May 2017

Coking Resistance of Alumina Forming Cast Austenitic Stainless Steels

Lizeth Nayibe Ortiz Reyes
University of Wisconsin-Milwaukee

COKING RESISTANCE OF ALUMINA FORMING CAST AUSTENITIC STAINLESS STEELS

by

Lizeth Nayibe Ortiz Reyes

A Thesis Submitted in

Partial Fulfillment of the

Requirements for the Degree of

Master of Science

in Engineering

at

The University of Wisconsin-Milwaukee

May 2017

ABSTRACT

COKING RESISTANCE OF ALUMINA FORMING CAST AUSTENITIC STAINLESS STEELS

by

Lizeth Nayibe Ortiz Reyes

The University of Wisconsin-Milwaukee, 2017
Under the Supervision of Dr. Benjamin C. Church

Coking is the process of carbon deposition from a gas phase that is encountered in many reforming, cracking and other high temperature processes. Coking in certain petrochemical processes can lead to carbon build up causing reduced process efficiency, corrosive attack, and degradation of the alloy. Steam cracking of hydrocarbons is one of the most important process for manufacturing many base chemicals such as ethene, propene and other. A major influence on the energy efficiency and economics is the formation of coke on the inner wall of the reactors. With the accumulation of coke on the walls, eventually metallurgic constraints of the reactor material will force to stop the process and de-coke the reactors resulting in loss of efficiency with negative effect on the economics of the process.

Materials used in these processes are fabricated from HP alloys that rely on the formation of a chromium oxide (chromia) layer as a protective layer between the bulk material and chemical byproducts. However, strong oxidation, carburization, sulfidation or nitriding can occur if the environment does not promote chromium oxide formation or if the protectivity of the scale is destroyed by other mechanisms.

More recent alloys that form an alumina-based oxide layer have been recently developed for structural use in aggressive oxidizing environments. These alloys, commonly known as AFA alloys, form a protective layer of aluminum oxide (alumina) showing a promising combination of oxidation resistance, creep resistance, tensile properties, and potential for good welding behavior.

An experimental high temperature coking atmosphere was constructed and used to evaluate the effects of temperature, time and metal surface roughness on the carbon deposition of two alumina forming alloys (2.6% and 3.7% Al content each). Coking conditions were simulated with multiple atmospheres including CO-H_2 mixtures at moderate temperatures and ethane at higher temperatures. Carbon deposition was tracked using specific mass change of the samples as a function of exposure times and conditions. Results obtained with the alumina forming alloys were compared to a baseline HP alloy. The materials were analyzed using XRD, SEM, and optical microscopy to characterize the oxide layer formation, carbon deposition layers and carbon attack, and changes to base metal microstructure. Raman spectroscopy was used to characterize the carbon deposits.

The overall resistance of the alumina-forming alloys relative to the traditional chromia forming alloys is described. Overall, AFA alloys showed better coking resistance to more aggressive environments that involve high temperature and longer times of exposure than traditional chromia-forming alloy. Therefore, this particular coking resistance make AFA alloys suitable for a wide range of energy production, chemical and process industry applications, resulting in significant cost and energy savings as well as reductions in environmental emissions.

To

My loving parents,

Jorge and Mabel

whose words of encouragement and support

have taught me to work hard for the things that I aspire to achieve.

TABLE OF CONTENTS

LIST OF FIGURES

LIST OF TABLES

LIST OF ABBREVIATIONS

AFA	Alumina-forming austenitic stainless steel alloy
SS	Stainless Steel
HK, HP	Heat-resistant chromia-forming alloys
BSE-SEM	Back-scatter detector

ACKNOWLEDGMENTS

I would first like to thank my advisor Dr. Benjamin Church for accepting me into his research group. His continuous support since the beginning of the project and his guidance helped me consistently to take the right path. By supporting my attendance at various conferences, engaging me in new ideas, and demanding a high quality of work, he made me not only a better student but also, with his example of teaching, working and human being, made me a better person.

I would like to thank my committee members Dr. Hugo Lopez and Dr. Ronald Perez. Thanks to Dr. Lopez for the knowledge gained through his class and for the interest on my research. Thanks to Dr. Perez for his support during my Master's studies.

I would also like to thank Jim Myers of MetalTek for providing his industrial insight, time and resources throughout the project. Additionally, thanks to Dr. Steven Hardcastle for his time and resources in the AAF, especially with the SEM and XRD trainings.

I would like to thank the research group members, Kao Yang, Elmer Prenzlow and Wen-Chieh Lee, for their continuous help and friendship. Every result described in this document was accomplished with their help and their support.

Finally, I must express my gratitude to my parents and to my host family, for providing me with unfailing support and continuous encouragement through my Master's Studies. This accomplishment would not have been possible without them.

This work was sponsored by ARPA-E, DE-AR0000690. Without their financial support this work could have not been possible.

CHAPTER 1. INTRODUCTION

Applications such as power generation, chemical processing, fuel cells, and high temperature heat exchangers are exposed to high temperature aggressive gaseous environments which limit the life expectancy. Coking is the process of carbon deposition from a gas phase that is encountered in many reforming, cracking and other high temperature processes that can lead to carbon build up causing reduced process efficiency as well as corrosive attack and degradation of the alloy.

The ethylene production process and other petrochemical processes can be improved by developing materials that resist coking, retain long-term oxidation and corrosion resistance, and yet remain economically favorable for implementation. Typical alloys used in these applications are austenitic Fe-Ni-Cr heat resistance steels which form a protective chromium oxide (chromia) layer during exposure. The chromia layer acts as a diffusion barrier that restricts the transport of gas-phase constituents (oxygen, carbon) and alloy constituents (Fe, Ni, Cr, and others) so that the inevitable reactions between the gas and solid are slowed (1), (2). These heat resistant stainless steels rely on chromia scales for protection from high temperature oxidation but their performance is limited in many industrial environments. Depletion of chromium in the alloy due to carburization can degrade the alloy's ability to regenerate a protective oxide scale thus resulting in faster coke build-up and further carburization.

More recently, research into alloys which produce protective layers of aluminum oxide (alumina) have been explored as a way to further slow the rates of high temperature oxidation and coke build-up (3), (4). Alumina-forming austenitic stainless steel alloys are

thought to be an alternative to the traditional alloys due to more stable oxide scale as well as superior corrosion and creep resistance for many industrial environments (5). The protective oxide layer enables the use of these alloys at higher temperatures and for longer time periods than stainless steel alloys that form a protective chromium oxide surface layer. This oxide layer make them suitable for a wide range of energy production, chemical, and process industry applications, where the use of more durable materials capable of withstanding higher temperatures can result in significant cost and energy savings as well as reduction in environmental emissions (6). Development and commercial implementation of such alloys is not trivial; a modification to chemical composition alters the manufacturability of the material and long-term performance remains an unproven, yet critical, variable.

1.1. Background

Ethylene (C_2H_4), or ethene, is a hydrocarbon material used as a raw building block for many industrially critical materials such as polyethylene, PVC, polystyrene, ethylene glycol, and countless other products. The annual world-wide production is over 100 million tons with US production representing roughly 25% of the total. US based production is expected to increase from an average of 1.25 million barrels per day (b/d) in 2016 to 1.7 million b/d in 2018.[1] Ethylene as one of the great buildings blocks in chemistry is produced in large volumes mainly by thermal cracking of hydrocarbons in the presence of steam, and by recovery from refinery cracked gas.

[1] U.S. Energy Information Administration. “U.S. Gas Plant Production of Ethane-Ethylene”. www.eia.gov . Accessed on 01/17/17

More than half of the production of ethylene is used to produce polyethylene, one of the most important materials today. The market grows continuously with an average rate of 4% worldwide and can be related to the gross national product growth in an area or a certain country (7).

The production of ethylene today is based on feedstocks derived from crude oil or from natural or associated gas (Natural Gas). The leading technology applied for production of ethylene is steam cracking, a high temperature pyrolysis in the presence of steam, which was developed in the 1960s, and has remained largely unchanged since that time (7). It is commonly produced in steam crackers where gaseous feed stocks such as ethane or propane are cracked and formed into the ethylene structure. Hydrocarbons and steam pass through tubes that are heated to temperatures above 900°C in many cases exceeding 1100 °C. The systems for producing this raw chemical incorporate large reactors that are made of alloys that provide 1) high temperature mechanical strength and 2) chemical resistance to attack under the aggressive carbon-rich conditions of the system. Typical alloys for the reactor tubes are stainless steels or Fe-Cr-Ni centrifugal cast alloys (HK, HP). It is important to select the alloy composition or control the environment to minimize the damage produced by interactions with aggressive oxidants (8). Even with good alloys and tight process control, carbon build-up (coking) is inevitable. Most production facilities are periodically taken off-line so that the reactor system can be “de-coked” using steam and air to “burn off” coke deposits. The periodic maintenance results in a loss of production efficiency (~2-8% of annual capacity), added costs, and thermal cycling of the system which imparts additional wear on the reactor.

1.2. Literature review

1.2.1. Current materials

Heat-resistant structural and related iron and iron-nickel alloys are used in corrosive environments at temperatures above ~600 °C and up to ~1150 °C. These steels are used in high temperatures environments that include air, ammonia, carburizing gases, oxidizing and reducing flow gases. Such applications demand an optimum combination of microstructural stability, creep resistance, excellent oxidation resistance, and additionally, resistance to coking and carburization in case of ethylene pyrolysis applications (9). These alloys utilize Cr_2O_3-based scales for protection. However, this chromia scale can be susceptible to accelerated oxidation in the presence of water vapor (10). The excellent metallurgical compatibility of chromium in Fe/Fe(Ni) allows ready formation of a protective Cr_2O_3-based scale with wide alloy design flexibility optimizing oxidation resistance with other needed properties such as creep resistance, weldability, etc. (11). Because they combine good creep strength and oxidation resistance, are widely used in energy production and chemical processing environments. However, strong oxidation, carburization, sulfidation or nitriding can occur if the environment does not promote chromium oxide formation or if the protectivity of the scale is destroyed by other mechanisms (8).

1.2.2. AFA Alloys

Alumina-forming austenitic stainless steels have been recently developed for structural use in aggressive oxidizing environments at 600-900 °C. These alloys show a promising combination of oxidation resistance, creep resistance, tensile properties, and potential

for good welding behavior. Recently investigations indicate the potential to achieve superior oxidation resistance compared to conventional Cr_2O_3-forming iron- and nickel-based heat-resistant alloys (11). This is due to the slower growth rate and greater stability of alumina, particularly in the presence of water vapor species encountered in many industrial process and energy production environments (12).

Studies shown these alloys have potential in process environments involving aggressive water vapor, carbon, and sulfur species in temperatures ranging from 500 to 900°C. (6) It is speculated that the key factor controlling if and how long Al_2O_3 scale formation occurs in AFA alloys is oxygen solubility in the alloys. To promote protective Al_2O_3 scale formation, it has been explored that alloying addition levels of ~4-6 wt.% aluminum and ~10-25 wt.% chromium can destabilize the parent austenitic matrix structure, resulting in duplex ferritic/austenitic microstructure and a loss of creep resistance. This structure can be stabilized by additions of nickel so the AFA alloys can develop a good oxide scale and retain good creep resistance for the application (11) (see Figure 1 and Figure 2).

1.2.2.1. Alloying additions

The alloy's composition range have been studied so a material able to produce a good alumina oxide scale combined with a good creep resistance can be achieved. Researchers have been developed different grades of AFA alloys and have been tested in different oxidizing – carburizing environments at different high temperatures ranges (~600 - 1000 °C). Generally, the addition of Al and Cr to steel to increase its corrosion resistance but results in reduced creep strength (6). Over the past 30 years,

investigations have been focused in the balance between Al, Cr and other alloying elements so an optimal alloy can be developed.

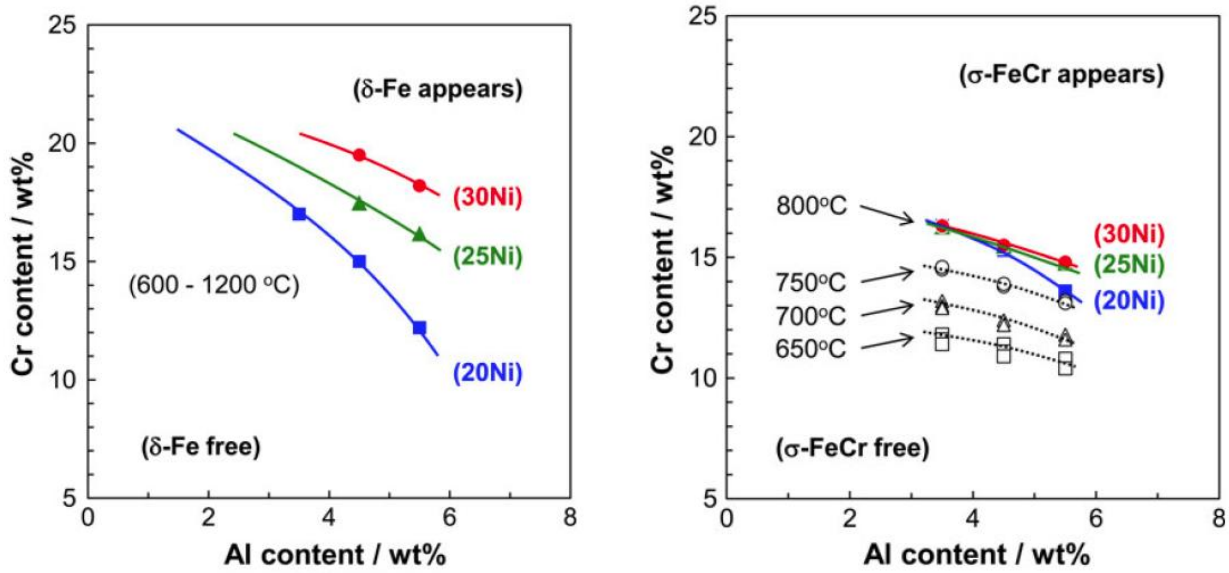

Figure 1. Phase diagram of Fe-Cr-Al-(20, 25, 30) Ni-1Nb-2Mo-0.1C showing limitations of Cr and al additions in a range of 600 to 1200 °C (right); and at 650, 700, 750 and 800°C phases, predicted by thermodynamic calculation.[2]

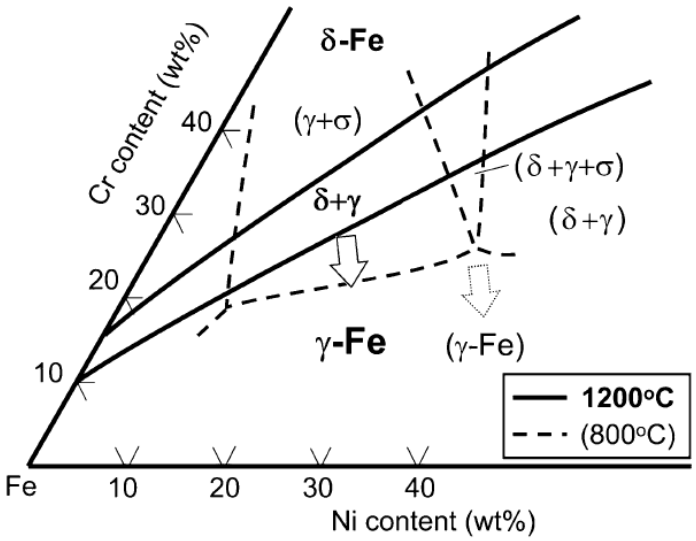

Figure 2. Superimposed ternary phase diagram of Fe-Cr-Ni near the Fe-rich corner at 1200 °C (bold lines) and at 800 °C (broken lines). Arrows indicate the direction of phase boundaries shifting by the Al addition due to the strong δ-Fe stabilizing effect of Al relative to γ-Fe.[2]

[2] Image taken from Yamamoto, Y. et al., "Overview of Strategies for High-Temperature Creep and Oxidation Resistance of Alumina-Forming Austenitic Stainless Steels", 2011. (15)

Studies on the alloy composition have explored the effects of alloying additions on oxidation and creep behavior concluding:

- It has been identified that AFA alloys with a relatively low Al and Cr contents (2.5 to 4 wt.% and 14 to 15 wt.% respectively, have formed alumina scale and permitted stabilization of an FCC austenitic matrix phase for creep strength with low additions of Ni (6).
- Niobium additions (0.6 to 3 wt.% Nb) seems to enhance the oxidation resistance, particularly in water-vapor containing environments (6) (11).
- Increasing niobium, aluminum, and/or nickel content all favor the establishment and maintenance of protective Al_2O_3 scale formation in these alloys (13).
- Some tolerance for vanadium and titanium is important because they can be used to enhance MC carbide formation for improved creep resistance (11).
- Use of nitrogen, titanium, and vanadium degrade the ability to form an alumina a surface layer in the AFA composition range and must be minimized (6).
- Alloys can be strengthened by gamma prime precipitates (γ'-Ni_3Al) with the proper balance of Al, Ni, Nb, and Ti additions (6).
- Carbides precipitates should be incorporated for creep strength (6). C levels of 0.3 – 0.4 wt.% C are required to balance creep properties with oxidation resistance (11).
- It has been found that cast AFA alloys containing 14wt.% Cr - 3.5 wt.% Al with approximately 25 wt.% Ni are restricted to maximum operating temperatures of 800-850 °C depending on the water vapor levels in the environment (9).

- The creep resistance of the alloys seems to be strongly dependent on the level of Nb additions. Al additions also help to increase the creep resistance (14), (15).

1.2.3. Al_2O_3 vs. Cr_2O_3

Different types of low cost Fe- and Ni- based alloys are widely used to meet the requirements of heat exchangers, steam crackers or tubes in the petrochemical applications. However, because of higher operating temperature and aggressive environment, most of the materials are not suitable for such applications. Above 700 °C, the commonly used alloys are susceptible to severe oxidation and creep deformation. The presence of water vapor (especially during the de-coking process), accelerates the rate of oxidation and increases Cr evaporation. The stability and the performance of the alloys are influenced by several factors such as microstructure, grain size, chemical composition, phase precipitation, scale formation, and operating temperature (16).

Al_2O_3 scales offer a superior degree of protection to Cr_2O_3 scales in many high-temperature environments (11), (17). Bhowmick et al. (16) studied the chromium evaporation from chromia and alumina forming alloys at 850 and 950 °C for 500 hours in air containing 2.6% and 12% water vapor. Chromium evaporation rate from thermally grown alumina scales is approximately two orders of magnitude lower than that formed on a conventional chromia forming alloy. They explained that the lower Cr evaporation rate in the alumina-forming alloy is due to the development of thin protective alumina scale on the surface along with the formation of Cr, Fe and Ni-rich islands.

A comparison of the advantages and disadvantages of the alumina scale versus chromia scale in presented in Table 1.

Table 1. Comparison of Al_2O_3 vs Cr_2O_3 oxide scales

Al_2O_3	Cr_2O_3
Al_2O_3 scales grow at a rate that is 1 to 2 orders of magnitude lower than that of Cr_2O_3. (see Figure 3).	The presence of water vapor, accelerates the rate of oxidation and increases Cr evaporation
Diffusion of carbon (D_C) is lower through alumina than chromia. Aluminum additions also reduce D_c within austenitic matrix.	Chromia (and spinel) prevent inward carbon diffusion under certain conditions by means of very low diffusion rate of carbon (D_c)
Alumina is more thermodynamically stable to higher temperatures and for longer time periods than chromia. (See Figure 3). $Al_2O_3 > SiO_2 > Cr_2O_3$	Loss of Cr through evaporation of Cr_2O_3 and/or $CrO_2(OH)_2$ at high oxygen partial pressures >1850 °F (~1000 °C) which represents a temperature limitation.
Greater stability in the presence of water vapor (11). Significant oxidation volatility is not typically observed until temperatures reach ~1200 °C (6).	Volatile chromium oxy-hydroxide species can form and significantly reduce oxidation lifetime of the alloy (6).
A uniform and dense alumina scale can reduce the propensity for catalytic coke formation.	Local breakdowns in scale and subsequent transport of carbide or Fe ions to surface act as nucleation sites for catalytic coking.

It has been proven to be particularly beneficial in the presence of aggressive carbon- or sulfur-species encountered in combustion and chemical process industry applications (11), (17).	Above ~1900°F(1040°C) in the presence of carbon (i.e. coke layer), Cr carbide is thermodynamically favorable and its formation will cause eventual failure of oxide layer

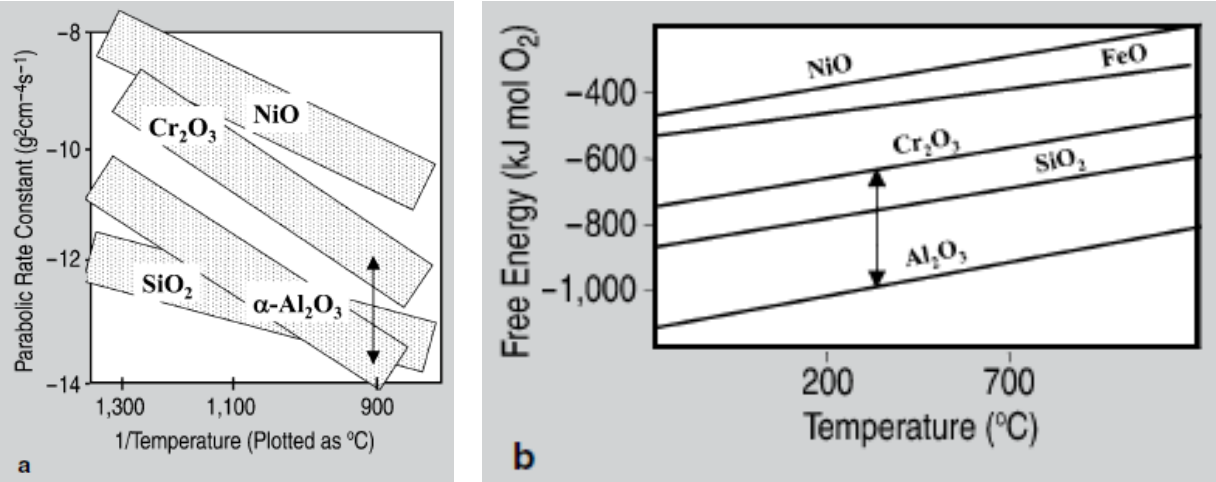

Figure 3. A schematic representation of (a) growth rate data and (b) thermodynamic stability data for specific oxides.

The arrows demark differences between Al_2O_3 and Cr_2O_3.[3]

1.2.4. Crystal structure of AFA alloys

Ferritic Fe-Cr-Al-based alloys capable of forming Al_2O_3 are widely used in specialty applications such as heating elements and furnace liners. However, they are not suitable for structural applications above ~500-600°C because of its poor creep resistance resulting from their open body-centered cubic structure. Investigations have shown that to obtain a good creep resistance, an austenitic face-centered cubic structure is needed.

[3] Image taken from Brady, M. P. et al. "The development of alumina-forming austenitic stainless steels for high-temperature structural use", 2008. (11)

Austenitic stainless steel has a face-centered cubic (FCC) crystal structure that is stabilized by nickel; exhibits better high-temperature creep strength than ferritic stainless steel, which features a body-centered cubic (BCC) crystal structure.

Studies in the role of Manganese in the high-temperature oxidation resistance of AFA alloys have been done above 800 °C in air and in air with 10% water vapor. Manganese is a strong face-centered cubic stabilizer and much cheaper than nickel, usually added into austenitic steels to realize solid-solution strengthening, stabilize the austenite matrix, and reduce the raw material cost. AFA alloys usually have between 1% and 2% Mn, but its role in the oxidation process is not well clarified yet. Researchers have found that excessive additions of Mn in AFA alloys tend to stimulate formation of the coarse spinel $CrMn_{1.5}O_4$ and Cr_2O_3 which is responsible for the degradation in the oxidation performance. Therefore, Xiangqi et al., have concluded that exists an upper limit for the Mn addition, and the tolerable amount of Mn in these alloys is decreased with the increase of the service temperatures and presence of water vapor. Also, they found the oxidation resistance was moderately degraded with additions of larger than 1% Mn at 800 C, even in dry air (18).

1.2.5. Oxidation

The oxidation phenomenon is considerate as the most important corrosion reaction at high temperature and is one of the primary considerations that determine the durability of heat-resistant alloys. The metals and alloys oxidize when are exposed to air or environments with high oxygen potential, at elevated temperature with a strong effect of temperature over oxidation rate (17). The key factor for a good oxidation resistance is to establish an external, continuous layer of a slow-growing, thermodynamically stable

oxide phase (11). For high-temperature applications, such as higher than 600 °C, Cr_2O_3 and Al_2O_3 are the principal oxides used for the protection of metallic alloys.

Muralidharan et al., tested an AFA alloy (CAFA 7) cetrifugally cast in an oxidation environment of air with 10 vol. % water vapor, and laboratory air (no added water vapor). Oxidation exposures were conducted in 100 h cycles at 750 and 800 °C, and 800°C and 900 °C for 1000-2000 h using 500h cycles respectively. Their results show that the oxidation resistance of the alumina forming stainless steels was superior to the chromia-forming alloys (HK[4] and HP[5] steel). Figure 4 shows a BSE-SEM images of their alloys after exposure to air for 2000 hours at 800 °C. It is noticeable that the oxide layer formed by the AFA alloy is thinner than that formed by the HP alloy for the same exposure conditions. They also report that in some regions of the AFA alloy, the oxide layer was multi-layered, with the outside layer comprising of a locally nodular-like Fe-Ni-Cr rich oxide, undercut by a continuous alumina layer. The oxide on HP was multilayered in some regions as well, with the same nodular-like Fe-Ni-Cr rich oxide followed by an interior layer being rich in Cr (9).

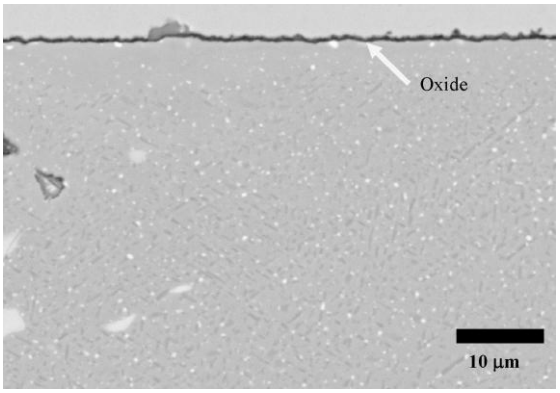

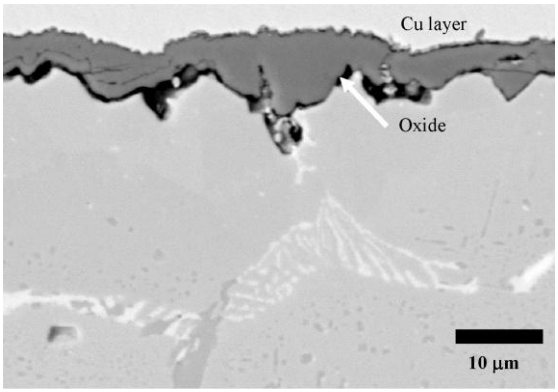

[4] HK austenitic s.s.: 24-28 wt.% Cr, 18-22 wt.% Ni
[5] HP austenitic s.s.: 24-28 wt.% Cr, 33-37 wt.% Ni

Figure 4. BSE BSE-SEM image from CAFA7 (left) and HP (right) alloy tested at 800°C in air for 2000 hours.[6]

Since the formation of the alumina scale in the AFA alloys occurs at a slow growth rate, the change in mass for the samples after exposure, even after 5000h have been reported as a positive mass gains around <0.5 mg/cm^2 (19). These small changes in mass are consistent with protective alumina scale formation in the range of a few microns thick (20). Researchers have found the scale to consist primarily of Al and O, with only minor amounts of Cr, Fe, Mn, and Nb (21).

Yamamoto et al. tested AFA alloys (range composition of 20wt. % Ni – 12-14 wt.% Cr – 2.5-4 wt.% Al) for 1000 hours in air and in air with 10% water vapor environments at 650 and 800 °C finding that none of the current compositions formed protective alumina scales at 1000 °C in air. However, excellent oxidation resistance at 650 and 700 °C was observed. The loss of protective oxidation behavior was associated with a transition to internal oxidation and nitridation of Al. Furthermore, the solubility of al in the austenitic matrix is on the order of ~2 to 2.5 wt.% Al, so that the higher-Al containing alloys, exhibited second phase dispersion of B2[(Ni,Fe)Al] (see Figure 5) acting as a Al reservoirs for the growth of alumina scales (19).

[6] Image taken from Muralidharan, G. et al. “Development of Cast Alumina-forming Austenitic Stainless Steel Alloys for use in High Temperature Process Environments”. (9)

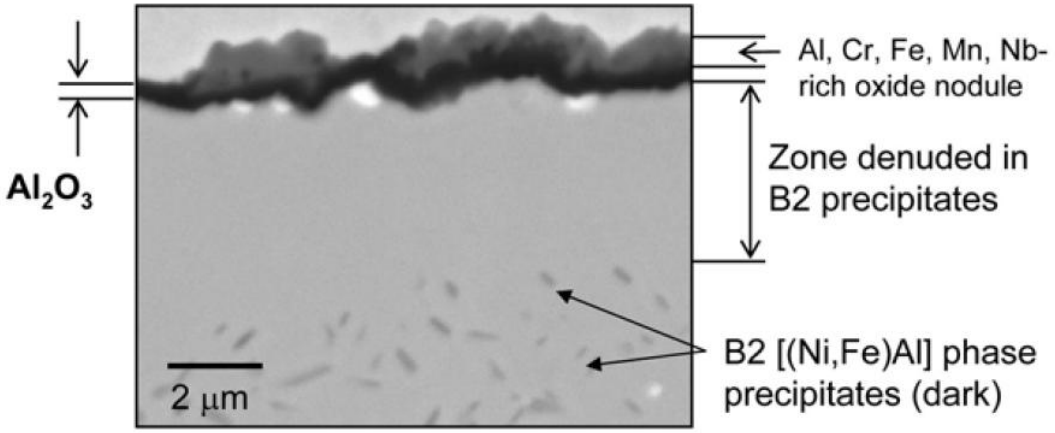

Figure 5. BSE-SEM of AFA 4-1 (4Al/0.6Nb/0.1ti) after 100h at 900 °C in air.[7]

1.2.5.1. Thermodynamics

Thermodynamically, it is probable the formation of an oxide over a metal surface when the oxygen potential in the atmosphere is higher than the partial pressure of oxygen in equilibrium with the oxide. This partial pressure in equilibrium could be determined from the standard free energy change (ΔG) for the oxide formation, considering this reaction:

$$\boldsymbol{M_{(s)} + O_{2\,(g)} \leftrightarrow MO_2} \qquad (1.1)$$

$$\boldsymbol{\Delta G = -RT\, Ln\left(\frac{a_{MO_2}}{a_M * P_{O_2}}\right)} \qquad (1.2)$$

Assuming the metal and oxide activities as the unity:

$$\boldsymbol{P_{O_2} = e^{\left(\frac{\Delta G}{RT}\right)}} \quad (1.3)$$

The standard free energy of formation for various oxides as a function of temperature and the relative partial pressures of oxygen in equilibrium with the oxide are summarized in Ellingham/Richardson diagram as shown in Figure 6. From this diagram, it is possible to determine the potential of oxygen in oxidizing atmospheres (P_{O2}) and reducing atmospheres with gas mixtures (P_{CO}/P_{CO2}) (22). Comparing the oxygen

[7] Image taken from Yamamoto, Y. et al., "Development of Alumina-Forming Austenitic Stainless Steels", 2008. (19)

potential in the gaseous environment with the oxygen partial pressure in equilibrium with the evaluated oxide, it is possible to determine thermodynamically if this is stable or not under conditions worked in the laboratory.

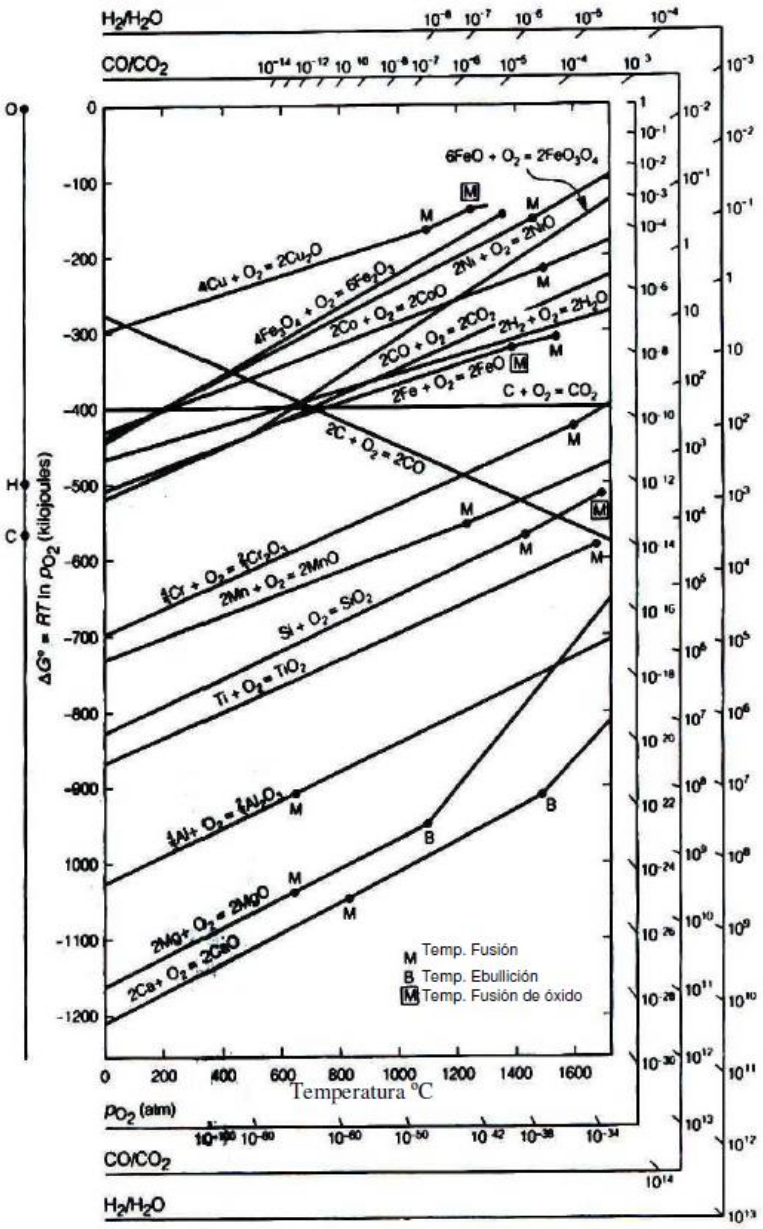

Figure 6. Ellingham/Richardson diagram for metal oxides. Standard free energies of formation in function of Temperature.[8]

[8] Image taken from Lay, G.Y. "High Temperature Corrosion of Engineering Alloys",1990 (17).

Millward et al. (23) used published algorithms to evaluate the free energy changes, ΔG, for the various oxidation reactions that can take place in the metal's surface as show in Figure 7.

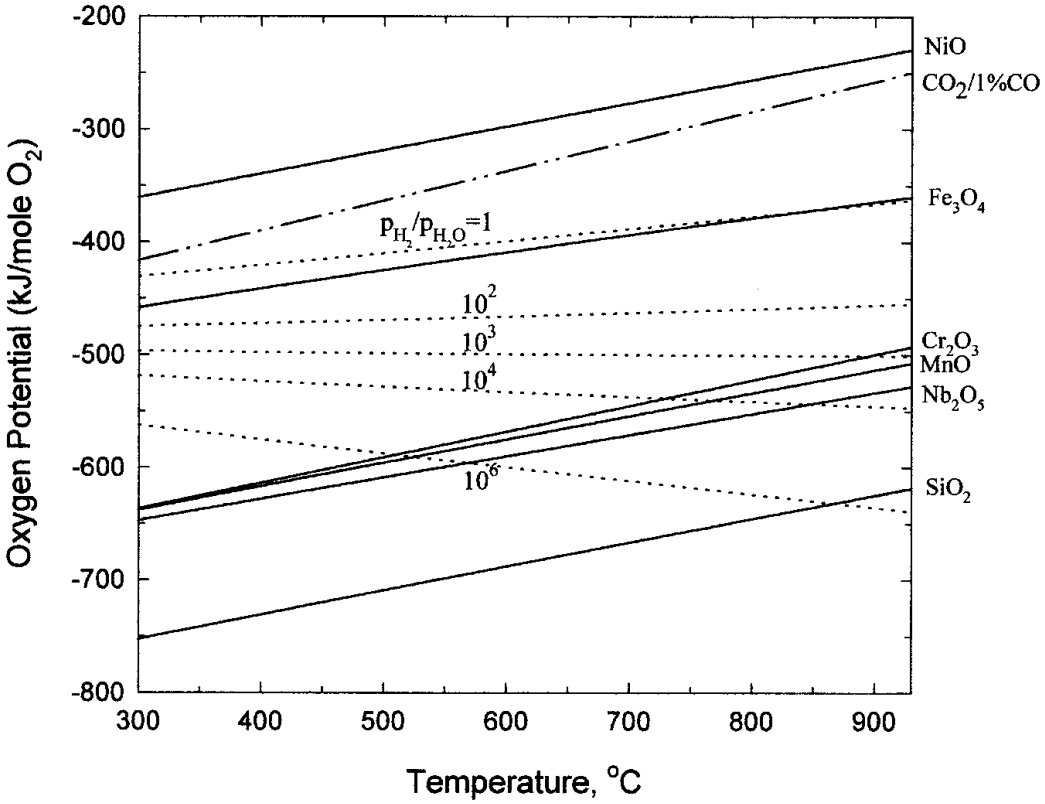

Figure 7. Free energy changes, ΔG, expressed as oxygen potential for various oxidation reaction temperatures.[9]

From Figure 7, it is appreciated that at temperatures of 850 – 915 °C, temperatures worked for the oxidation tests of this document, ratios of 10^2 -10^3 of H_2/H_2O are required to form a Cr_2O_3 scale oxide on the surface of the metals.

[9] Image taken from Millward, G. R., Evans, H. E., Aindow, M., & Mowforth, C. W. (2001). "The Influence of Oxide Layers on the Initiation of Carbon Deposition on Stainless Steel" **(23)**

1.2.5.2. Kinetics

Church et al. (24), evaluated the relative oxide formation of a traditional chromia-forming alloy (35Cr-45Ni-0.4) against two alumina forming alloys (27Cr-35Ni-0.4C) containing varying amounts of aluminum (2.7%Al and 2.6%Al). The oxidation treatment was intended to produce a stable surface oxide on the samples. Their environment conditions were 850°C for 12 h and raised the temperature up to 915°C for 1, 10 and 100 hours in 100% steam. They concluded that the alumina forming alloys had parabolic oxidation kinetics while the chromia forming alloy had significant departures from parabolic behavior likely due to chromia volatilization. Furthermore, both alumina-forming alloys were able to form a continuous layer during 100% steam oxidation. The chromia-forming alloy showed mass changes that were non-linear with the root of time indicating that is likely to had competing mechanisms of a) oxidation and b) chromia volatilization that resulted in the observed mass change behavior.

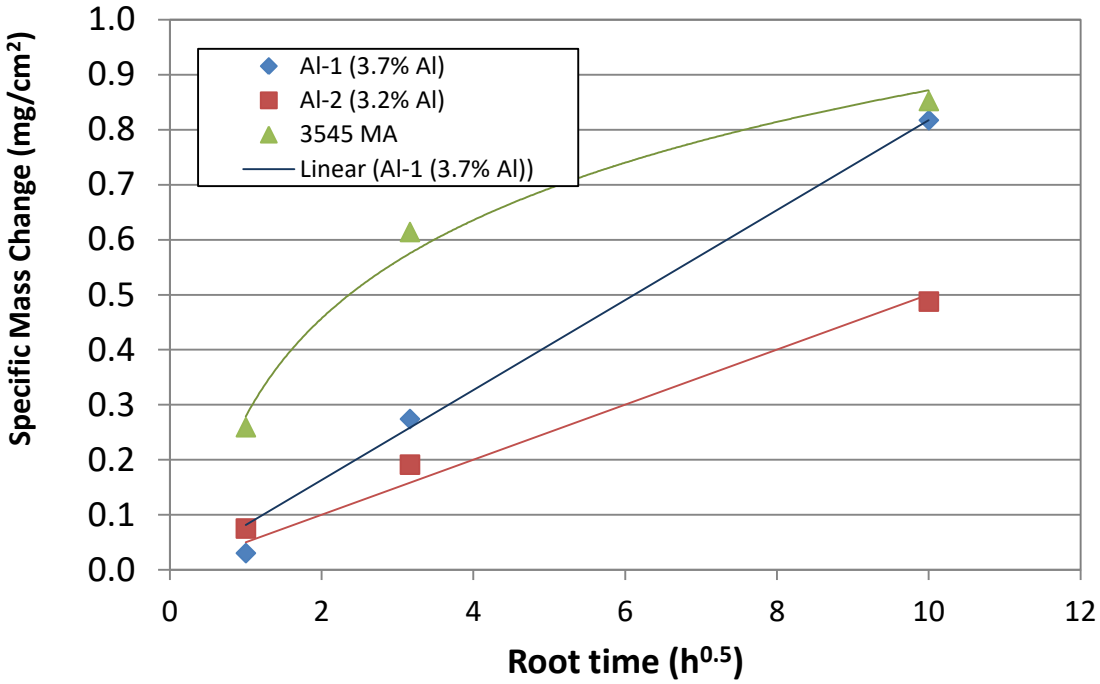

Figure 8. Mass change of samples during steam pre-oxidation treatments at 915 °C. Linear trend lines were forced to originate at the origin to emphasize ideal parabolic ($\Delta m \propto t0.5$) kinetics.[10]

1.2.6. Coking

The formation of carbon deposits (coking) has been described in the literature and is a function of several factors including the balance of hydrocarbon to steam, incorporation of process gas dopants (e.g. sulfur compounds), and the surface chemistry of the materials that make up the reactor (25), (26). Understanding the relation between the alloy's surface chemistry and coking resistance is a primary goal which will allow for the design of alloys with improved coking resistance.

1.2.6.1. Thermodynamics

The industrial environments normally connected to the metal dusting – problem contains CO, H_2 and sometimes also other gaseous components, i.e. synthesis gas mixtures.

[10] Image taken from Church, B., Ortiz, L., Prenzlow, E, et al. "An Initial Evaluation of the Effect of Alloy Composition and Oxide Layer on High Temperature Coking Resistance of Heat Resistant Alloys", 2016 (24)

Basically, there are two reactions that bring about solid carbon or coke deposition in H_2-CO mixtures:

$$\boldsymbol{2CO_{(g)} \leftrightarrow C_{(s)} + CO_{2\,(g)}} \text{ (1.4)}$$

$$\boldsymbol{CO_{(g)} + H_{2\,(g)} \leftrightarrow C_{(s)} + H_2O_{(g)}} \text{ (1.5)}$$

Reaction (1.4) corresponds at Boudouard equilibrium and (1.5) to Steam-carbon equilibrium.

Szakálos et al. (5) investigated the kinetics of these reactions as a function of CO/H_2 content and temperature on pure iron. The results showed that reaction (1.4) dominates at higher CO concentrations and reaction (1.5) dominates at higher H_2 concentrations (5).

Thermodynamically, the carbon activity in the environment is determined according with the present gaseous species like CO, CO_2, H_2O and H2, based on (1.4) and (1.5) reactions. The, the carbon activity in the environment could be calculated from reaction (1.5):

$$a_c = e^{\left(\frac{-\Delta G}{RT}\right)} * \frac{P_{H_2}\, P_{CO}}{P_{H_2O}} \qquad (1.6)$$

Being:

ΔG	Gibbs energy change
T	Temperature of the system
P_i	Partial pressure
a_c	carbon activity in the gaseous environment

Considering the equilibrium constant of the reaction (1.5), then, it is possible to get an approximation of the carbon activity (a_c) of the environment.

$$Ln\ K_{1.2} = \frac{-\Delta G}{RT} \quad (1.7)$$

$$a_c = Ln\ K_{1.2} * \frac{P_{H_2}\ P_{CO}}{P_{H_2O}} \quad (1.8)$$

The values of a_c increase with decreasing temperature and may easily reach a_c=100 or 1000 at low P_{H_2O}. The carbon from the reaction (1.5) may

a) be transferred into solid solution in the phase metal,
b) be consumed by carbide formation or
c) deposited as more or less graphitic carbon (27).

The thermodynamic condition to predict if an alloy would be carburized or decarburized depends on the carbon activity (a_c) in the environment and the interior of the alloy (28). The alloy tends to be carburized or gain carbon from the environment when:

$$a_{C\ \ environment} \gg a_{C\ alloy}$$

The alloy tends to be decarburized or lost carbon from the metal matrix when:

$$a_{C\ environment} \ll a_{C\ alloy}$$

It may be concluded that during carbon deposition of high alloyed steels and Ni-base alloys, two additional reactions take place which produce carbon from the gas phase according to the reactions

$$CO_{(g)} + M_{(s)} \rightarrow C_{(s)} + MO_{(s)} \quad (1.9)$$

$$CO_{2\,(g)} + 2M_{(s)} \rightarrow C_{(s)} + 2MO_{(s)} \quad (1.10)$$

It has been demonstrated that, metal dusting is caused by the strong tendency for graphite formation, either by “graphitization” as in the case of nickel and Ni-base alloys or by carbide, mainly M_3C decomposition as in the case of iron and steels (27).

Metal dusting has been also observed in refineries cause by naphtha and in principle also in cracking tubes for ethylene production. Then, the carbon activity results from the decomposition of hydrocarbons

$$C_xH_y = \frac{y}{2}H_2 + xC \qquad (1.11)$$

$$a_c = \left(\frac{P_{C_xH_y}}{K_{1.7} * P_{H_2}^{\frac{y}{2}}} \right)^{\frac{1}{x}} \qquad (1.12)$$

If the environment contains CH_4, the carbon activity of the environment will be dominated by the reaction (1.13).

$$CH_4 = C_{abs} + 2H_2 \quad (1.13)$$

Where carbon activity can be expressed as

$$a_c = K_{1.9} * \left(\frac{P_{CH_4}}{P_{H_2}^2} \right) \quad (1.14)$$

If the environment contains $CO_2/CO/C_2H_4$ gas mixture, the carbon activity of the CO_2/CO equilibrium will be negligible compared with that produced by the reaction of ethylene (C_2H_4) with other constituents. Various possible overall dissociation reactions can be identified (23):

$$C_2H_4 + 2CO_2 \rightarrow 2C + 2CO + 2H_2O \qquad (1.15)$$

$$C_2H_4 + 2CO \rightarrow 4C + 2H_2O \qquad (1.16)$$

$$C_2H_4 + CO_2 \rightarrow 3C + 2H_2O \qquad (1.17)$$

The carbon activity of this environment is uncertain, since it depends on which of the reactions (1.15), (1.16), or (1.17) will dominate and how closely equilibrium is approached. Even so, carbon activities far greater than unity can be expected and that the gas, will provide a potentially highly depositing environment.

Serna et al. (8) report that boundary grain precipitation is the main mechanism of carburization in austenitic Fe-Ni-Cr (HP-40) alloys was observed for samples extracted from ethylene furnace tubes. They saw internal carburization only in areas where the oxide film was absent. For austenite, carbon solubility is high, but carbon diffusivity is low, and chromium diffusivity is low. For ferrite, carbon solubility is much less but carbon diffusivity is much higher; chromium diffusivity is much higher.

1.2.6.2. Kinetics

In general, three coke formation mechanisms have been described in the literature: the heterogeneous catalytic mechanism, the heterogeneous free-radical mechanism, and the homogeneous droplets condensation/tar deposition mechanism (29).

The catalytic mechanism, accounts for the coil materials, with nickel and iron acting as catalysts for the formation of carbonaceous deposits in carbon-rich atmospheres. In this mechanism, as shown in Figure 9, hydrocarbons are chemisorbed on the metal surface, subsequently losing hydrogen atoms which react and desorb into the gas phase. The carbons left at the surface start diffusing into the alloy. As carbon keeps depositing, the particles keep being lifted by carbon filaments growing out of the surface. Simultaneously, the radical carbon formation increases the diameter of the filament and

eventually covers the particle, encapsulating it. Therefore, the relative importance of radical coking compared to that of catalytic coking increases over time (29).

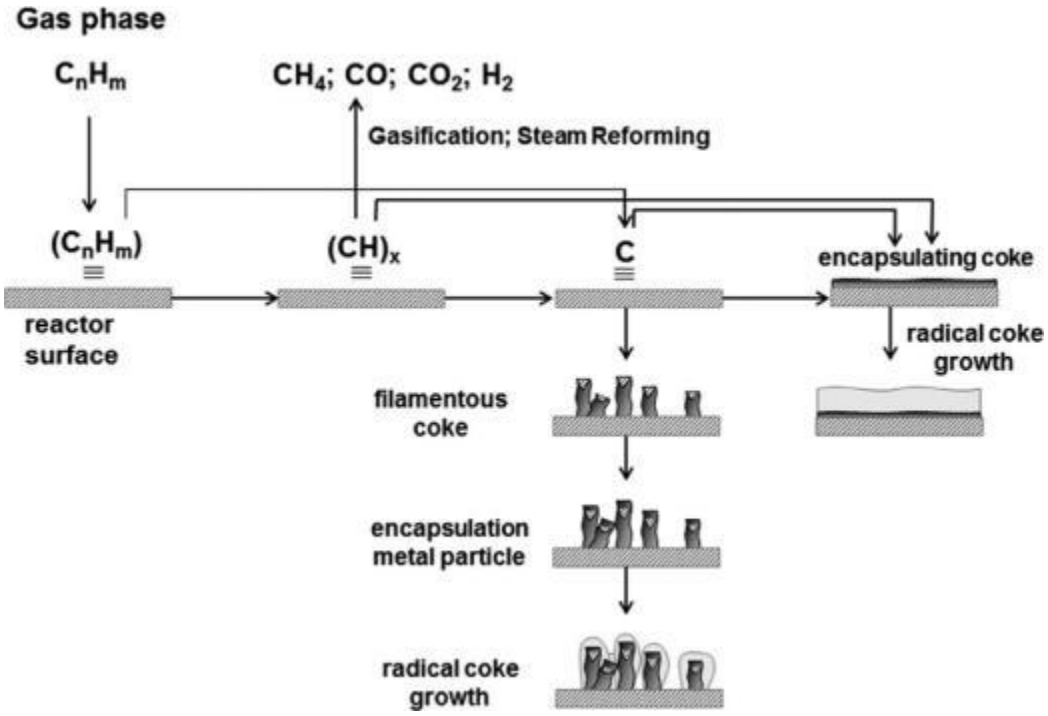

Figure 9. Schematic diagram of the heterogeneous catalytic mechanisms for coke deposition.[11]

Respect to the heterogeneous free-radical mechanism can be explained by five radical reactions: hydrogen abstraction, substitution, addition by gas phase radicals, addition to gas phase olefins and cyclization. This radical mechanism is present throughout the entire run length of the coil, and its relative importance increases over time as the catalytic sites of the surface are covered (29).

The homogeneous droplet condensation mechanism applies when heavy polynuclear aromatics are present in the atmosphere. Its importance relies when cracking heavier feeds, such as gas oils, vacuum residue, and bitumen are cooled (29).

[11] Image taken from Andres Munoz et al., "Influence of the Reactor Material Composition on Coke Formation during Ethane Steam Cracking", 2014. (29)

Kinetics of coke formation have been studied in some alloys in atmospheres similar to petrochemical industry atmospheres. Jackson et al., studied the coking kinetics of several commercial Fe-Ni-Cr alloys used as materials for ethylene steam crackers. Temperatures of 450 to 1000°C in hydrogen-propylene atmosphere using a microbalance reactor were used. They found that the rate of coke formation on alloys increased continuously between 500 and 1000 °C. Between 900 and 1000°C, steady state kinetics were controlled by gas-phase pyrolysis and similar reaction rates were observed for all materials. Also, they conclude that differing catalytic activities resulted in significant differences in coking rates below 900 °C; whereas significant differences in reaction rates of alloys due to formation of filamentous coke was observed only below 800°C (30).

Munoz et al. (29), studied the influence of the reactor material composition on coke formation during ethane steam cracking, finding that coke deposition is strongly affected by the composition of the material. Also, that Al-enhanced alloys had a better resistance to coke formation than those without aluminum in their formulation. In general, they conclude that for all alloys, independent on composition, the formation of a uniform layer of a protective oxide is essential, because the stability of the surface after pre-oxidation or decoking has a significant impact on the coking rate and not the bulk composition.

1.2.6.3. Composition and morphology of coke

Depending on the composition of the alloy and gas mixture, the coke will grow as a fur uniformly on the samples, locally and/or in form of noodles, cones or leeches. On high alloy steels the metal dusting and coke growth start locally in most cases, at spots where there are defects in the oxide scale. In the process plants, the coke Is generally

carried away by the gas flow and deposited somewhere in corners or dead ends. Chemical analysis can prove if the coke is from metal dusting, where will always contain metal elements. The metal components of the corroding alloys are transferred into the coke always in ratios corresponding to the alloy composition as carbides or oxides. Then, the morphology of coke can be very different depending on the steel, its surface state, the reaction temperature, and other parameters (27).

1.2.6.4. Metal dusting – $CO/H_2/H_2O$ gas atmospheres

Metal dusting is a corrosion phenomenon that deteriorates iron, low and high alloy steels, and other materials in strongly carburizing gas atmospheres, with carbon activity $a_c>1$ and at higher temperatures (usually 400-800°C). It is also defined as the disintegration of alloys into carbon and metal particles during high-temperature exposure to carbon-bearing gases (2). Corrosion products are graphite, metal, carbide, and oxide particles, mixed in finely divided form. Depending on the composition of the alloys and environment conditions, different mechanisms of metal dusting have been described in the literature.

J. Zhang et al. (31) characterized the coke formed by carburizing a pure iron sample at 700°C in a 24.81 – 94.81 vol.% H2, 5-75 vol.% CO and 0.19 vol.% H_2O gas mixture covering a range of carbon activities ($15.8 \leq a_c \leq 82.9$). They found the carburization is fast at the early stage of the reaction, then this rate decreases slightly and finally increases drastically after 2-hour reaction. Formation of a cementite with a graphite layer was found on the surface of the cross sections of the samples. Also, after 4 hours of carburization, a thick coke layer was found on the surface. They conclude that nature of the particles in the coke layer depends on the gas atmosphere. At low CO contents

(a_c=15.8), a major part of α-Fe particles together with cementite and some Fe_2C can be found on the surface. If the CO content exceeds 30% only iron carbide is observed in the coke for a test with pure iron samples.

Toh et. al (2) studied Fe-Cr and Fe-Ni-Cr alloys under 68%CO-26%H_2-6%H_2O gas mixtures at 680 °C (a_c = 2.9) under thermal cycling conditions. They assumed that interstitial diffusion of carbon into the alloy is much faster than substitutional diffusion and the process is one of carbon enrichment in a system in which the Fe/Cr ratio remains fixed. Depending on the composition of the alloy and the Fe/Cr ratio, a diffusion path may be followed in the ternary diagram of the Fe-Cr-C system.

Based on Figure 10, the corresponding diffusion path for an Fe-46Cr alloy is shown. This composition is critical since at lower chromium levels, the formation of Fe_3C is predicted whereas at higher levels it is not. Then, alloys containing more than 46% Cr would be predicted to resist dusting. However, additions of Ni to the Fe-Cr-C system results in destabilization of both ferrite and Fe_3C. At nickel levels of 10 and 25%, the Fe_3C phase is completely suppressed and only the chromium-rich carbides are predicted to form under the conditions of the test. They concluded that loss of chromia-reheating ability was followed by spinel formation, internal carburization, and surface cementite formation was found on the alloys after being tested. The difference in the nature of the “metal-dust” particles was reflected in the coke morphology and corresponded to large differences in metal-wastage rates (2).

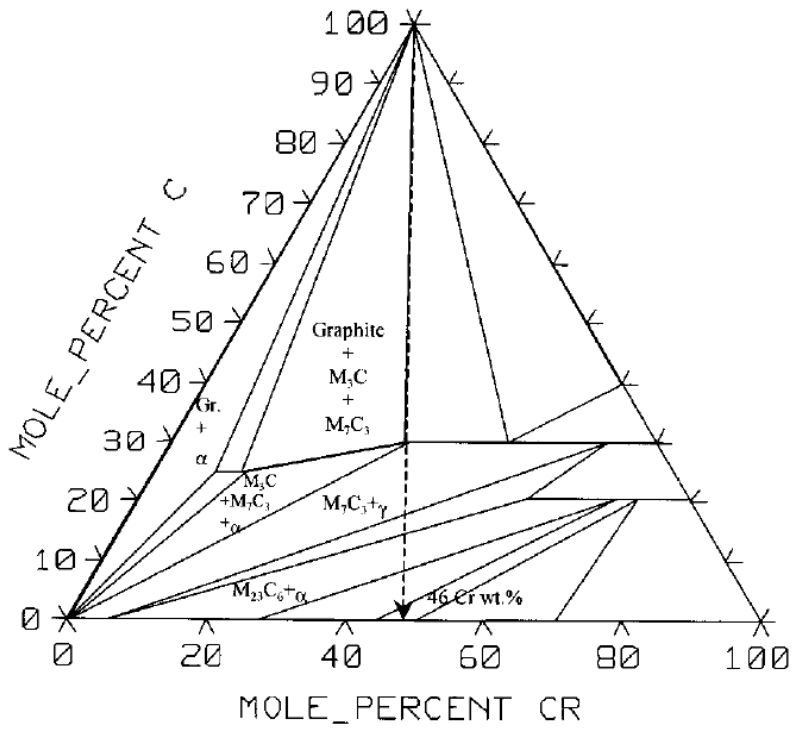

Figure 10. Isothermal ternary diagram for Fe-Cr-C system at 680 °C.
Dashed line shows a possible diffusion path for $D_c >> D_m$ for a Fe-46Cr alloy[12].

1.2.6.5. Hydrocarbons atmospheres

In the refinery and petrochemical industries, austenitic and ferritic alloys are usually used for tubes in fired furnaces where environments are combustion product gases and hydrocarbon gases with low oxygen potentials and high carbon potentials. Usually, the temperature range for exposure of austenitic alloys is 800-1100 °C, and for ferritic alloys 500-700 °C. These processes involve carbon deposition (coking) on the inner diameter, carbon absorption at the metal surface, diffusion of carbon inside the alloy, and precipitation and transformation of carbides to a depth increasing with service (8).

During thermal and steam cracking operation, carbon is deposited in the form of coke on the internal surfaces of the tubes. The efficiency of heat transfer is reduced and the

[12] Image taken from "Metal Dusting of Fe – Cr and Fe – Ni – Cr Alloys under Cyclic Conditions. Oxidation of Metals", 2002. (2)

metal skin temperature increased to maintain the process temperature. The presence of coke eventually leads to carburization of the tubes when it is periodically removed by oxidation in water vapor and air (de-coking) (8).

Serna et al. (8) compared the morphological differences in the carbon deposition occurred in austenitic and ferritic alloys exposed for a long time in environments with carbon activity over one in many cases concluding:

- In a sample of a ferritic alloy Fe-9Cr-1Mo extracted from a tube closed to the outlet of the radiation zone, exposed for 102000 hours at 600 °C showed the evident bulk carburization through all the cross section along the inside diameter. Although this alloy had an oxide layer over the internal surface, the carburization was homogeneous along the internal diameter.
- A tube alloy of austenitic Fe-Ni-Cr (HP40) extracted from a coil of the radiation zone of the furnace exposed for 88000 hours over 900 °C, carburization only occurred along the austenitic grain boundary. A pre-existing oxide scale over the internal surface in this alloy, formed in air before exposure to the carburization environment, reduced or inhibited carburization. Internal carburization was present only in areas where the oxide film was absent.

Investigations of carbon deposition on stainless steels have been done as well. Millward et al. (23) studied the influence of oxide layers on the initiation of carbon deposition on stainless steels. With a $10^2 < a_c < 10^7$, they tested two 20Cr-25Ni-Nb-stabilized austenitic steels containing either zero or 0.56 wt.% Si using $CO_2/CO/C_2H_4$ gas mixture at 550 °C. Their research confirmed that carbon filaments are not readily nucleated on chromia layers, in particular for the Si-free steel. By using Si-free and Si-bearing

versions of the alloy, neither chromia nor magnetite catalyzed carbon deposition under those test conditions. However, carbon deposits may have formed in regions covered by iron-rich oxides provided there is gas access to catalytic sites within the alloy substrate. They have postulated that these are regions of metallic nickel formed (see Figure 11) as a result of the selective oxidation of chromium and iron by the depositing gas.

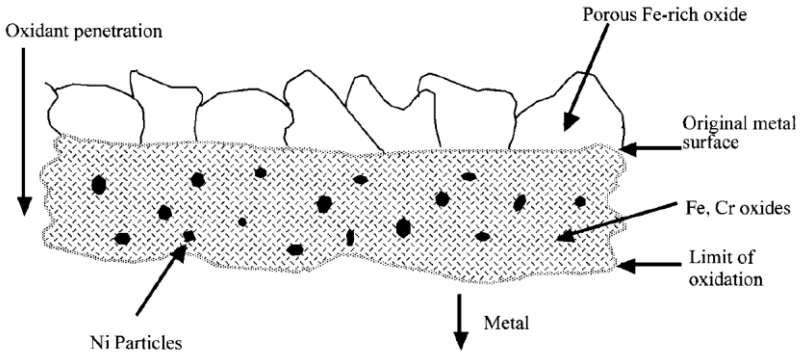

Figure 11. Schematic depth profile illustrating a suggested mode of formation of nanoparticles of Ni that can act as potential catalytic agents for producing carbon filaments[13].

1.2.7. Cyclic conditions

Investigations on HP40Nb alloys previously preoxidized and subsequently exposed to an alternating carburizing/oxidizing/carburizing atmosphere at 1000°C have concluded that a thick Cr_2O_3 layer formed on surface which partly spalled off during cooling to room temperature, in this way chromium depleted areas resulted at the surface (32). Additionally, during second exposures to the carburizing atmosphere there is more catalytic coke formation compared to the first exposure showing that, the reduction of the oxides promotes the formation of (Fe, Ni)-particles which show strong catalytic activity towards coke formation (30).

[13] Image taken from "The Influence of Oxide Layers on the Initiation of Carbon Deposition on Stainless Steel", 2001 (23).

The catalytic coke formation during thermal cracking in hydrogen rich hydrocarbon atmospheres is cause by the presence of a porous (Fe, Ni, Cr-) spinel layer at the metal surface which is formed during the oxidation step. However, severe pre-oxidation of the metallic surface followed by rapid cooling and spalling of the oxide layer causes chromium depletion. Once there is chromium depletion and there is contact with a carburizing atmosphere, formation of rich carbide decreasing the chromium concentration of the metallic matrix. Finally, repeated coking operations result in the reduction of the spinels into highly catalytic Fe and Ni particles leading to grow a catalytic surface and therefore an increasing in the coking rate (32), (33).

CHAPTER 2. METHODOLOGY

An experimental high temperature coking atmosphere was constructed and used to evaluate the effects of temperature, time and metal surface roughness on the carbon deposition of two alumina forming alloys. Furthermore, the same alloys were evaluated in one coking/de-coking cycle to compare early-stage performance and identify if oxide spallation would be observed. Coking conditions were simulated with multiple atmospheres including CO-H_2 mixtures at moderate temperatures and ethane at higher temperatures. Carbon deposition was tracked using specific mass change of the samples as a function of exposure times and conditions. Results obtained with the alumina forming alloys were compared to a baseline HP alloy. The materials were characterized using SEM and EDS to characterize the oxide layer formation, carbon deposition layers and carbon attack, and changes to base metal microstructure. Raman spectroscopy was used to characterize the carbon deposits.

2.1. Material Composition

A series of alloys were produced via centrifugal casting process and provided by MetalTek International, were received as sections of pipe. The production process used is identical to that used to produce production tubes for ethylene service. Following horizontal centrifugal casting, the cast tubes were pull-bored to machine the inner diameter. The inner diameters of the tubes were pull bored and the outer diameter was left in the as-cast condition. Three alloys were chosen for the experiments. The nominal alloy compositions are shown in Table 2. Two AFA alloys against one chromia forming are being tested. The difference between AFA alloys is the Aluminum compositions which varies for a low Al of 2.6% to a high Al of 3.7 %. Cr-Fe and Ni-Fe ratios are

relatively similar. The chromia former alloys does not have aluminum and its Cr-Fe and Ni-Fe ratios are similar to the AFA alloys.

Table 2. Nominal compositions of the alloy samples.

		Nominal Composition wt%								
	Designation	**Fe**	**Al**	**Cr**	**Ni**	**Nb**	**Si**	**Mn**	**C**	**MA additions**
H	3.7 % Al	Remainder	3.7	27	34	0.8	1.3	0.6	0.4	Ti, Zr added
L	2.6 % Al	Remainder	2.6	28	38	0.7	1.3	0.8	0.4	Ti, Zr added
C	HP-Nb	Remainder	0	27	34	0.8	1.3	0.6	0.4	Ti, Zr added

Both 3.7% Al and 2.6% Al are designed as alumina-forming austenitic alloys (AFA). The HP-Nb is a Chromia forming heat resisting alloy. For easy handling of the samples, “C” refers to the chromia forming, “H” to the 3.7% Al and “L” to the 2.6% Al AFA alloys. Change in mass was tracked during all steps of the experiments.

2.2. Sample preparation

Samples were prepared from as-cast pipe sections, cut down with an abrasive saw to pieces of roughly the same dimensions (see Figure 13). Variables “x’ and “y” represent the inner and outer diameters; “t” the thickness of the samples and “h” the height. Following this, samples were ground to 600-grit in all sides of the cut surfaces, and cleaned with hand soap followed by methanol and by acetone.

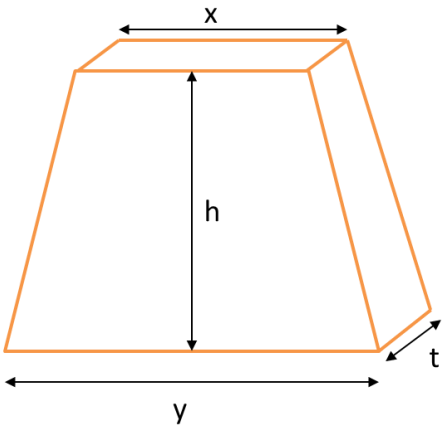

Figure 12. Notation for dimensions of samples after cutting

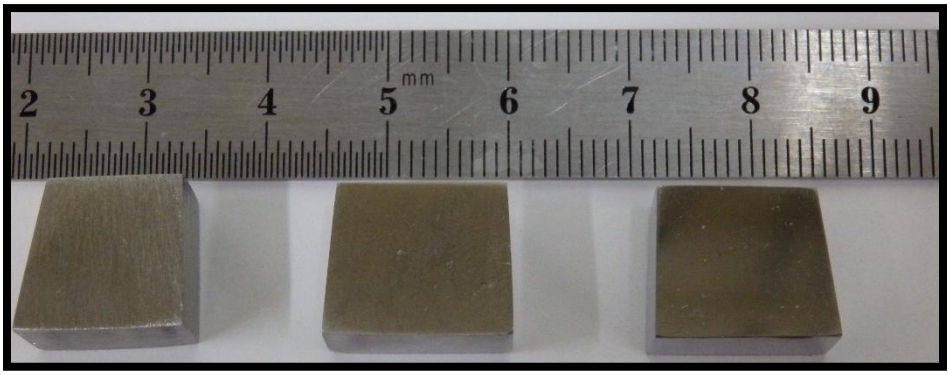

Figure 13. Some of the samples used for tests.

Prior to any test, samples were subjected to measurements. Each sample was assumed to take the generic shape of a trapezoidal prism as shown in Figure 12. Samples were ground until all sides were flat until there was no curvature from ID or OD sides. Surface area of each samples was calculated using equation (2.1).

$$SA = t\left[\left(x + y + 2 * \sqrt{h^2 + \frac{1}{4}(y - x)^2}\right) + (x + y)\right] \qquad (2.1)$$

Where SA denotes surface area; “t” is thickness, “x” and “y” are the horizontal measurements and “h” is the height of the sample, all depicted in Figure 12.

2.2.1. Influence of surface roughness

The surface roughness that the material will have depends on the grit paper used. The experiment used three different sandpapers to generate different surface finish on the samples. These are shown in Table 3.

Table 3. Surface roughness average for each grit sandpaper used.

Std. ANSI Grit	Grit Median Diameter (micron)	Surface roughness Ra (micron)
80	180	1.14
320	40.5	0.23
1200	2.5	0.02

Different samples were cut from the cast tubes, ground to 80-, 320- and 1200-grit on the surfaces, and cleaned in methanol followed by acetone. Samples were averaged 7.35 cm^2 for the CO-H_2-H_2O atmosphere and 7.90 cm^2 for the C_2H_6 atmosphere test as shown in Table 4 and Table 5. Specific dimensions for each sample can be found in APPENDIX A – DIMENSIONS OF SAMPLES.

Table 4. Surface area of samples for test of surface roughness under CO-H_2-H_2O atmosphere

Surface area (cm^2)			
	Surface roughness		
	80	320	1200
Al - 3.7%	6.67	7.57	9.47
Al - 2.6%	6.72	7.87	6.82
HP - Nb	7.86	6.63	6.55

Table 5. Surface area of samples for test of surface roughness under C_2H_6 atmosphere

Surface area (cm^2)			
Sample	Surface roughness		
	80	320	1200
Al - 3.7%	8.90	8.41	7.57
Al - 2.6%	7.05	7.28	6.76
HP - Nb	8.75	8.59	7.74

2.2.2. Influence of time and temperature under C_2H_6 atmosphere

Experiments at 850, 950 and 1050 °C were performed for 1, 6 and 24 hours each. The two AFA alloys were tested against the chromia-forming alloy under these conditions. Samples were ground to 320- grit SiC paper. Under these conditions, nine experiments were performed and the designation for the samples for each experiment are shown in Table 6.

Table 6. Designation for experiments for the evaluation of time and temperature.

	Temperature								
Time	**850**			**950**			**1050**		
1	C1	H1	L1	C4	H4	L4	C7	H7	L7
6	C2	H2	L2	C5	H5	L5	C8	H8	L8
24	C3	H3	L3	C6	H6	L6	C9	H9	L9

Samples were averaged 6.99 cm^2 in surface roughness for the C_2H_6 atmosphere test as shown in Table 7. Specific dimensions for each sample can be found in APPENDIX A – DIMENSIONS OF SAMPLES.

Table 7. Surface area of samples for test of time and temperature under C_2H_6 atmosphere

Surface roughness (cm^2)									
Time	**Temperature**								
	850			**950**			**1050**		
1	6.72	7.28	6.54	7.59	7.37	7.31	7.42	6.23	7.88
6	5.95	7.53	6.73	6.29	7.36	6.84	6.71	8.05	6.89
24	6.41	7.85	6.22	7.16	7.12	6.13	6.79	6.51	7.88

2.2.3. Cyclic conditions

Samples were ground to 320-grit on the surfaces, and cleaned in methanol followed by acetone. Experiments of pre-oxidation, coking, de-coking with air and de-coking with steam were performed. Surface area of samples were averaged 6.80 cm^2 as shown in Table 8. Specific dimensions for each sample can be found in APPENDIX A – DIMENSIONS OF SAMPLES.

Table 8. Surface area of samples for cyclic test.

Surface area (cm^2)				
Sample	1	2	3	4
	Pre-oxidation	**Coking**	**de-coking air**	**de-coking steam**
HP-Nb	6.96	7.44	7.09	7.68
3.7 % Al	6.13	7.71	6.28	7.05
2.6 % Al	6.65	6.52	6.26	5.81

"1" denotes samples that will go until pre-oxidation; "2" coking; "3" de-coking with air; and "4" until de-coking with steam step.

2.3. Pre-Oxidation test

The purpose of the pre-oxidation procedure was to develop a known and controlled distribution of oxide on the specimen surface prior to coking test. The apparatus is designed so that temperatures of up to 1000 °C can be achieved in the furnace, while steam is constantly flowed throughout the chamber. The process to obtain an environment of pure steam includes the purging of the system with nitrogen prior to switching to steam flow. It was used a small exchange furnace to produce steam allowing only steam vent through the chamber while the flow rate of steam is held at sufficient levels to there was no back flow.

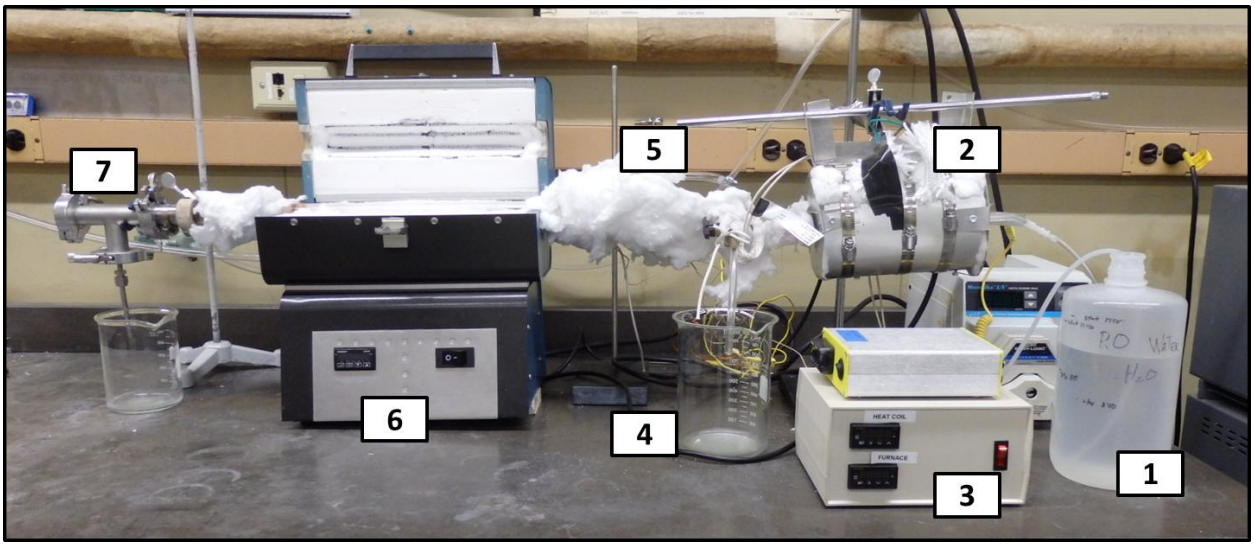

Figure 14. Oxidation Apparatus

Features of the testing setup (see Figure 14) are:

1. Peristaltic pump
2. Furnace for steam generation
3. Heating/Temperature controllers
4. Steam overflow vent during nitrogen use
5. Three-way heated inlet valve for nitrogen/steam change and three-way valve for steam to furnace/atmosphere
6. Tube furnace with quartz 1” tube, and programmable temperature controller
7. Heated steam exit vent

Steam pre-oxidation was carried out using 100% steam environment as described in Figure 15, running for 12 hours at 850°C followed by raising the temperature up to 915 °C for 1 hour.

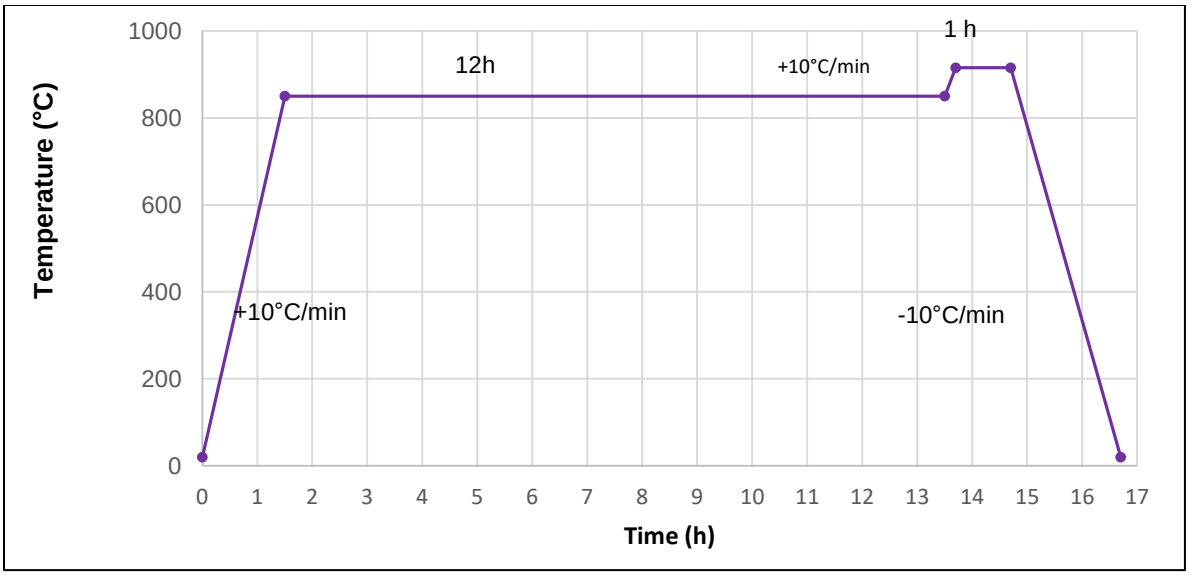

Figure 15. Thermal pre-oxidation under 100 % steam used to prepare samples prior to coking tests.

2.4. Coking test

Samples were placed in an alumina boat and set in the hot zone of the furnace. The furnace was first purged with argon for several hours and then the coking atmosphere introduced prior to heating. Heating and cooling rates were 10 °C/min. The test atmosphere was maintained with mass flow controllers at a total flow rate of 400 ml/min with a 25%CO - 25%H_2 - 49.5%Ar - 0.5% H_2O gas composition and 25%C_2H_6 - 75% Ar for the ethane tests. The CO and C_2H_6 gas flow was introduced at the temperature of test, during heating and cooling rates only Argon was flowed.

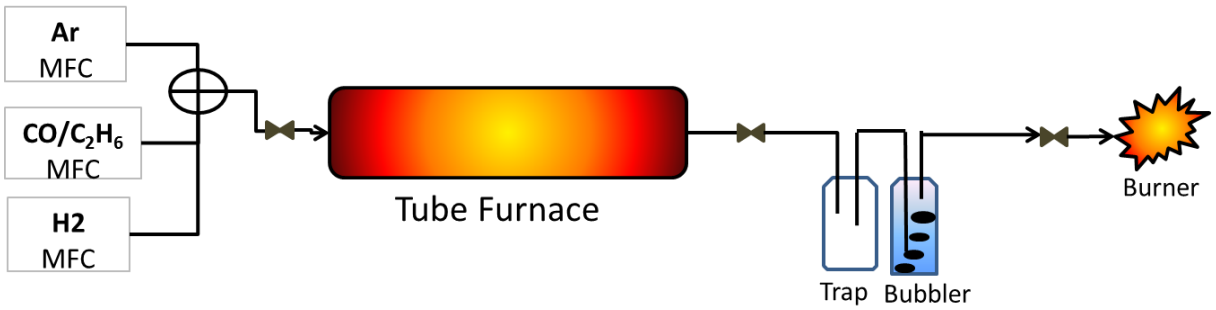

Figure 16. Scheme of the coking furnace used.
MFC: Mass flow controller

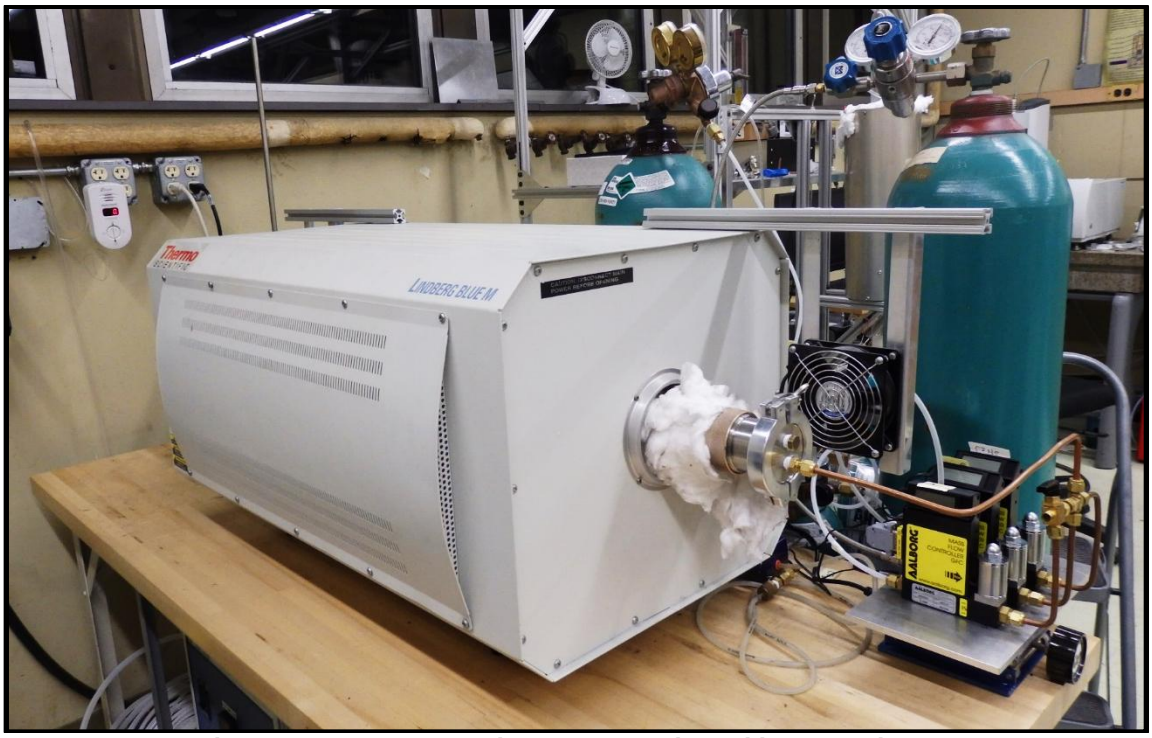

Figure 17. Furnace used to carry out the coking experiment.

2.4.1. Influence of surface roughness and atmosphere

Samples with no pre-oxidation treatment were placed in the hot zone of the furnace following the profile temperature depicted in Figure 18. The first test gas atmosphere was 25% CO, 25% H_2, 49.5% Ar, 0.5% H_2O. These conditions created a total carbon activity of approximately 19.7 and a P_{O2} of 10^{-26} atm at the 600°C hold temperature for the 169 hour hold time. The second test atmosphere was 25% C_2H_6, 75% Ar at 850°C for 100 hours.

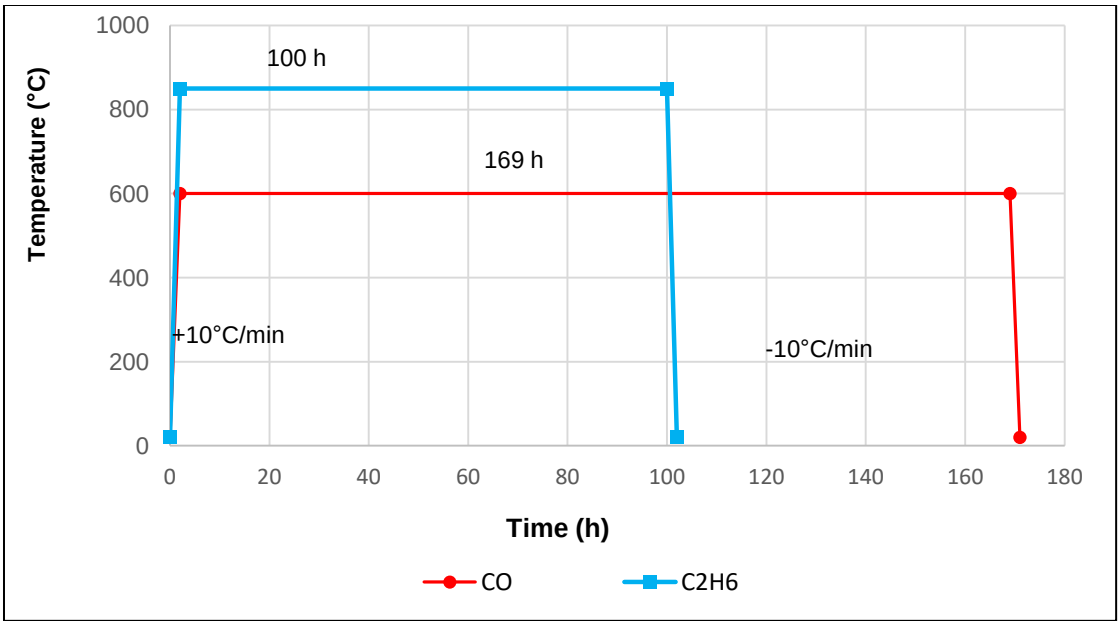

Figure 18: Coking profile temperature carried out. The time at the peak temperature (600 °C) was 169 h with CO/CO_2 atmosphere; for C_2H_6 atmosphere the time at the peak temperature (850 °C) was 100 h.

2.4.2. Influence of time and temperature under C_2H_6 atmosphere

Experiments at 850, 950 and 1050 °C were performed for 1, 6 and 24 hours each under 25% C_2H_6-75% Ar atmosphere. The design of experiments is shown in Figure 19. Two AFA ("H" as a 3.7% Al and "L" as a 2.6% Al) alloys were tested against the chromia-forming alloy ("C" as a HP-Nb) under these conditions.

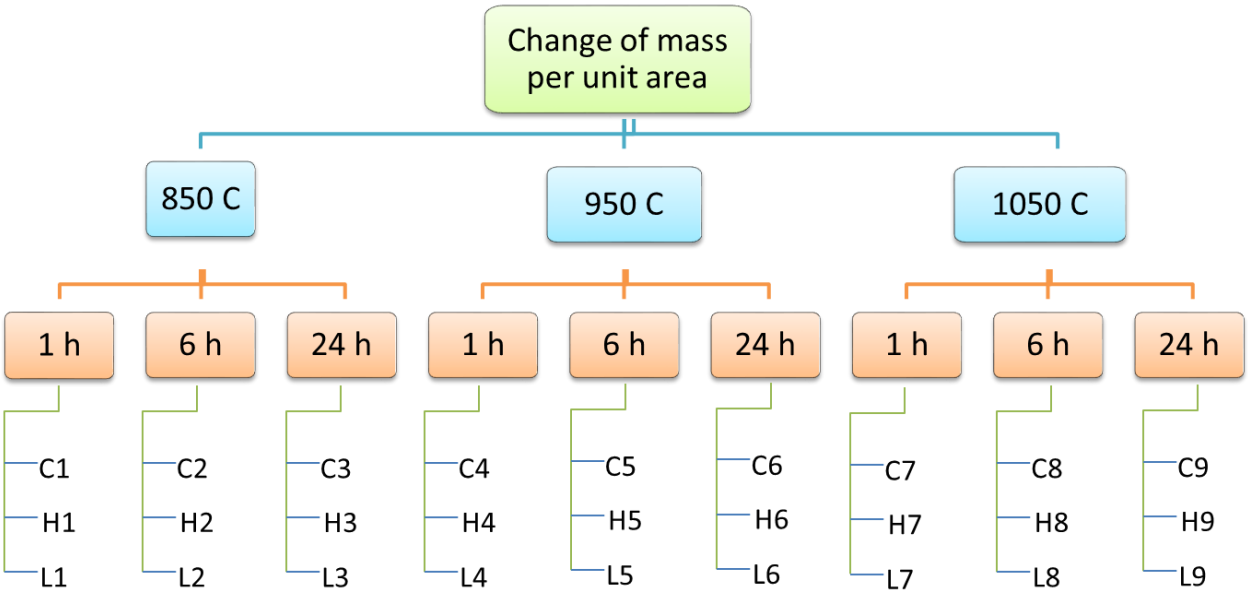

Figure 19. Design of experiments for the evaluation of temperature and time under C_2H_6 gas atmosphere

2.5. Cyclic conditions

Steam pre-oxidation was carried out using 100% steam environment as described in Figure 15, running for 12 hours at 850°C followed by raising the temperature up to 915 °C for 1 hour. Coking test was performed with an atmosphere of 25% C2H6, 75% Ar gas composition at 1050°C. Samples pre-oxidized with steam were exposed to this condition for one continuous run for 6 hours. De-coking with air was performed at 1050 °C for 15 min followed by continued de-coking with 100% steam at 915 °C for 1 hour. Heating and cooling rates for each stage in the cycle was 10 °C/min.

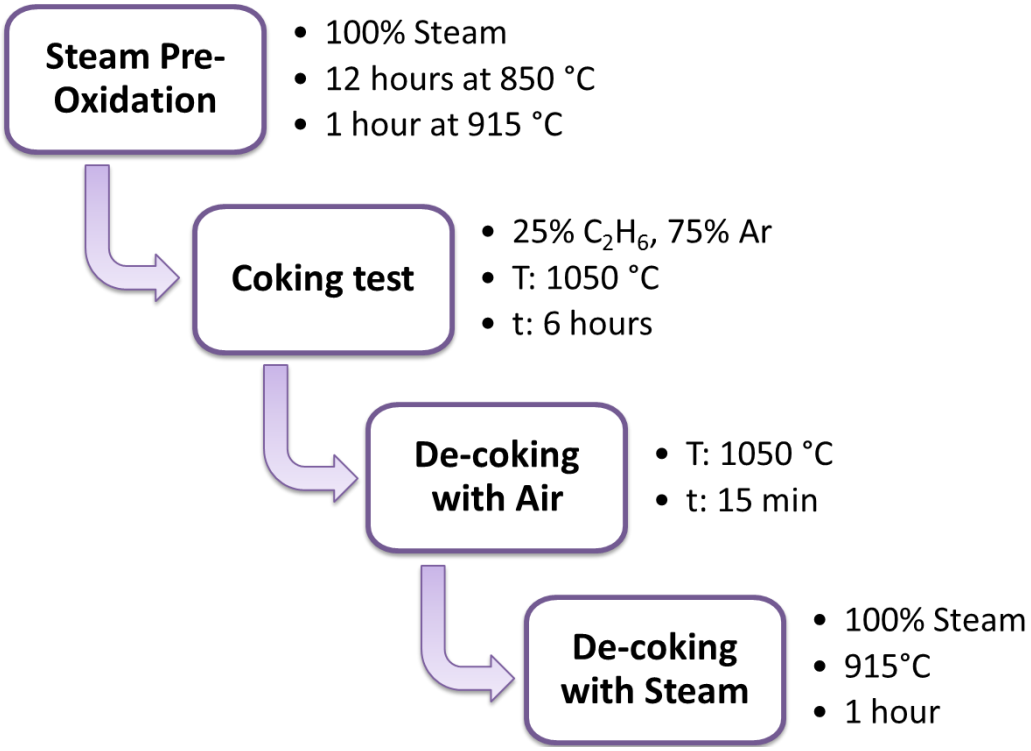

Figure 20. Experimental procedure carried out for cyclic conditions

2.6. Characterization

Samples for metallographic and scanning electron microscopy (SEM) analysis were sectioned with a water-cooled diamond saw, mounted in bakelite, and prepared using common metallographic techniques. Microstructural analysis was performed using light microscopy, SEM, and energy dispersive spectroscopy (EDS). Raman Spectroscopy was used to characterize the carbon deposits on each alloy formed during the coking tests.

2.6.1. Change in mass

Mass measurements before and after exposure were made with a 0.01 mg resolution analytical balance.

For coking experiments, samples including the crucible were weighed before and after exposure to the carbon atmosphere so the carbon deposited on samples that would fell off on crucible would be measure as well. An empty crucible was also introduced in the furnace for each test, so the carbon gained for the crucible could be subtracted from the total change in mass. Changes in mass were calculated using (2.2).

$$\Delta m = m_{final} - m_{initial} - \Delta m_{crucible} \quad (2.2)$$

Where:

$$m_{final} = m_{sample} + m_{crucible}\ (after\ exposure)$$

$$m_{initial} = m_{sample} + m_{crucible}\ (after\ exposure)$$

$$\Delta m_{crucible} = m_{crucible,final} - m_{crucible,initial}$$

2.6.2. Scanning Electron Microscopy (SEM)

High magnification images of developed oxide layers were taken with a JEOL scanning electron microscope in order to determine the continuity of the oxide layer, carbon layer or internal damage. Images were taken using an accelerating voltage of 15 keV.

2.6.3. Energy Dispersive Spectroscopy (EDS)

In order to identify elemental composition of oxide layers formed, a EDS was used. Each EDS scan was to track elemental data for the elements Fe, Cr, Ni, al, O and C as this allowed for interpretation of the beginning of the oxide layer, carbon layer, any elemental mixtures, and the base metal.

2.6.4. Raman Spectroscopy

Samples were analyzed on the ID using a Renishaw 1000 Micro Raman spectroscope in order to characterize the carbon deposits on each alloy formed during the coking

tests. A laser of 633 nm, grating of 1800 l/mm, and a focal lens of 50X was used in the collection of peak data.

CHAPTER 3. RESULTS

An experimental high temperature coking atmosphere was constructed and used to evaluate the effects of temperature, time and metal surface roughness on the carbon deposition of two alumina forming alloys. Furthermore, the same alloys were evaluated in one coking/de-coking cycle to compare early-stage performance and identify if oxide spallation would be observed. Coking conditions were simulated with multiple atmospheres including CO-H_2 mixtures at moderate temperatures and ethane at higher temperatures. Carbon deposition was tracked using specific mass change of the samples as a function of exposure times and conditions. Results obtained with the alumina forming alloys were compared to a baseline HP alloy. The materials were characterized using SEM and EDS to characterize the oxide layer formation, carbon deposition layers and carbon attack, and changes to base metal microstructure. Raman spectroscopy was used to characterize the carbon deposits.

3.1. Influence of surface roughness and gas atmosphere

Samples with no oxidation treatment were exposed to two atmospheres; to a CO-H_2-H_2O atmosphere for 169 h at 600 °C and to a C_2H_6 atmosphere for 100 h at 850 °C. Samples were exposed directly to the carbon atmosphere so the environment conditions are more aggressive to the material than when is already pre-oxidized. Depletion of chromium, developing of oxide scale, formation of intermetallic or internal damage as well as coke layer is described if there is any.

3.1.1. Carbon deposition in CO-H_2-H_2O atmosphere

Samples of average 7.35 cm^2 in surface area were exposed to a carbon-rich coking atmosphere of 25% CO, 25%H_2, 49.5% Ar, 0.5% H_2O gas composition. Samples prior to coking test are shown in Figure 21. These conditions created a P_{O2} of 10^{-26} atm at the 600°C hold temperature for 169 hours and a total carbon activity of approximately 19.7.

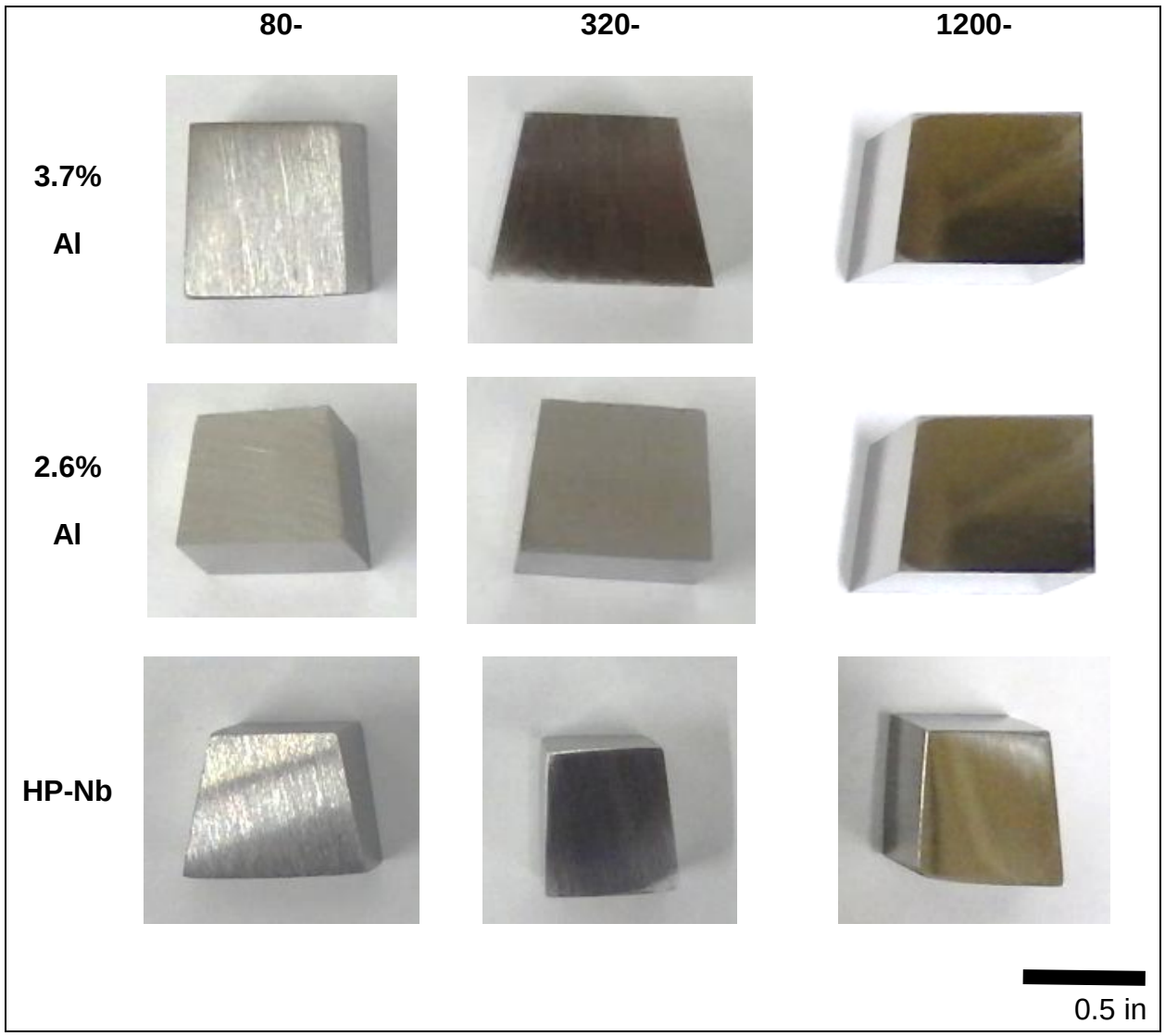

Figure 21. Samples prior to coking test of CO-CO_2-H_2O atmosphere

Mass change for each material as a function of surface roughness was tracked. Samples had not evident carbon deposition on their surfaces as shown in Figure 23. Respect to the changes in mass, shown in Figure 22, there was not clear effect of the surface roughness on the mass change of alloys in this exposure condition. This may indicate that the atmosphere was not aggressive enough to generate a significant mass of change.

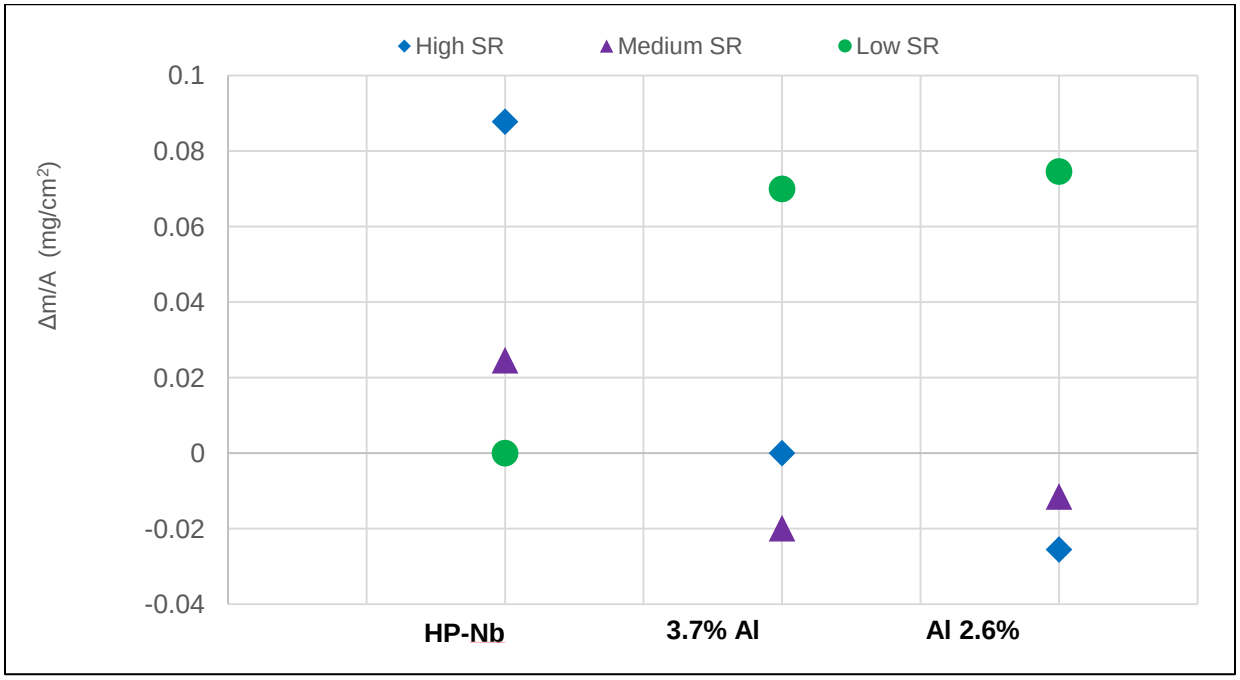

Figure 22. Mass difference per surface area of samples after exposure to CO/H_2 for 169h at 600°C.
SR: Surface Roughness. Note that High SR (1.14 μm) denotes samples polished with 80-grit, Medium SR (0.23 μm) with 320-grit and Low SR (0.02 μm) with 1200-grit sandpaper

The surfaces of the samples ground to 1200-grit were observed by SEM as shown in Figure 25. Presence of some particles of carbon onto the surface of the three alloys was found. Isolated surface features were identified as oxides and sometimes carbides containing elements such as Al, Cr, Nb and Si.

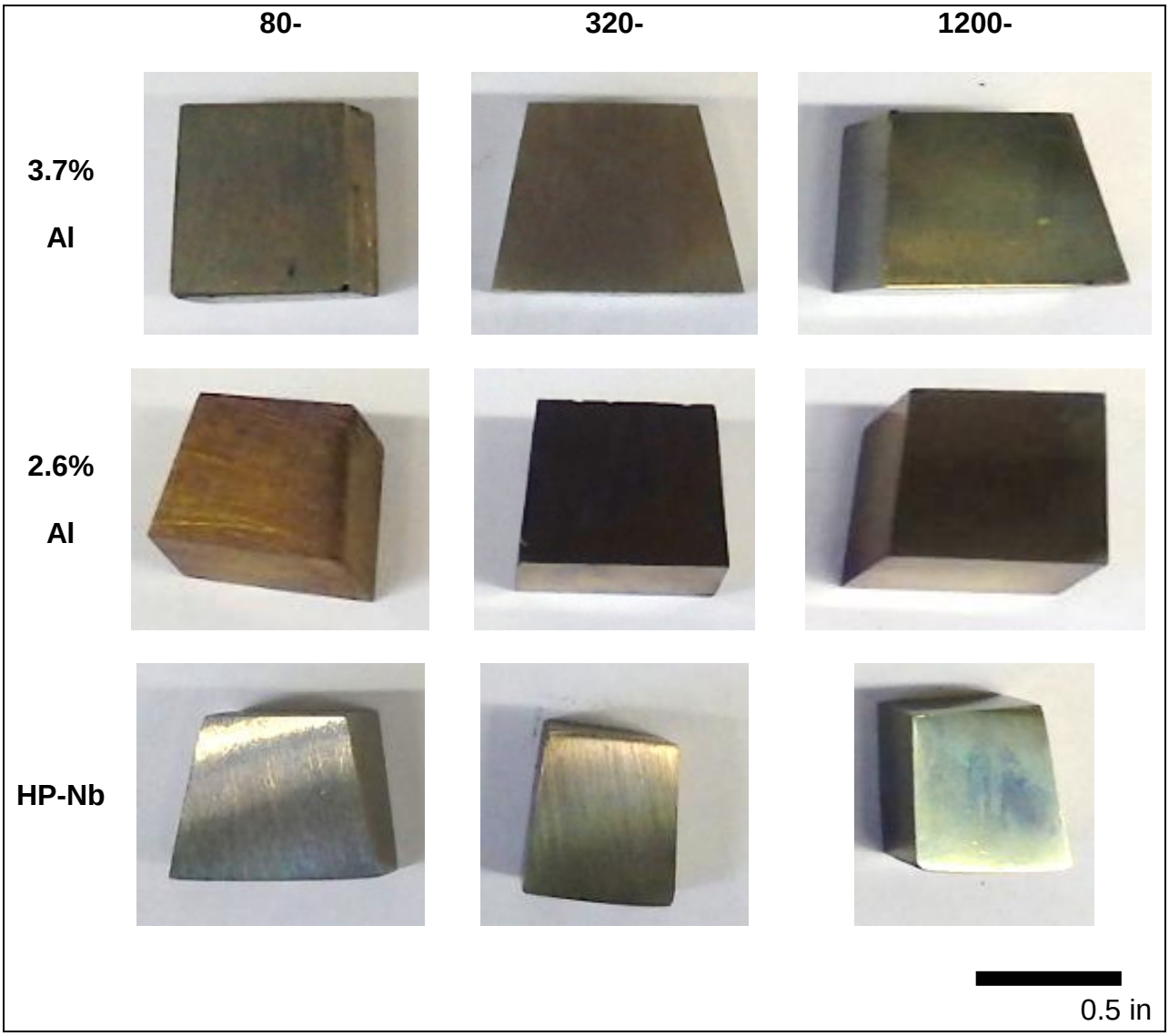

Figure 23. Samples after coking with CO CO-CO_2-H_2O at 600 °C for 169 h.

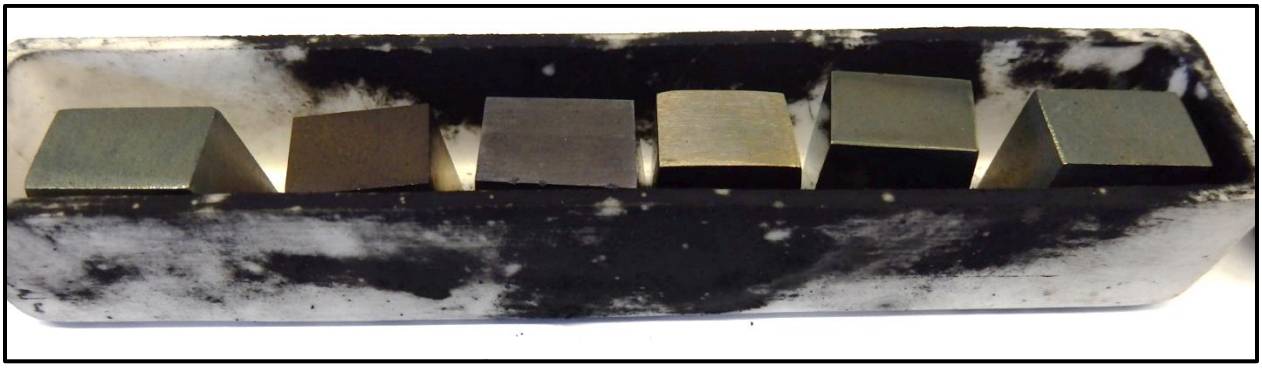

Figure 24. Photo of the crucible with samples after coking with CO CO-CO_2-H_2O at 600 °C for 169 h

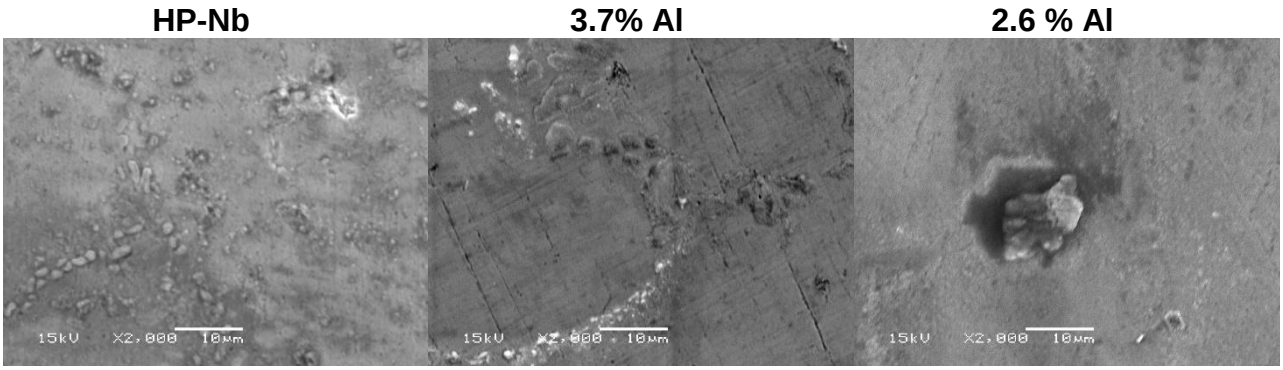

Figure 25.SEM Images at 2000x of the surface after exposition to CO/CO2 atmosphere at 600°C for 169 hours.

Thin oxide layers were observed with SEM after cross-sectioning as shown in Figure 26. The alumina forming alloys had a thin (<0.5 µm thickness), well-formed oxide layers that were identified as mainly Al and O via EDS analysis. No presence of an oxide layer in the chromia-former alloy was observed. Regions of spalling or significant internal attack were not observed.

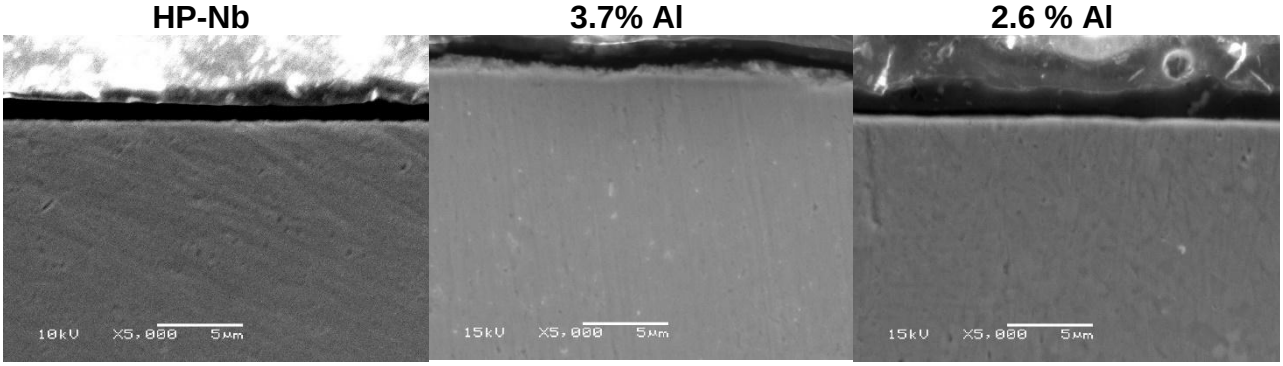

Figure 26: SEM cross-sections images at 5000x of samples after exposition to CO/CO_2 atmosphere at 600°C for 169 hours.

3.1.2. Carbon deposition in C_2H_6/Ar atmosphere

Samples were exposed to a carbon-rich coking atmosphere of 25% C_2H_6, 75% Ar gas composition at 850°C for 100 hours. Mass change for each material as a function of surface roughness was tracked. Carbon deposition was evident after the removal of the samples from the furnaces (see Figure 28).

Raman spectroscopy was performed on the carbon deposits (see Figure 27) and indicated that the carbon formed during the test was carbon black, results are shown in Figure 30.

Figure 27. Carbon deposited during C_2H_6 atmosphere at 850 C for 100 hours

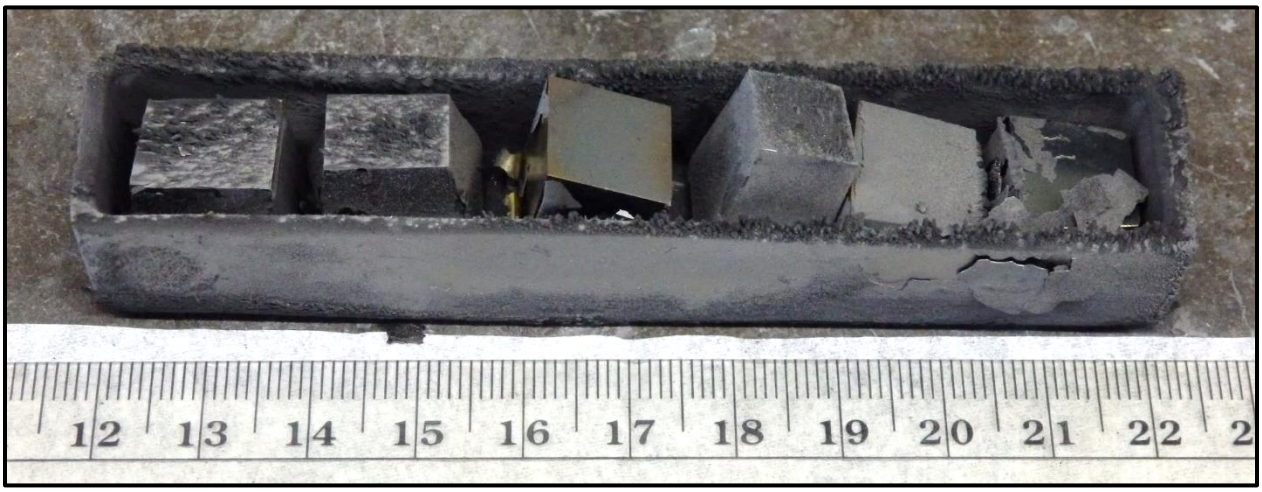

Figure 28. Photo of the crucible with some of the samples after coking with C_2H_6 at 850 C for 100 hours.

Coke deposited onto the surface was different for each material. The carbon deposited on the AFA alloys fell off easily after handling or moving the sample while the carbon deposited on the HP-Nb alloy, stayed there and even after trying to remove it, remained on surface. This indicates that the adhesion of the carbon to the surface of the material it may depend on the surface, in this case, the oxide layer that is formed on the surface

of the material. It is well known that diffusion of carbon is lower in Alumina than in Chromia.

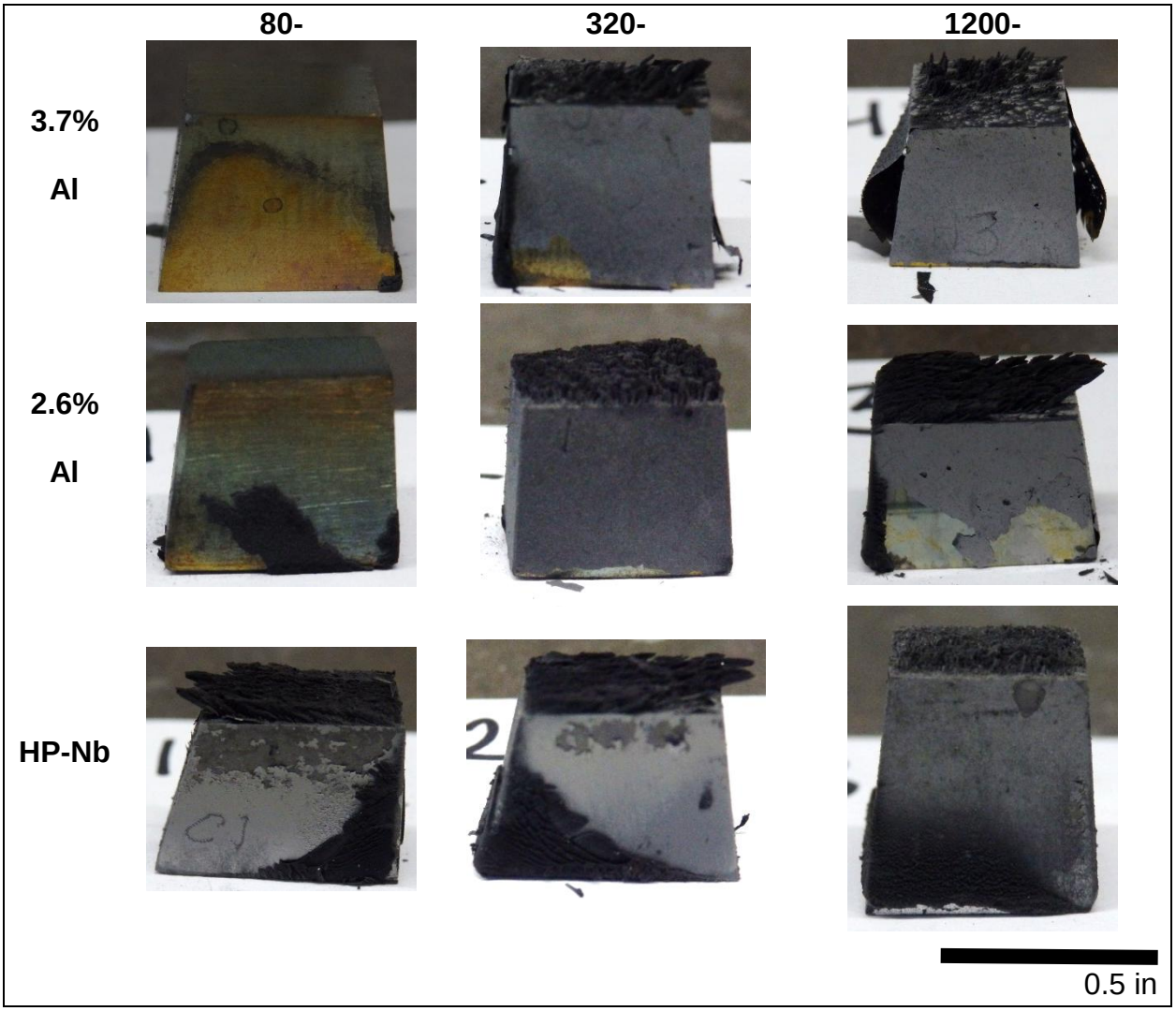

Figure 29. Samples after coking with C_2H_6 at 850 C for 100 hours.

There is a clear gain in mass which corresponds to the carbon deposition on surface of each sample. These mass changes were higher compared to those of CO/H_2 atmosphere test. While the overall magnitude of mass change was more significant, there was still no clear trend relating surface roughness and change in mass (see Figure 31).

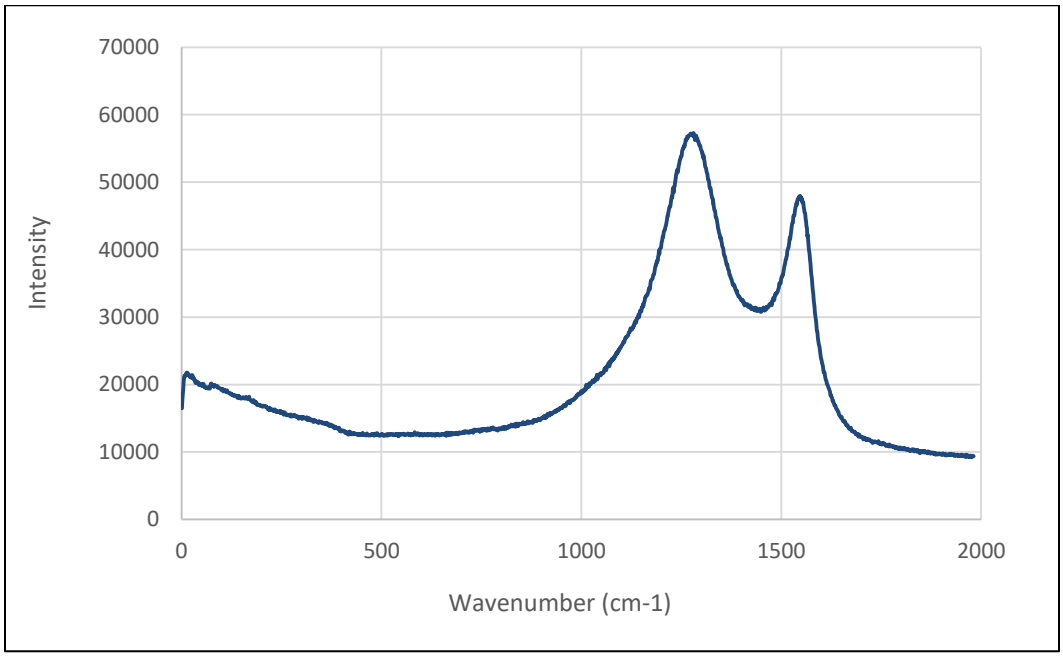

Figure 30. Results of Raman Spectroscopy performed on the carbon deposits.

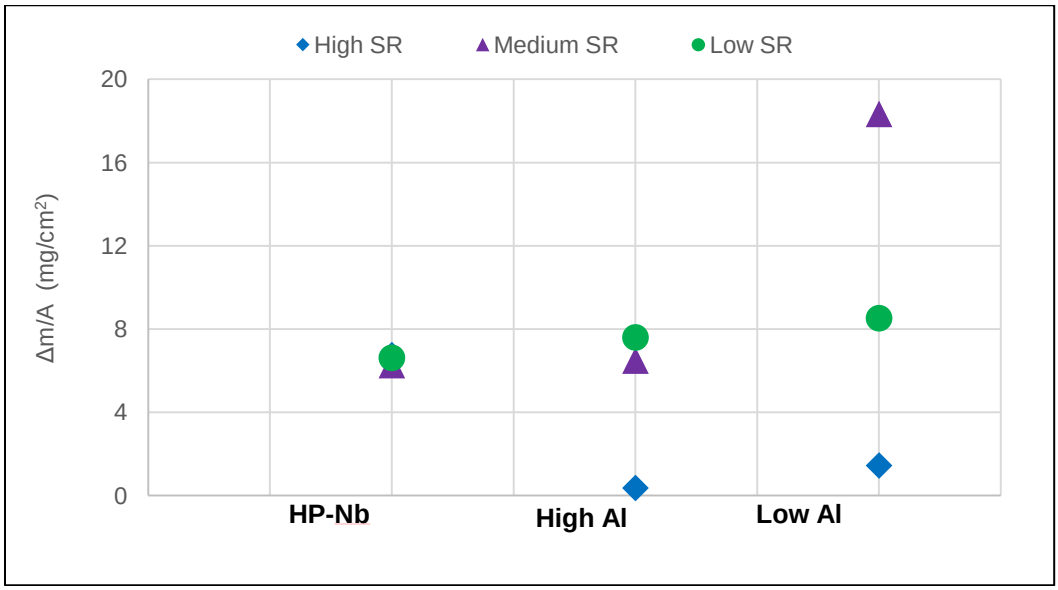

Figure 31. Mass difference per surface area of samples after exposure to C2H6 for 100h at 850 °C.

SR: Surface Roughness. Note that High SR (1.14 μm) denotes samples polished with 80-grit, Medium SR (0.23 μm) with 320-grit and Low SR (0.02 μm) with 1200-grit sandpaper.

The surfaces of the samples ground to 1200-grit were observed by SEM as shown in Figure 32. Presence of carbon on the surface was noticeable across all three samples.

Surface EDS scans showed only the deposits of carbon with no other elements observed.

Carbon deposited on the 3.7% Al alumina-former alloy fell from the sample upon removal of the sample from the furnace in spite of gentle handling. The surface image for that sample in Figure 32 corresponds to the surface of the sample without the carbon deposits. A more detailed EDS analysis of locations on the 3.7% Al sample is shown in Figure 33.

Presence of aluminum, chromium and oxygen as well as carbon deposits are found on surface of the 3.7 % Al. A formation of a thin alumina scale is expected followed by a thin chromia scale on surface. Regions of chromium oxide are found on surface indicating that the alumina scale is not uniform across the sample.

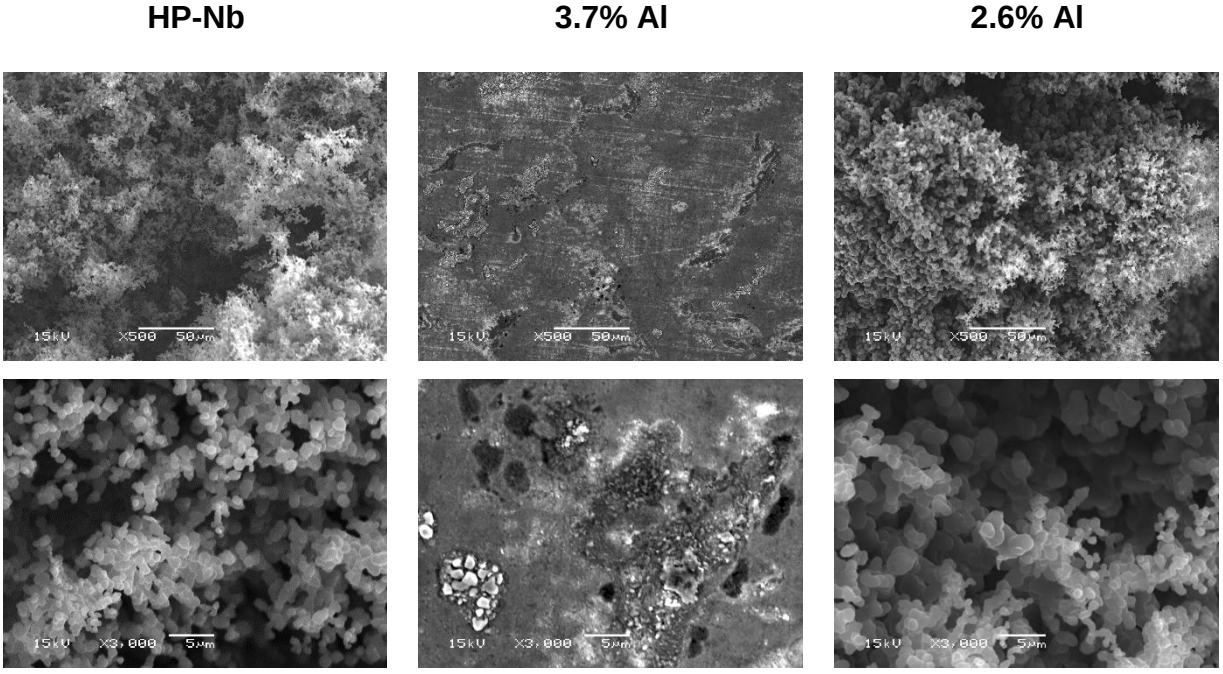

Figure 32: SEM images of the surface of samples after exposure to C_2H_6/Ar atmosphere at 850 °C for 100 hours.
Carbon deposits of the 3.7% Al sample came out during handling.

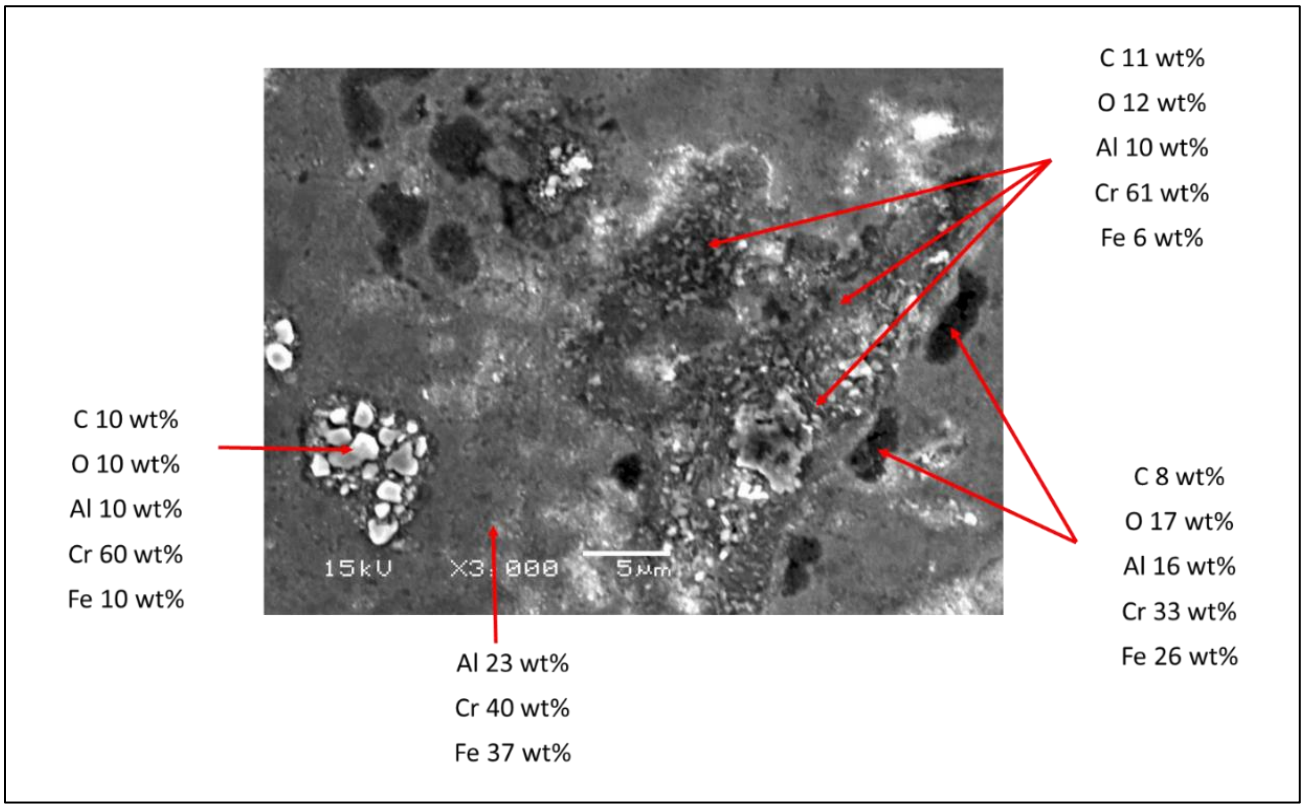

Figure 33. SEM image of the surface at 3000x of 3.7%Al alloy with EDS results.

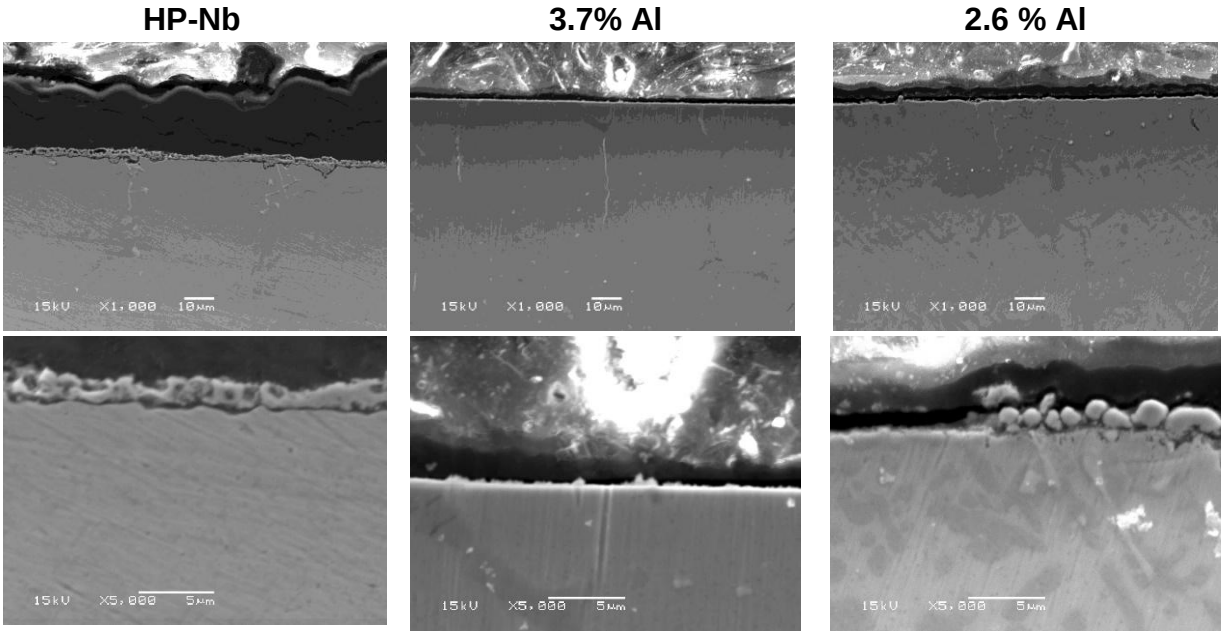

Figure 34: SEM cross-sections of samples after exposure to C_2H_6/Ar atmosphere at 850 °C for 100 hours.

Cross-sections images of the three alloys are shown in Figure 34. Coke layer of ~20 µm followed by a chromia layer on the HP-Nb alloy with a uniform ~2.5 µm thickness was found across all the sample. The presence of Cr and O in the HP-Nb scale was determined by EDS analysis (see Figure 35).

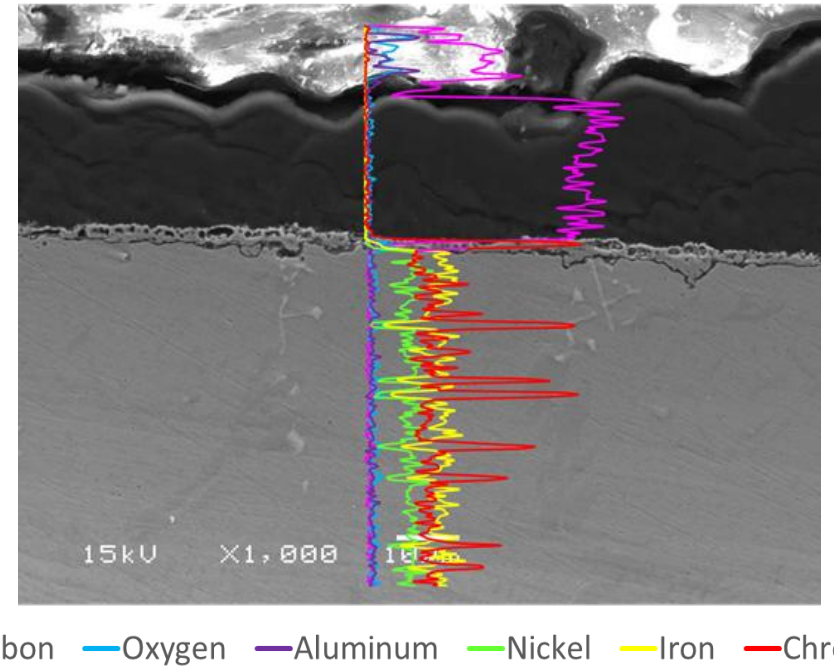

Figure 35. EDS linescan of cross section of HP-Nb alloy exposed to C_2H_6/Ar atmosphere at 850 °C for 100 hours.

Nodules of ~1.4 µm thickness of Cr were found in the 2.6% Al alloy. Similar nodules were observed sporadically at several locations on the sample but their presence was not uniform. Additionally, formation of an intermetallic phase near the surface in the 2.6% Al alloy were found. It has been reported that the formation of this intermetallic corresponds to FeNiAl precipitates that act as Al reservoir to maintain alumina (1). A uniform thin layer of alumina was found on the 3.7% Al sample. EDS analysis indicated only Al and O were present in the oxide scale. It is also seen that chromium oxide is underneath this alumina scale (see Figure 36).

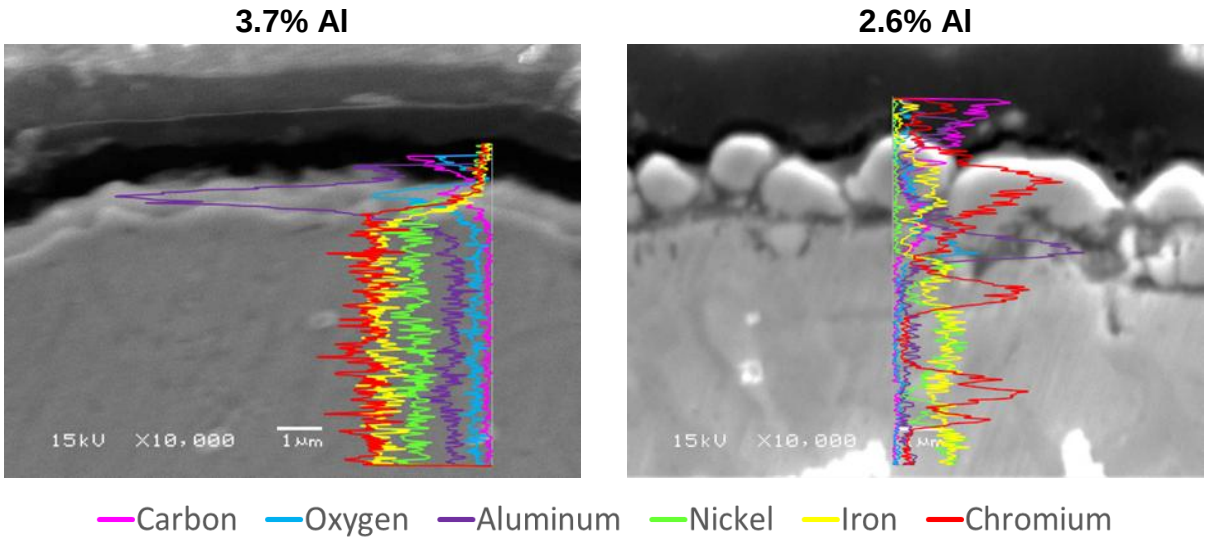

Figure 36. EDS linescan of cross section of 3.7%Al and 2.6%Al AFA alloys exposed to C_2H_6/Ar atmosphere at 850 °C for 100 hours.

3.1.3. Summary

- Alloys were exposed to $CO/CO_2/H_2O/H_2/Ar$ and to C_2H_6 atmosphere. Exposure to $CO/CO_2/H_2O/H_2/Ar$ atmosphere at 600 °C showed no damage to the alloys and formation of a thin (<0.5µm thick) oxide layer after exposure. Exposure to C_2H_6 atmosphere at 850 °C, alloys showed carbon deposition onto the surface of materials, and formation of a thick oxide layer (~1.5 µm) in the 2.6% Al and HP-Nb alloys.
- There is not a clear trend relating surface roughness and mass changes as well carbon deposition.
- Ethane atmosphere was more aggressive to the alloys compared to the CO atmospheres. A higher carbon activity can be achieved by using ethane as a coking atmosphere and allows a higher temperature to work with.

3.2. Influence of time and temperature under C_2H_6 atmosphere

Samples with pre-oxidation treatment were exposed to 850, 950 and 1050 °C for 1, 6 and 24 hours for each temperature, under 25%C_2H_6 - 75%Ar atmosphere. The design of experiments was shown in Figure 19. The study of the influence of time and temperature on the change in mass, oxide layer formation and internal damage for two alumina-forming alloys against a chromia-forming alloy, is described.

3.2.1. Pre-oxidation treatment

All of the samples that were exposed to coking conditions were pre-oxidized first. Industrial practice includes a pre-oxidation stage in steam at similar temperatures for newly installed tubes. Therefore, a known and controlled distribution of oxide on the specimen surface could be obtained prior to coking test. Oxidation was done in 100% steam at 850 °C for 12 hours and then 915 °C for 1 hour as described in Figure 15.

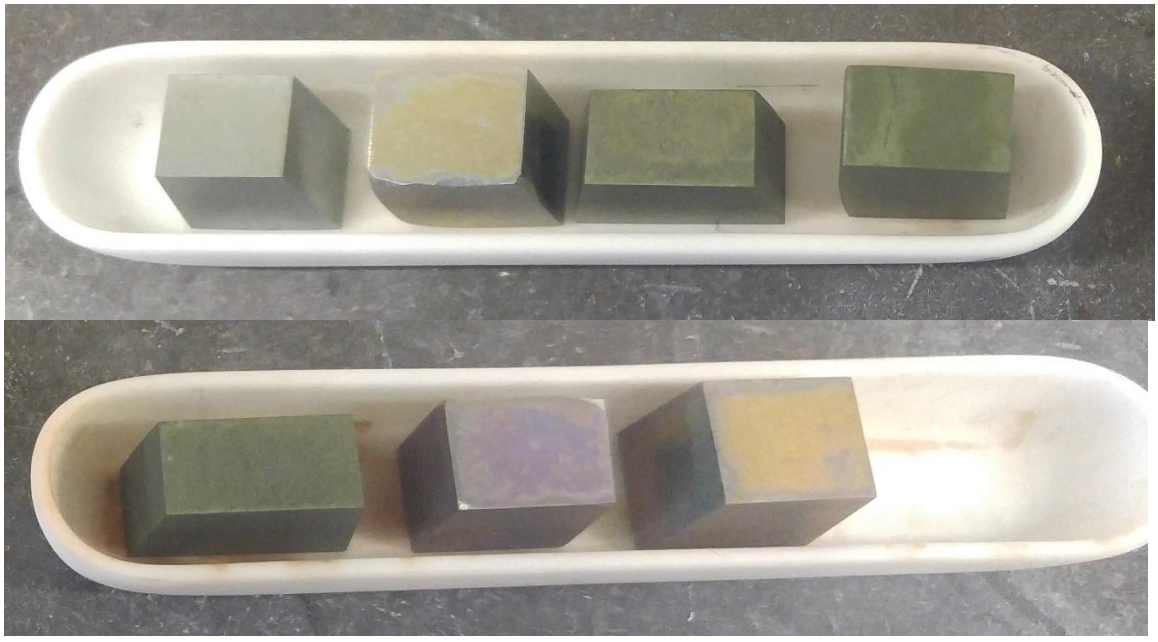

Figure 37. Samples after pre-oxidation treatment

A total of nine samples per material were pre-oxidized. HP-Nb alloys had a green-like color on surfaces after oxidation while AFA alloys had between yellow- and purple-like color on its surfaces. The change in mass was tracked and the average of it was obtained (see Figure 38 and Table 9). Standard deviation and standard error was calculated so an estimate of which material has the highest change in mass could be obtained. It is expected that a bigger change in mass represent a thick oxide layer on surface and therefore, better coking resistance.

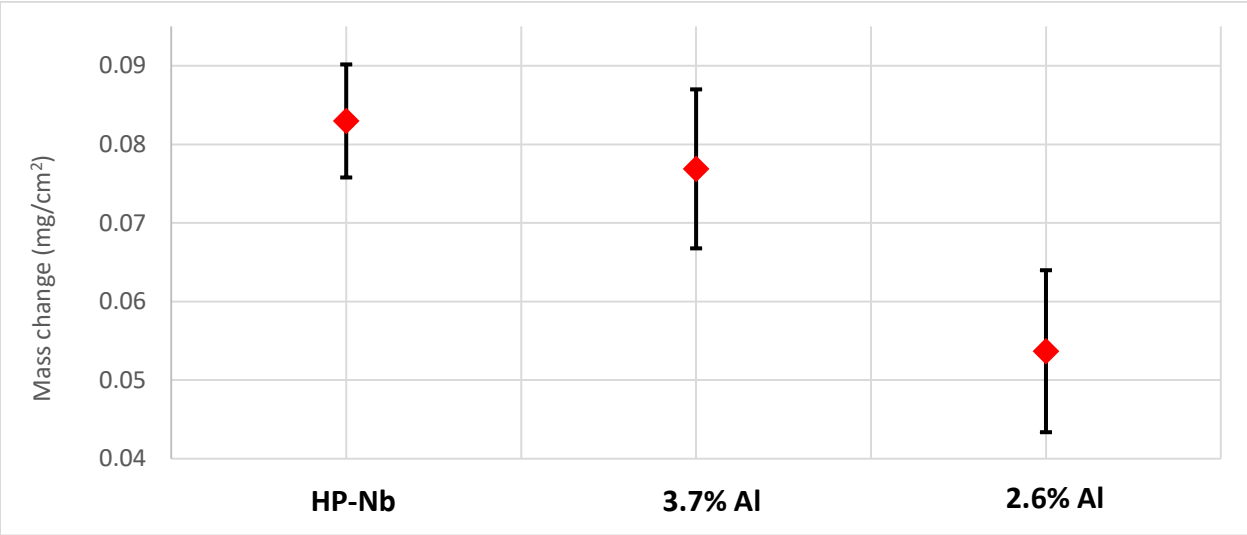

Figure 38. Average of change in mass after pre-oxidation treatment

Table 9. Average of change in mass after pre-oxidation treatment.

Material	Average	Standard deviation
HP-Nb	0.0830	0.022
3.7% Al	0.0769	0.030
2.6% Al	0.0537	0.031

Based on Figure 38, the HP-Nb alloy had the highest change in mass after oxidation treatment. This indicates the formation of a chromia layer is expected across all surface. In case of the AFA alloys, the change in mass should reflect a developed thin alumina

scale followed by a thin chromia scale underneath. Highest aluminum content in the alloy leads to a thicker alumina scale and therefore, better coking resistance is expected.

3.2.2. Influence of time and temperature

Samples with pre-oxidation treatment were exposed to an atmosphere of 25% C_2H_6 - 75% Ar for 1, 6 and 24 hours at 850, 950 and 1050 °C. The change in mass was tracked so a trend could be obtained for each of the materials (see Table 10). Based on Figure 39, the change in mass for each alloy based on time is described. The mass measurement was done including the sample and the crucible weight. Then, the change in mass was obtained before and after test, as is described in the methodology using equation (2.2). The carbon gained by the crucible, was subtracted of the total change in mass.

Table 10. Change in mass per sample for different times and temperatures of exposure.

		Coking - Oxidation Mass difference per area (mg/cm^2)		
		Temperature (°C)		
Material	**Time (h)**	**850**	**950**	**1050**
HP-Nb	1	0.1280	0.1568	1.0221
	6	0.9660	0.7933	6.1068
	24	21.8416	11.4531	24.7577
3.7 Al	1	0.1882	0.2728	1.3068
	6	1.1829	1.1655	4.8068
	24	26.9620	17.3275	36.7757
2.6 Al	1	0.7021	0.4498	1.6569
	6	0.9192	2.0194	6.7320
	24	48.8897	48.0140	33.1679

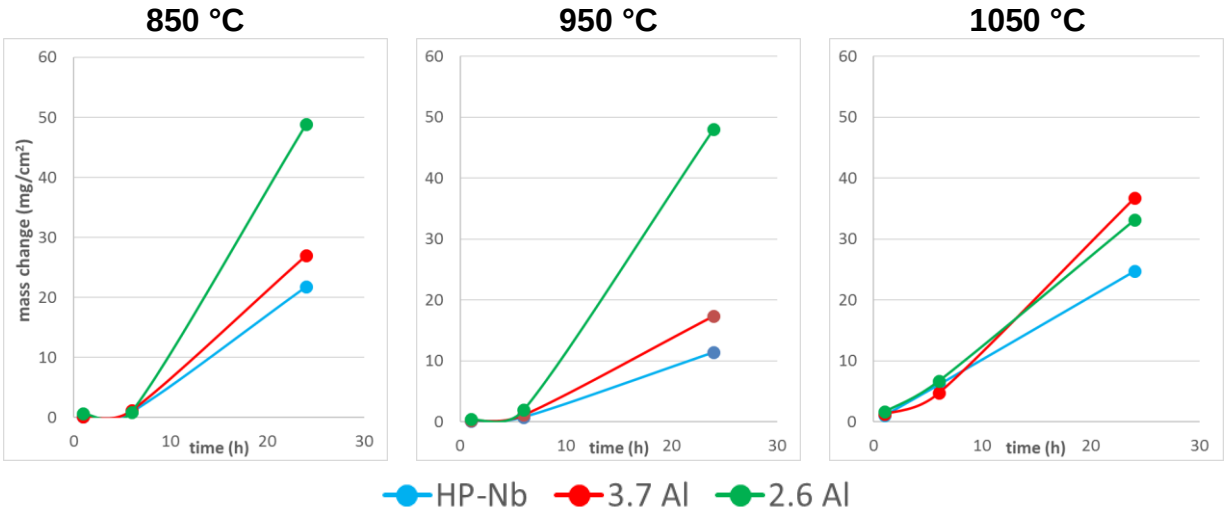

Figure 39. Change in mass of samples after exposure to C_2H_6 for 1, 6 and 24 hours at 850, 950 and 1050 °C at each temperature.

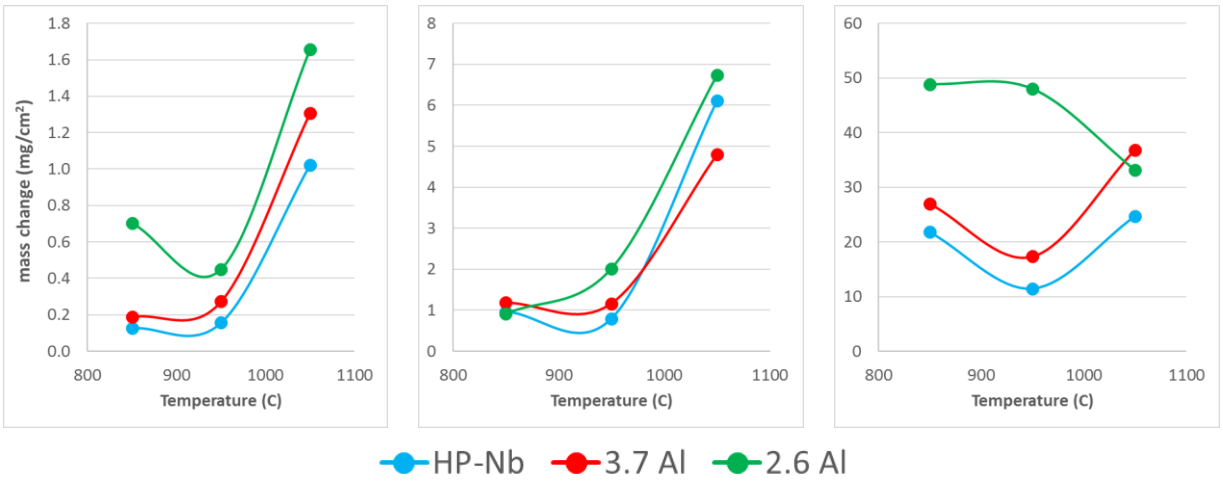

Figure 40. Change in mass of samples after exposition to C2H6 for 1, 6 and 24 hours at 850, 950 and 1050 °C.

Analyzing the effect of temperature on the change in mass, based on Figure 40, the 2.6% Al had the highest gain in mass for all three times at different temperature. The 3.7% AFA alloy, seems to be the more resistant at 850 and 950 °C since formation of intermetallic compounds or oxide spallation is not visible. However, at 1050 °C, the chromia layer formed in the AFA alloys started to deplete and internal damage is seen.

For the 2.6% Al, formation of intermetallic is clear at 950 °C and 1050 °C for 24 hours each. Oxide spallation of the chromia scale is noticeable as well in the 2.6% Al alloy. It is also possible to predict that there is change in mechanism at 1050 °C for 24 hours for this alloy since the material starts to loss mass.

The HP-Nb alloy, the chromia former, was the alloy that had less gain in mass compared to the Alumina alloys. However, it is noticeable that the carbon deposited on surface of the alloys is different for the Chromia-former compared to the AFA alloys. As shown in Figure 41, the HP-Nb alloy has a “gray” color across all surface while the AFA alloys, its carbon fell off due to handling and the color of the alloy after oxidation treatment remained same.

The influence of time on the coking resistance for these alloys shows that in general, longer exposure times represent bigger gain in mass. In terms of the oxide layer and cross section SEM pictures, longer times show more damage to the materials especially at 1050 °C.

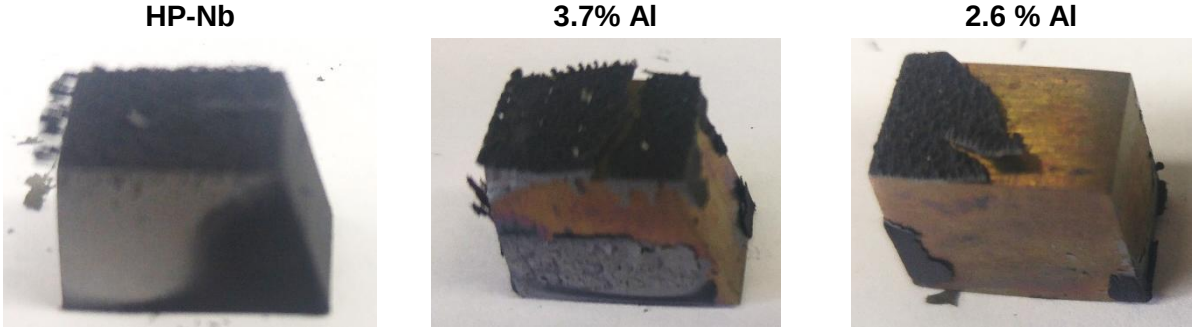

Figure 41. Samples after exposure to C_2H_6 for 24 h at 850 °C.

SEM cross sections of the samples for the different times of exposure are shown in Figure 42, Figure 43 and Figure 44. Additional SEM images of samples, can be found in APPENDIX C – SEM OF INFLUENCE OF TIME AND TEMPERATURE

Respect to the carbon layer, it is possible to see the increment on the thickness of the coke layer especially for alloys at 850 °C.

The AFA alloys (3.7%Al and 2.6% Al) show no internal damage or depletion of the oxide scale at 850 and 950 °C. At 1050 °C, these alloys start to show formation of intermetallic, depletion of chromia layer and internal damage indicating that at this temperature, these alloys are not appropriate. HP-Nb alloy at 950 and 1050 °C, especially for the longest time show on its cross section the depletion of the chromia scale along with internal damage, indicating that this alloy may not be suitable for temperatures above ~850°C in presence of carbon.

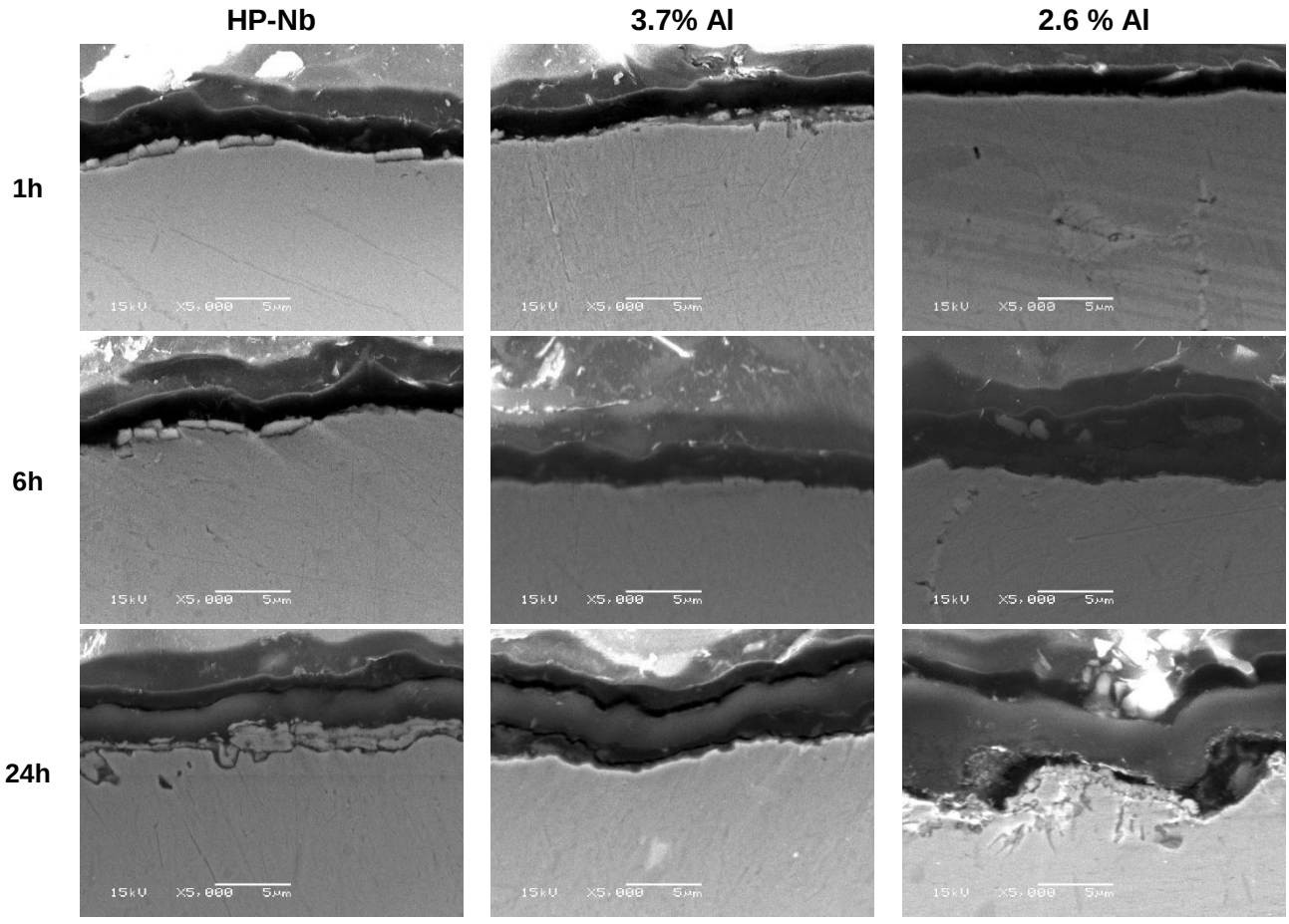

Figure 42. SEM cross section of samples after exposure to C_2H_6 at 850 °C

At 850 °C, the HP-Nb alloy oxide spallation starts to appear at 24 h test, the carbon layer and the oxide layer is noticeable. At 950 °C, for 24 hours the internal damage is bigger compared to the 850 °C and for 1050 °C that, even for 6 hours, the alloy started to show oxide spallation.

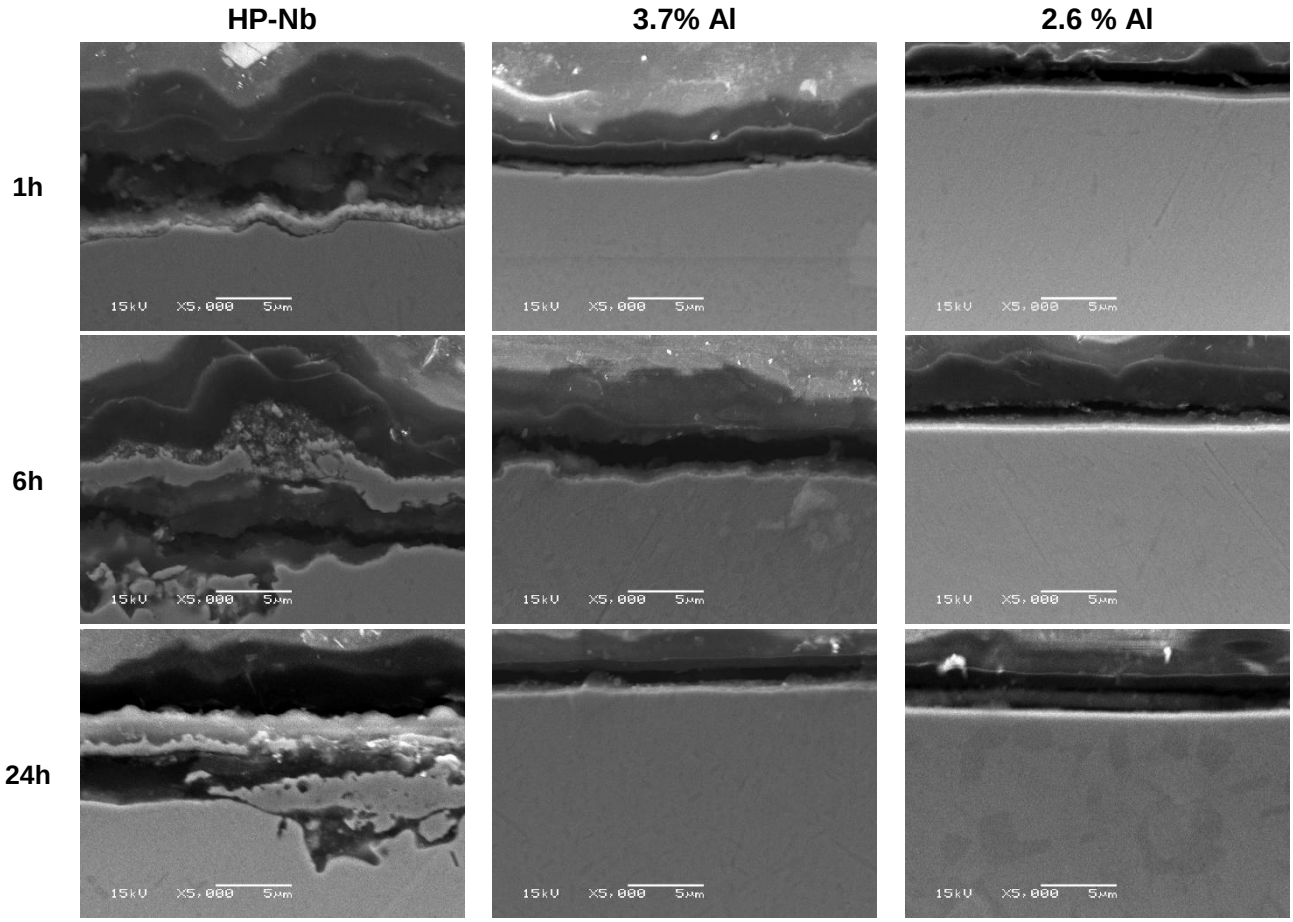

Figure 43. SEM cross section of samples after exposure to C_2H_6 at 950 °C

The 3.7% Al and 2.6% Al EDS line scans, shows presence of Al and O on surface, indicating the formation of a thin alumina oxide scale. Underneath of it, presence of chromium and oxygen is found. Spallation of oxide scale it is seen in the 3.7% Al alloy, indicating that the chromia scale came out to surface and started to deplete while the alumina scale remained on surface. Chromia volatilization starts to appear at temperatures of 950 °C when exposure has been done for at least 6 hours.

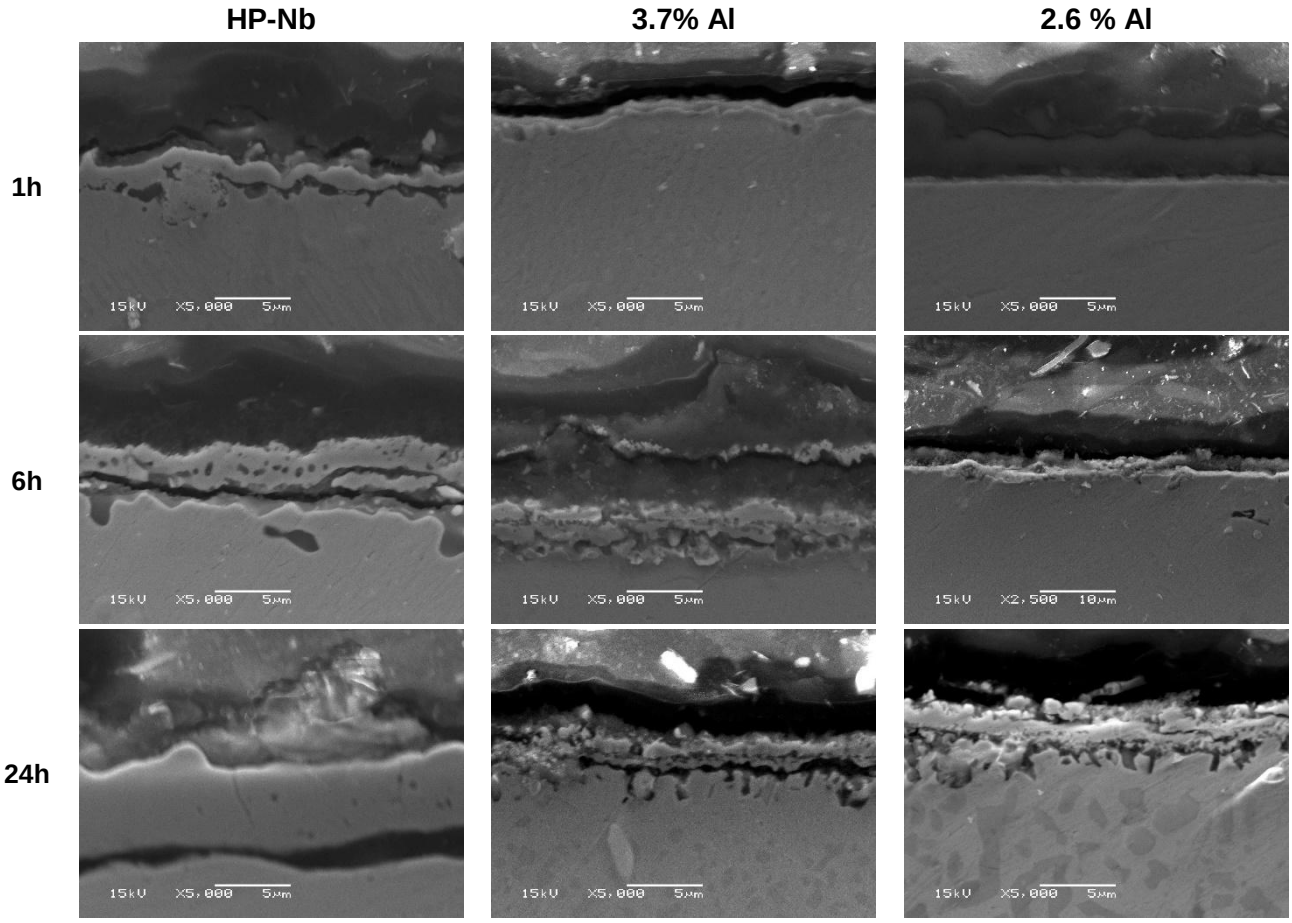

Figure 44. SEM cross section of samples after exposure to C_2H_6 at 1050 °C

A EDS on samples exposed to C_2H_6 for 6 hours at 1050 °C is shown in Figure 45. HP-Nb alloy shows presence of chromium and oxygen indicating the formation of the chromia scale on surface, of around ~2µm thick. Underneath the oxide scale, base metal is found with no formation of intermetallic.

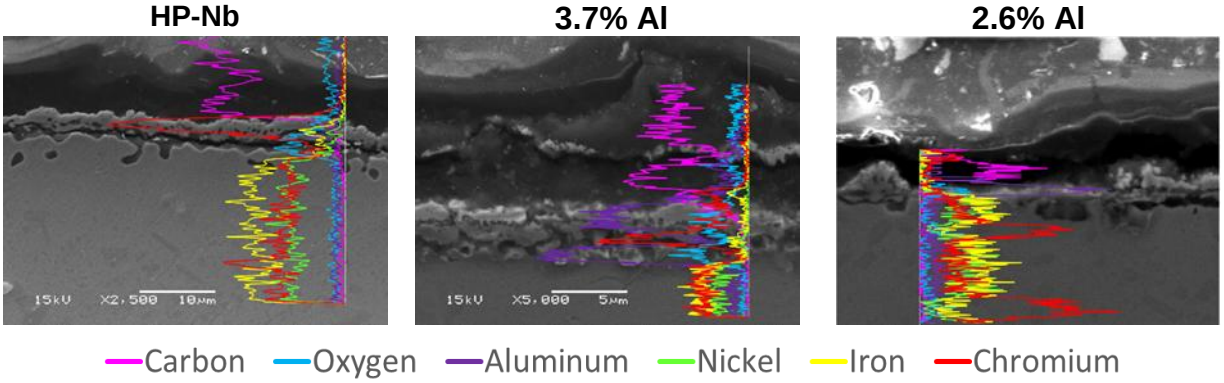

Figure 45. EDS of cross section of alloys exposed to C_2H_6 atmosphere at 1050 °C for 6 hours.

3.2.3. Summary

Samples with pre-oxidation treatment were exposed to 850, 950 and 1050 °C for 1, 6 and 24 hours for each temperature, under 25%C_2H_6 - 75%Ar atmosphere. The influence of time and temperature on the effect of carbon deposition onto the alloys was studied.

- Carbon adhered more to the HP-Nb alloys than the AFA samples.
- HP-Nb alloy showed poor resistance to atmospheres of 850 °C or above in presence of carbon since internal damage and oxide spallation was seen.
- 2.6%-Al alloy showed a different trend in the change of mass at 1050 °C compared to the 850 and 950 °C trends.
- 3.7%-Al alloy showed good coking resistant to the C_2H_6 atmosphere at the different temperatures and times. However, formation of intermetallic started to appear at the highest temperature (1050 °C) and longest time (24 hour).

3.3. Cyclic conditions

A pre-oxidation treatment in steam was intended to produce a stable surface oxide on the samples. Industrial practice includes a pre-oxidation stage in steam at similar temperatures for newly installed tubes. One cycle of coking/de-coking was performed on samples after the pre-oxidation treatment. The mass change was tracked for each step of the cycle as shown in Figure 46. A gain in mass after the pre-oxidation was seen for all of the samples, with a higher gain in mass for the HP-Nb alloy followed by the 3.7% Al alloy and the 2.6% Al Alloy. Then, the alloys were exposed to C_2H_6 for 6 hours at 1050 °C, the three alloys showed a slight additional gain in mass after exposure. The

HP-Nb alloy showed the highest gain in mass compared to the alumina-former alloys. Two different atmospheres were used to de-coke the alloys. The first was an atmosphere of 100% air at a temperature of 1050 °C for 15 min. The three alloys showed a small loss in mass after being exposure to air. Therefore, majority of mass gain occurred as a result of the initial pre-oxidation and coking. Slight mass loss was observed upon decoking but not the extent to where mass returned to the pre-coked level. This indicates than some oxidation may have resulted during the decoking stage of the cycle. No significant weight loss that would indicate spallation was observed for any of the alloys.

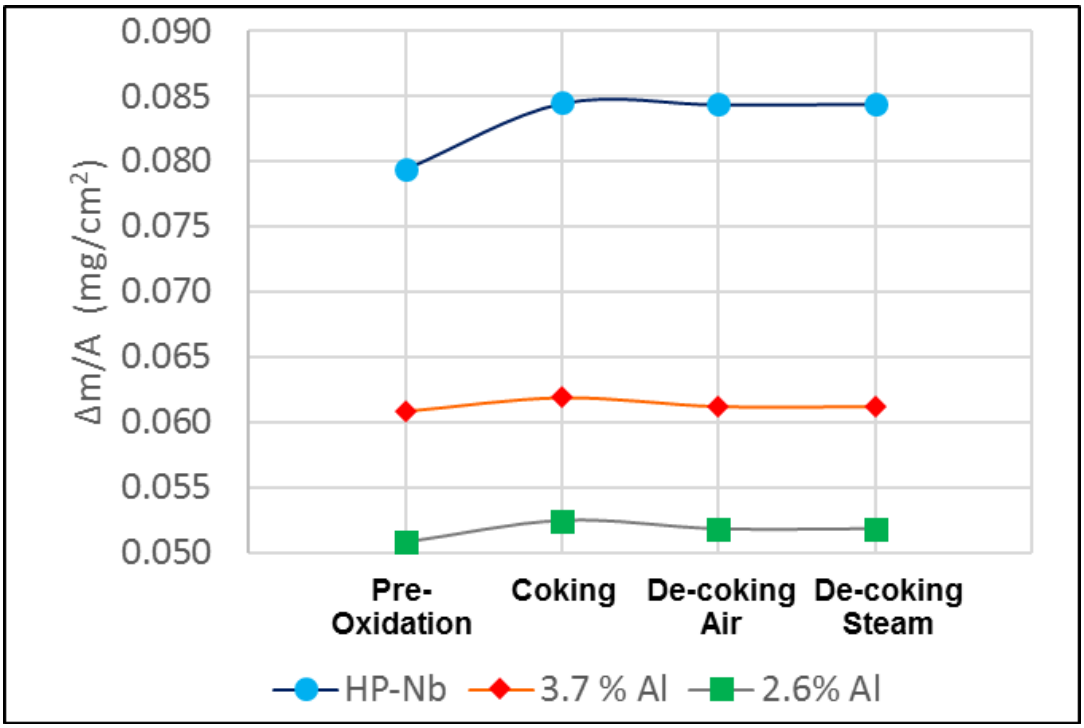

Figure 46. Mass change for each step of one cycle coking/de-coking

Cross sectional images of the samples for each step of the cycle are shown in Figure 47. For the pre-oxidation treatment, the HP-Nb alloy showed a uniform oxidation layer of 1.2 µm. EDS analysis confirmed the presence of Cr and O elements in this layer. For

the alumina-former alloys, in the case of the 3.7% Al alloy, a uniform layer of 0.5 μm thick of alumina and a thinner (~0.1 μm) chromia layer underneath was found across the sample. In the 2.6% Al alloy, a similar oxide layer as the 3.7% Al was observed and several nodules of alumina and chromia were observed sporadically.

After the pre-oxidation treatment, the samples were exposed to coking conditions. The SEM cross sections shown no presence of carbides or internal damage to the alloys. The previous chromia layer formed from the pre-oxidation remained for the HP-Nb alloy but presence of intermetallic appeared in the microstructure of the alloy. Additionally, spaces between chromia layer and base metal starts to seem noticeable indicating possible future spallation of layer. For the alumina-former alloys, a thicker alumina layer was found in the 3.7% Al compared to the formed in the pre-oxidation treatment. It was uniform and the sample was free of carbides or internal damage. In the 2.6% Al alloy, the same alumina layer from the pre-oxidation treatment was found followed by a thicker chromia layer underneath it. Presence of formation of intermetallic was found in some regions of the alloy.

De-coking with air for 15 min at 1050 °C was done after exposure to coking conditions. It is possible to see internal damage, beneath the chromia layer in the HP-Nb alloy because of depletion of Cr due to the strong atmosphere. Furthermore, higher presence of Oxygen was found in the chromia layer on this alloy. Alumina-former alloys did not change significantly after de-coking in air. No internal damage was found indicating that these alumina-former alloys may have better resistance to the de-coking atmosphere than the chromia-former alloy at high temperatures. The 2.6% Al alloy showed a thicker alumina layer and bigger intermetallic that based on EDS analysis are mainly Cr.

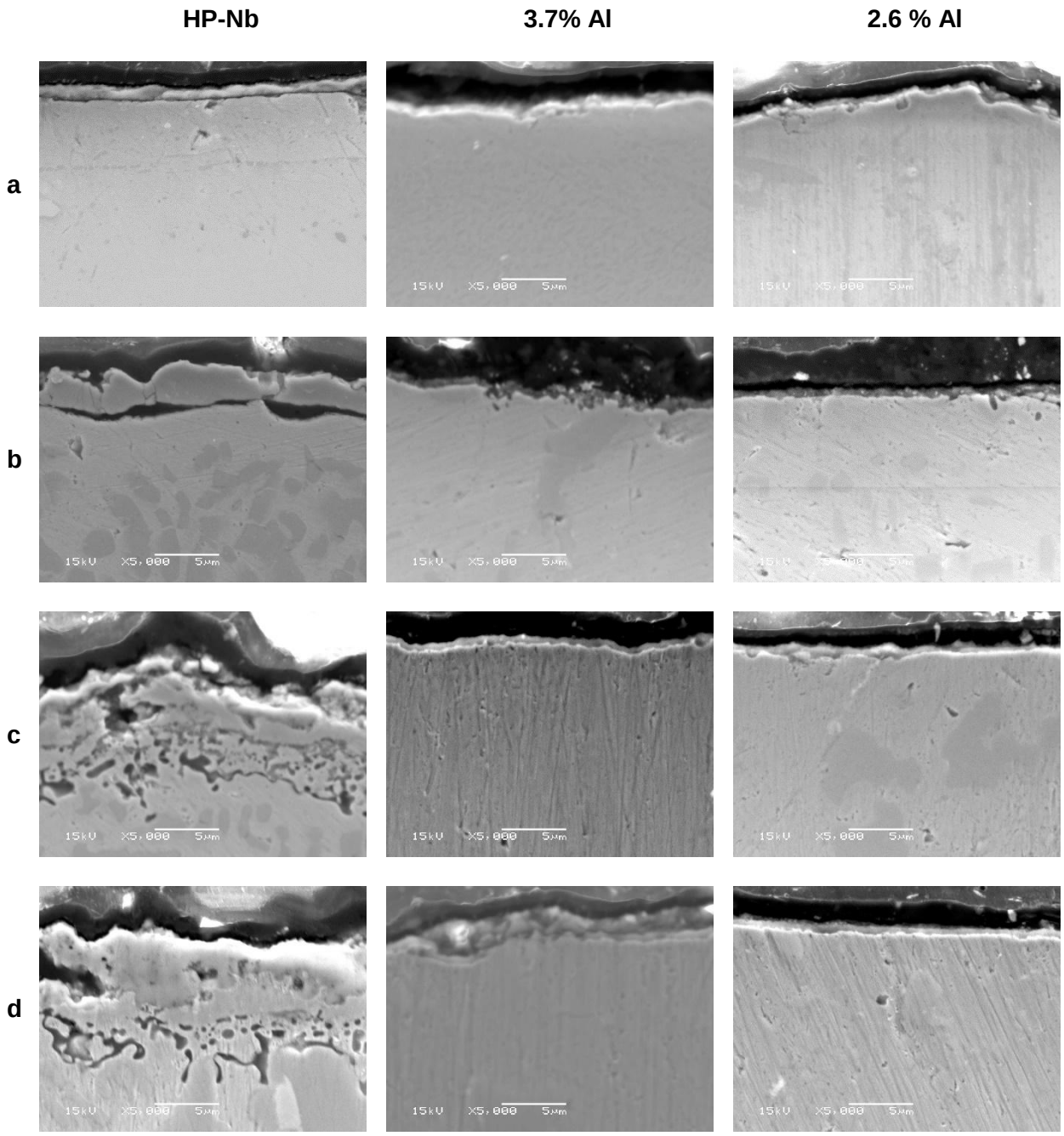

Figure 47. SEM cross-sections at 5000x magnification. a) Pre-oxidation with 100% steam for 12 h at 850°C and 1 h at 915°C; b) coking with 25%C_2H_6/75%Ar for 6 h at 1050°C; c) de-coking with air for 15 min at 1050°C; d) de-coking with 100% steam for 1 h at 915°C

De-coking with 100% steam for 1 hour at 915 °C was done after exposure to air. There was no significant difference in the microstructure or oxide layers of the samples after

exposure to steam. The internal damage of the HP-Nb alloy remained unchanged after the exposure to steam.

3.3.1. Summary

One cycle of coking/de-coking was performed on samples after the pre-oxidation treatment. Cyclic effects between coking and de-coking conditions of a one cycle was studied.

- **Pre-oxidation:**

  HP-Nb alloy showed a uniform and ~1.5 μm thick chromia layer after exposure.

  Both alumina-forming alloys were capable of forming a continuous thin (~0.5 μm) alumina layer

- **Coking**

  Found possible spallation of the chromia layer due to high temperature in the HP-Nb alloy.

  Alumina-forming alloys showed a thicker oxide layer (~1 μm) and no presence of internal damage.

- **De-coking**

  HP-Nb alloys showed internal damage

  AFA alloys showed no presence of internal damage. Oxide layer remained same

CHAPTER 4. ANALYSIS AND DISCUSSION

4.1. Influence of surface roughness and gas atmosphere

Samples with no oxidation treatment were exposed to two atmospheres; to a CO-H_2-H_2O atmosphere for 169 h at 600 °C and to a C_2H_6 atmosphere for 100 h at 850 °C. Samples were exposed directly to the carbon atmosphere so the environment conditions are more aggressive to the material than when is already pre-oxidized. Surface roughness was also studied. Samples were polished to 80-, 320- and 1200- grit SiC paper, a surface roughness from 0.02 μm to 1.14 μm was studied.

Samples exposed to CO-H_2-H_2O atmosphere, had not evident carbon deposition on their surfaces. Therefore, there was not clear effect of the surface roughness on the mass change of alloys in this exposure condition. This indicated that CO-H_2-H_2O atmosphere was not aggressive enough to generate a significant mass of change and/or carbon deposition on samples. Additionally, SEM analysis on cross-section of the samples showed no presence of internal attack or spalling on the samples.

Samples exposed to C_2H_6 atmosphere, showed evident carbon deposition on the surface of the samples. Based on Raman Spectroscopy analysis, the carbon deposits correspond to carbon black. Respect to the change in mass, there is a clear gain in mass which corresponds to the carbon deposition on surface of each sample. While the overall magnitude of mass change was more significant, there was still no clear trend relating surface roughness and change in mass. SEM and EDS analysis showed presence of a coke layer and an oxide layer across the alloys. A uniform oxide layer of around ~2.5 μm thickness was found across all HP-Nb alloy, while a thin oxide layer

with nodules of ~1.4 μm thickness of Cr were found in the 2.6% Al alloy with a alumina layer underneath. The 3.7% Al sample, had a thin oxide layer across all sample and no presence of nodules or chromia scale was found on it.

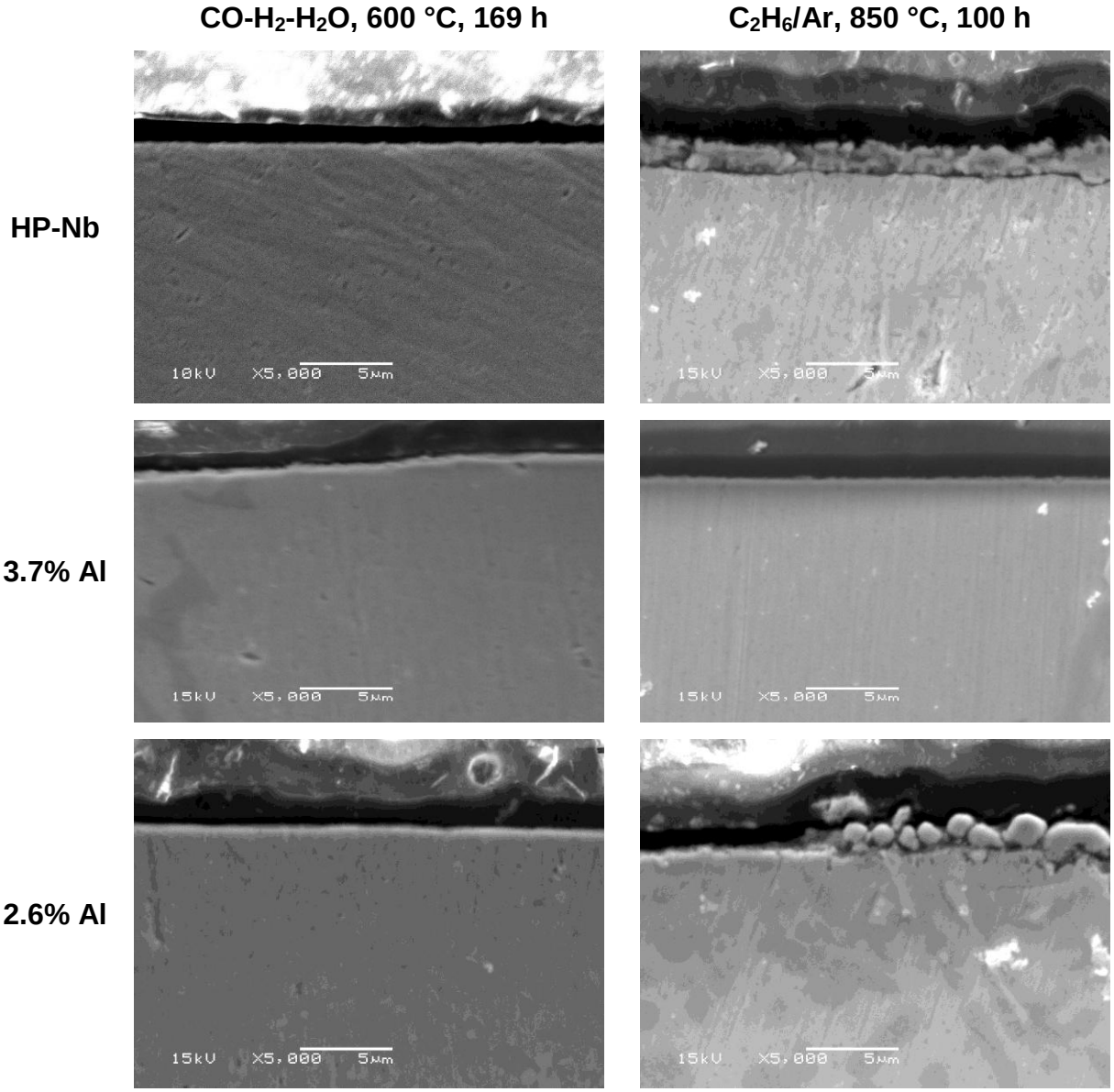

Figure 48. Comparison of effect of atmosphere on cross sections of samples

Exposition to C_2H_6 atmosphere showed a stronger effect of the atmosphere on the samples than exposition to $CO\text{-}H_2\text{-}H_2O$ atmosphere (see Figure 48). The HP-Nb alloy had a clear coke layer followed by the chromia layer on surface. The development of

the alumina layer on the AFA alloys was noticeable on samples exposed to the ethylene atmosphere. Therefore, higher carbon activity was achieved with the ethylene atmosphere and the higher temperature that this atmosphere allows to work with, allowed more aggressive conditions closer to the petrochemical industry environments.

4.2. Influence of time and temperature under C_2H_6 atmosphere

Samples were subjected to a pre-oxidation treatment for 815 °C for 12 hours and 915 °C for 1 hour under 100% steam in order to develop a uniform oxide layer across all surfaces of each alloy. Then, same alloys were exposed to 850, 950 and 1050 °C for 1, 6 and 24 hours for each temperature, under 25%C_2H_6 - 75%Ar atmosphere. The influence of time and temperature on the change in mass, oxide layer formation and internal damage for two alumina-forming alloys against a chromia-forming alloy was studied.

4.2.1. Pre-oxidation in Steam

A total of 9 samples per material were exposed to oxidation conditions. The HP-Nb alloy had the highest gain in mass compared to the AFA alloys indicating that this alloy developed a thicker oxide scale on its surface. Respect to the AFA alloys, the higher aluminum content in the alloy, the higher the gain in mass after oxidation treatment. This is correlated with similar studies done by Prenzlow (36), where he found that, oxidation under 100% steam, the higher aluminum content in the AFA alloy, the thicker the oxide layer developed and therefore, a bigger gain in mass.

4.2.2. Influence of time and temperature

After pre-oxidation treatment, alloys were exposed to an atmosphere of 25% C_2H_6 - 75% Ar at 850, 950 and 1050 °C for 1, 6 and 24 hours at each temperature.

Tests performed at 850 and 950 °C show a similar mechanism in the kinetics of carbon deposition on the alloys. There was more carbon deposition on the 2.6% Al alloy since had the highest gain in mass compared to the 3.7% and HP-Nb alloys. Despite the HP-Nb alloy had the lowest change in mass, the carbon deposited on it was different to the deposited on the AFA alloys. This carbon remained on its surface after handling while the carbon on AFA alloys fell off and the color of the alloy after oxidation treatment remained same. Respect to the cross section, AFA alloys showed no internal damage or depletion of the oxide scale. The HP-Nb alloy had good oxide layer at 850 °C while at 950 °C depletion of oxide scale is seen. This indicates this alloy may not be suitable for temperatures above ~850°C in presence of carbon.

Test performed at 1050 °C, seems to have a different mechanism on the kinetics of carbon deposition on these alloys. Indication of a linear trend for all three alloys it is suggested. It is noticeable that at this temperature, alloys are not strong enough to resist the high temperature since the HP-Nb alloy showed internal damage and oxide spallation; while the AFA alloys started to show formation of intermetallic and depletion of chromia layer.

In general, the influence of time on the coking resistance for these alloys shows that in general, longer exposure times represent bigger gain in mass. The thickness of the coke layer increases as alloys are exposed to longer times. The 3.7% Al alloy seems to

be the more resistant to the coking conditions. However, at longer exposure time and higher temperature (1150 °C and 24 hours), formation of intermetallic started to appear in the 3.7% Al alloy.

4.3. Cyclic conditions

Cyclic effects between coking and de-coking conditions of a one cycle was studied. The HP-Nb alloy showed a uniform and ~1.5 μm thick chromia layer after exposure. Both alumina-forming alloys, containing 3.7% and 2.6% wt Al, were capable of forming a continuous thin (~0.5 μm) alumina layer during 100% steam pre-oxidation. Mass changes showed that the HP-Nb alloy had the higher gain in mass compared to the alumina-former alloys. Between the alumina-former alloys, the higher the aluminum content, the higher the gain in mass after pre-oxidation. Respect to the coking step, spaces between the chromia layer and base metal were found across the sample in the HP-Nb alloy indicating possible spallation of the chromia layer due to the high temperature. Alumina-forming alloys showed a thicker oxide layer (~1 μm) and no presence of carbides or internal damage was found. After de-coking with air, HP-Nb alloy showed internal damage in the base metal while the alumina-forming alloys showed the same oxide layer without presence of internal damage. Lastly, de-coking with 100% steam was done showing no change in the alloys, indicating there is no need to run steam after air has been run before in order to remove the carbon deposits. Therefore, it seems that the alumina-forming alloys have better resistance to the cyclic conditions than the chromia-former alloy at high temperatures.

CONCLUSIONS

Cast heat-resistant alloys designed to form aluminum oxide scales were compared to a traditional HP-Nb alloy for performance in coking conditions with and without pre-oxidation treatment and cyclic conditions with pre-oxidation treatment.

Coking experiments with $CO/CO_2/H_2O/H_2$/Ar atmosphere at 600 °C showed no apparent damage to the alloys and formation of a thin (<0.5μm thick) oxide layer after exposure. Experiments with C_2H_6 atmosphere at 850 °C, alloys showed carbon deposition onto the surface of the materials and formation of a thick oxide layer (~1.5 μm) in the 2.6% Al and HP-Nb alloys; a thin alumina layer (<0.5μm thick) was found in the 3.7% Al alloy.

There was not a clear trend relating surface roughness and mass changes as well carbon deposition or oxide layer formed in the alloys independently of the test atmosphere. However, the ethane atmosphere was more aggressive to the alloys compared to the CO atmospheres with significantly more carbon deposition, oxide formation, and internal damage observed in ethane conditions.

Carbon adhered more to the chromia former than AFA alloys. The carbon deposited on the AFA alloys fell off easily after handling or moving the sample while the carbon deposited on the HP-Nb alloy, stayed there and even after trying to remove it, remained on surface. It is suggested that chromia former alloy follows a different mechanism in the surface-carbon deposition interaction. From cross section analysis, HP-Nb alloy showed poor resistance resistance to atmospheres of 850 °C or above in presence of carbon since internal damage and oxide spallation was seen. The 2.6% Al alloy showed a different trend in the change of mass at 1050 °C compared to the 850 and 950 °C

trends. This indicates that formation of nodules oxide, formation of intermetallic and possible oxide spallation are influencing on the kinetics of carbon deposition on this alloy. The 3.7% Al alloy showed good coking resistant to the C_2H_6 atmosphere at the different temperatures and times. However, formation of intermetallic started to appear at the highest temperature (1050 °C) and longest time (24 hour). This implies an upper temperature limit for the AFA sample and while that limit is higher than traditional HP alloys, additional research into compositional or structure effects could result in further increasing that temperature limit.

Cyclic effects between coking and de-coking conditions over one cycle were studied.

- After pre-oxidation treatment, the HP-Nb alloy showed a uniform and ~1.5 μm thick chromia layer. Both alumina-forming alloys, containing 3.7% and 3.2% wt Al, were capable of forming a continuous thin (~0.5 μm) alumina layer during 100% steam pre-oxidation. Mass changes showed that the HP-Nb alloy had a higher gain in mass compared to the alumina-former alloys. Between the alumina-former alloys, the higher the aluminum content, the higher the gain in mass after pre-oxidation.
- After exposition to coking atmosphere, cracks and gaps between the chromia layer and base metal were found across the sample in the HP-Nb alloy indicating possible spallation of the chromia layer at the high temperature. Alumina-forming alloys showed a thicker oxide layer (~1 μm) and no presence of carbides or internal damage.

- After de-coking with air, HP-Nb alloy showed internal damage in the base metal while the alumina-forming alloys showed the same oxide layer without the presence of internal damage.
- Lastly, de-coking with 100% steam was done showing no change in both HP and AFA alloys, indicating there is no need to run steam to re-form the oxidation layers after air has been used to remove the carbon deposits.

Therefore, it seems that the alumina-forming alloys have better resistance to the cyclic conditions than the chromia-former alloy at high temperatures.

The alumina-forming cast heat resistant alloys were more resistant to carbon deposition compared with a traditional HP-Nb alloy. Aluminum content of the alloys within the range tested did not show a distinct difference in terms of carbon deposition.

FUTURE WORK

Coking kinetics could not be obtained with the test procedure used due to the ease at which carbon deposits would fall from samples during handling. Thermogravimetric analysis is suggested as a method to study the coking kinetics in greater detail.

The study of the stability of the alumina oxide layer at 1050 °C or higher temperatures based on aluminum content of alloy is suggested so alloy development could be improved based on exposure conditions.

The study of longer cyclic effects (cycling between coking and de-coking conditions) as well as thermogravimetric analysis to study the coking and de-coking kinetics in greater detail is suggested. Additionally, cyclic conditions with alloys of different aluminum content in order to study the stability of alumina and chromia under strong carbon-rich atmospheres.

Future work will also focus on comparative studies of alloy behavior in alternative feedstocks to explore performance in conditions similar to actual production environments.

REFERENCES

1. Brady, M. P., Magee, J., Yamamoto, Y., Helmick, D., & Wang, L. (2014). Co-optimization of wrought alumina-forming austenitic stainless steel composition ranges for high-temperature creep and oxidation/corrosion resistance. *Materials Science and Engineering A*, *590*, 101–115. http://doi.org/10.1016/j.msea.2013.10.014
2. Toh, C. H., Munroe, P. R., & Young, D. J. (2002). Metal Dusting of Fe – Cr and Fe – Ni – Cr Alloys under Cyclic Conditions. *Oxidation of Metals*, *58*(1–2), 1–21.
3. Zhang, J., & Young, D. J. (2008). Coking and Dusting of Fe–Ni Alloys in CO–H2–H2O Gas Mixtures. *Oxidation of Metals*, *70*(3–4), 189–211. http://doi.org/10.1007/s11085-008-9115-0
4. R.R. Kirchheiner, P. Becker, D.J. Young, R. D. (n.d.). Improved Oxidation and Coking Resistance of a New Alumina Forming Alloy 60 HT for the Petrochemical Industry. Houston, TX: CORROSION 2005.
5. Szakálos, P., Lundberg, M., & Pettersson, R. (2006). Metal dusting on an alumina forming Ni-base alloy. *Corrosion Science*, *48*(7), 1679–1695. http://doi.org/10.1016/j.corsci.2005.05.023
6. Larsen, K. R. (2015). Alumina-Forming Austenitic Alloys Resist High-Temperature Corrosion, 1–13.
7. Cai, H., Krzywicki, a., & Oballa, M. C. (2002). Coke formation in steam crackers for ethylene production. *Chemical Engineering and Processing*, *41*(3), 199–214. http://doi.org/10.1016/S0255-2701(01)00135-0

8. SERNA, A., & Rapp, R. A. (2003). Carburization of austenitic and ferritic alloys in hydrocarbon environments at high temperature. *Revista De Metalurgia*, *162*(c), 162–166.
9. Muralidharan, G., Yamamoto, Y., Brady, M. P., Walker, L. R., Meyer III, H. M., & Leonard, D. N. (2016). Development of Cast Alumina-Forming Austenitic Stainless Steels. *JOM*, *68*(11), 2803–2810. http://doi.org/10.1007/s11837-016-2094-8
10. Saunders, S. R. J., Monteiro, M., & Rizzo, F. (2008). The oxidation behavior of metals and alloys at high temperatures in atmospheres containing water vapor: A review. *Progress in Materials Science*, *53*(5), 775–837. http://doi.org/10.1016/j.pmatsci.2007.11.001
11. Brady, M. P., Yamamoto, Y., Santella, M. L., Maziasz, P. J., Pint, B. A., Liu, C. T., … Bei, H. (2008). The development of alumina-forming austenitic stainless steels for high-temperature structural use. *Jom*, *60*(7), 12–18. http://doi.org/10.1007/s11837-008-0083-2
12. Barbabela, G. D., de Almeida, L. H., da Silveira, T. L., & Le May, I. (1991). Role of Nb in modifying the microstructure of heat-resistant cast HP steel. *Materials Characterization*, *26*(3), 193–197. http://doi.org/10.1016/1044-5803(91)90053-7
13. Brady, M. P., Yamamoto, Y., Santella, M. L., & Pint, B. A. (2007). Effects of minor alloy additions and oxidation temperature on protective alumina scale formation in creep-resistant austenitic stainless steels. *Scripta Materialia*, *57*(12), 1117–1120. http://doi.org/10.1016/j.scriptamat.2007.08.032
14. Yamamoto, Y., Santella, M. L., Brady, M. P., Bei, H., & Maziasz, P. J. (2009). Effect of alloying additions on phase equilibria and creep resistance of alumina-forming

austenitic stainless steels. Metallurgical and Materials Transactions A: Physical Metallurgy and Materials Science, 40(8), 1868–1880. http://doi.org/10.1007/s11661-009-9886-1

15. Yamamoto, Y., Brady, M. P., Santella, M. L., Bei, H., Maziasz, P. J., & Pint, B. A. (2011). Overview of Strategies for High-Temperature Creep and Oxidation Resistance of Alumina-Forming Austenitic Stainless Steels. *Metallurgical and Materials Transactions A*, *42*(4), 922–931. http://doi.org/10.1007/s11661-010-0295-2

16. Sanjit Bhowmick, Gavin Lea, Atul Verma and Prabhakar Singh “Assessment of chromium evaporation from chromia and alumina forming alloys”, 2011. Advances in Solid Oxide Fuel Cells VII. Ceramic Engineering and Science Proceedings, Volume 32, Issue 4.

17. Grabke, H. J., Müller-Lorenz, E. M., & Schneider, A. (2001). Carburization and Metal Dusting on Iron. ISIJ International, 41(Suppl), S1–S8. http://doi.org/10.2355/isijinternational.41.Suppl_S1

18. Xu, X., Zhang, X., Sun, X., & Lu, Z. P. (2012). Roles of Manganese in the High-temperature Oxidation Resistance of Alumina-forming Austenitic Steels at above 800 C. *Oxidation of Metals*, *78*(5), 349–362. http://doi.org/10.1007/s11085-012-9311-9

19. Yamamoto, Y., Brady, M. P., Santella, M. L., Maziasz, P. J., & Pint, B. a. (2008). Development of Alumina-Forming Austenitic Stainless Steels, (865), 1–8.

20. Brady, M. P., Muralidharan, G., Leonard, D. N., Haynes, J. A., Weldon, R. G., & England, R. D. (2014). Long-Term Oxidation of Candidate Cast Iron and Stainless Steel Exhaust System Alloys from 650 to 800 C in Air with Water Vapor. *Oxidation of Metals*, *82*(5), 359–381. http://doi.org/10.1007/s11085-014-9496-1

21. Muralidharan, G., Yamamoto, Y., Brady, M. P., Walker, L. R., Meyer III, H. M., & Leonard, D. N. (2016). Development of Cast Alumina-Forming Austenitic Stainless Steels. *JOM*, *68*(11), 2803–2810. http://doi.org/10.1007/s11837-016-2094-8

22. Serna Gil, J. A. (2003). *Oxidacion, Carburacion y Sulfidacion de aleaciones ferriticas Fe-0-Cr-1Mo modificadas en ambientes con hidrocarburos a temperaturas entre 550 y 750 C*. Universidad Industrial de Santander, Colombia.

23. Millward, G. R., Evans, H. E., Aindow, M., & Mowforth, C. W. (2001). The Influence of Oxide Layers on the Initiation of Carbon Deposition on Stainless Steel. *Oxidation of Metals*, *56*(3/4), 231–250.

24. Church, B., Ortiz, L., Prenzlow, E., Li, S., dos Santos, B. L., Erwin, B., & Myers, J. (2016, June 14). An Initial Evaluation of the Effect of Alloy Composition and Oxide Layer on High Temperature Coking Resistance of Heat Resistant Alloys. NACE International.

25. Cai, H., Krzywicki, a., & Oballa, M. C. (2002). Coke formation in steam crackers for ethylene production. *Chemical Engineering and Processing*, *41*(3), 199–214. http://doi.org/10.1016/S0255-2701(01)00135-0

26. Young, D. J., Zhang, J., Geers, C., & Schütze, M. (2011). Recent advances in understanding metal dusting: A review. *Materials and Corrosion*, *62*(1), 7–28. http://doi.org/10.1002/maco.201005675

27. Muller-Lorenz, E. M., & Grabke, H. J. (1999). Coking by metal dusting of nickel-base alloys. *Materials and Corrosion*, *50*(11), 622–627. http://doi.org/10.1002/(SICI)1521-4176(199911)50:11<622::AID-MACO622>3.3.CO;2-I

28. Zhang, J., & Young, D. J. (2008). Coking and Dusting of Fe–Ni Alloys in CO–H2–H2O Gas Mixtures. *Oxidation of Metals*, *70*(3–4), 189–211. http://doi.org/10.1007/s11085-008-9115-0

29. Munoz Gandarillas, A. E., Geem, K. M. Van, Reyneris, M.-F., & Marin, G. B. (2014). Influence of the Reactor Material Composition on Coke Formation during Ethane Steam Cracking. Industrial & Engineering Chemistry Research, 53, 6358–6371. https://doi.org/dx.doi.org/10.1021/ie500391b

30. Zhang, J., Schneider, a., & Inden, G. (2003). Characterization of the coke formed during metal dusting of iron in CO-H2-H2O gas mixtures. *Corrosion Science*, *45*(6), 1329–1341. http://doi.org/10.1016/S0010-938X(02)00251-2

31. Jackson, P. R. S., Trimm, D. L., & Young, D. J. (1986). The coking kinetics of heat resistant austenitic steels in hydrogen-propylene atmospheres. *Journal of Materials Science*, *21*(9), 3125–3134. http://doi.org/10.1007/BF00553346

32. Steurbaut, C., Grabke, H. J., Stobbe, D., van Buren, F. R., Korf, S. J., & Defrancq, J. (1998). Kinetic studies of coke formation and removal on HP40 in cycled

atmospheres at high temperatures. *Materials and Corrosion-Werkstoffe Und Korrosion*, *49*(5), 352–359. Retrieved from isi:000073723400010

33. Young, D. J. (1999), Kinetic and morphological development of coke formation on heat-resistant alloys. Materials and Corrosion, 50: 675–680. doi:10.1002/(SICI)1521-4176(199912)50:12<675::AID-MACO675>3.0.CO;2-U

34. Leng, Yang. *Materials Characterization. Introduction to Microscopic and Spectroscopic Methods.* s.l. : Wiley-VCH, 2013.

35. Mell, Benjamin. *Sandpaper Roughness Measurement. Using 3D Profilometry.* s.l. : NANOVEA, 2010.

36. Prenzlow, Elmer A., "High Temperature Oxidation of Alumina Forming Cast Austenitic Stainless Steels Within an Environment of Pure Steam" (2016). *Theses and Dissertations*. 1403. http://dc.uwm.edu/etd/1403

APPENDIX A – DIMENSIONS OF SAMPLES

Influence of surface roughness

C – HP-Nb – chromia – forming alloy

H – 3.7% Al – AFA high aluminum content alloy

L – 2.6% Al – AFA low aluminum content alloy

Table 11. Dimensions of samples for test of surface roughness under CO-H_2-H_2O atmosphere

Sample	Length (in)				Surface area (in^2)	Surface area (cm^2)
	x	y	h	t		
C-80	0.540	0.705	0.562	0.336	1.218	7.86
C-320	0.476	0.502	0.557	0.335	1.028	6.63
C-1200	0.483	0.530	0.563	0.322	1.015	6.55
H-80	0.499	0.523	0.564	0.326	1.034	6.67
H-320	0.516	0.727	0.548	0.326	1.174	7.57
H-1200	0.616	0.759	0.547	0.381	1.468	9.47
L-80	0.481	0.578	0.457	0.343	1.042	6.72
L-320	0.534	0.597	0.470	0.381	1.220	7.87
L-1200	0.520	0.577	0.475	0.336	1.057	6.82

Table 12. Dimensions of samples for test of surface roughness under C_2H_6 atmosphere

Sample	Length (mm)				Surface area (mm^2)	Surface area (cm^2)
	x	y	h	t		
C-80	15.700	19.520	13.915	8.880	874.955	8.75
C-320	15.650	19.310	14.245	8.710	859.190	8.59
C-1200	11.330	13.260	14.510	9.890	774.032	7.74
H-80	13.070	15.440	12.280	10.900	890.466	8.90
H-320	13.180	13.810	12.365	10.690	841.496	8.41
H-1200	12.560	14.860	12.270	9.520	756.721	7.57
L-80	13.090	14.310	12.130	8.920	705.489	7.05
L-320	13.490	14.240	12.185	9.120	728.155	7.28
L-1200	14.260	16.010	12.035	7.980	675.695	6.76

Influence of time and temperature under C_2H_6 atmosphere

Table 13. Dimensions of samples for test of influence of time and temperature under C2H6 atmosphere

Experiment	Time (h)	Temperature (°C)	Sample	x (mm)	y (mm)	h (mm)	t (mm)	Surface area (mm^2)	Surface area (cm^2)
1	1	850	C	12.75	15.57	10.69	8.59	671.78	6.72
1	1	850	H	13.05	15.70	12.45	8.82	727.92	7.28
1	1	850	L	11.89	12.18	12.21	9.01	653.78	6.54
2	6	850	C	11.70	14.75	11.12	7.90	595.25	5.95
2	6	850	H	13.24	15.25	12.54	9.17	753.23	7.53
2	6	850	L	13.03	13.93	12.19	8.60	673.44	6.73
3	24	850	C	11.64	14.78	10.77	8.59	640.79	6.41
3	24	850	H	12.60	15.31	12.95	9.59	784.96	7.85
3	24	850	L	13.26	12.24	12.33	8.22	622.32	6.22
4	1	950	C	10.40	13.47	11.19	10.79	758.75	7.59
4	1	950	H	12.97	14.68	12.59	9.15	736.83	7.37
4	1	950	L	12.96	14.53	12.24	9.20	731.49	7.31
5	6	950	C	12.46	15.70	10.60	8.09	629.05	6.29
5	6	950	H	12.35	13.13	12.50	9.69	736.17	7.36
5	6	950	L	13.10	14.73	12.21	8.54	684.35	6.84
6	24	950	C	14.78	17.94	11.30	8.11	715.79	7.16
6	24	950	H	13.05	14.00	12.26	9.05	711.59	7.12
6	24	950	L	11.79	13.41	12.13	8.20	612.66	6.13
7	1	1050	C	15.82	18.00	11.85	8.11	741.58	7.42
7	1	1050	H	11.60	14.95	9.06	8.71	622.92	6.23
7	1	1050	L	12.55	13.57	12.10	10.31	788.21	7.88
8	6	1050	C	10.86	13.48	9.15	9.99	670.90	6.71
8	6	1050	H	13.68	15.25	12.54	9.70	804.90	8.05
8	6	1050	L	13.46	14.03	12.23	8.67	688.80	6.89
9	24	1050	C	15.51	17.62	11.81	7.55	679.30	6.79
9	24	1050	H	12.64	12.82	11.71	8.76	651.14	6.51
9	24	1050	L	12.69	14.21	12.19	10.07	787.75	7.88

Cyclic conditions

Sample notation is defined as a: “1” for samples that will go until pre-oxidation; “2” coking; “3” de-coking with air; and “4” until de-coking with steam step.

Table 14. Dimensions of samples for cyclic conditions test.

Sample	Length (mm)				Surface area (mm^2)	Surface area (cm^2)
	x	y	h	t		
C1	11.81	14.01	14.55	8.61	695.80	6.96
C2	13.41	14.30	14.47	8.82	744.18	7.44
C3	11.83	13.20	14.54	8.96	709.38	7.09
C4	14.20	16.03	14.34	8.61	767.91	7.68
H1	12.45	12.53	12.28	8.23	613.22	6.13
H2	13.12	12.75	12.51	10.04	770.60	7.71
H3	11.88	12.06	12.30	8.66	627.68	6.28
H4	12.95	13.76	12.41	9.01	705.06	7.05
L1	12.41	14.19	12.00	8.61	665.26	6.65
L2	12.16	12.19	12.17	8.93	652.25	6.52
L3	12.25	12.69	12.05	8.46	625.90	6.26
L4	11.95	12.59	12.03	7.95	581.45	5.81

APPENDIX B – SEM OF INFLUENCE OF SURFACE ROUGHNESS

Carbon deposition in CO-H_2-H_2O atmosphere

3.7% Al

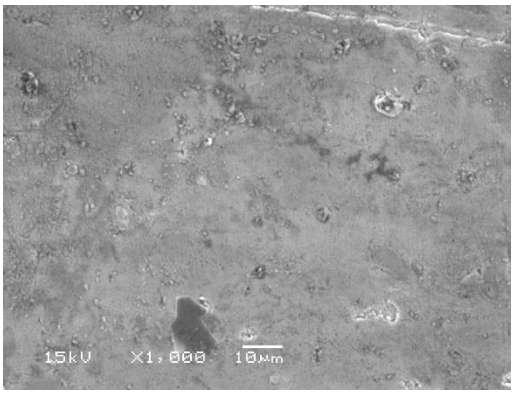

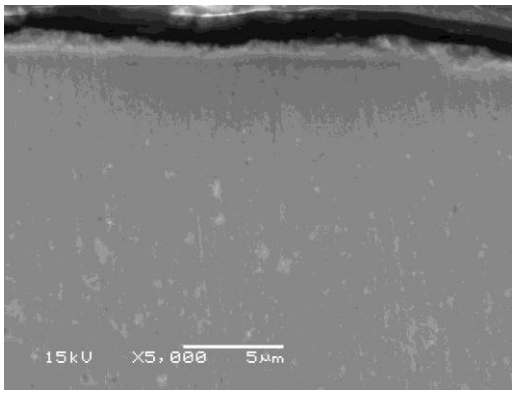

2.6% Al

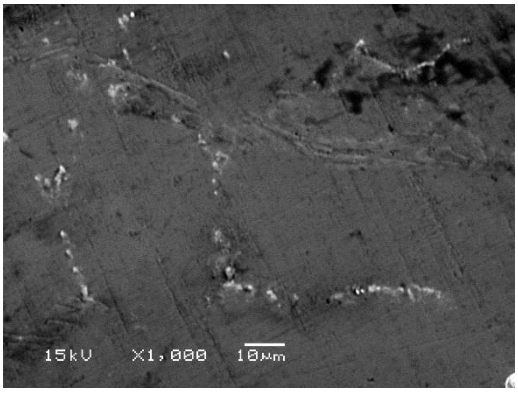

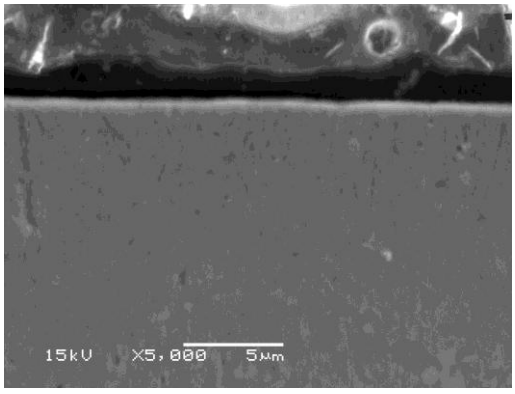

HP-Nb

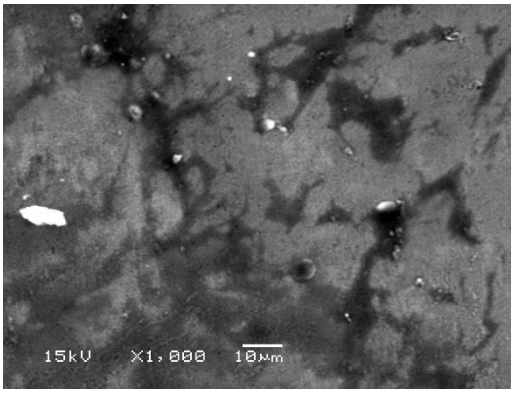

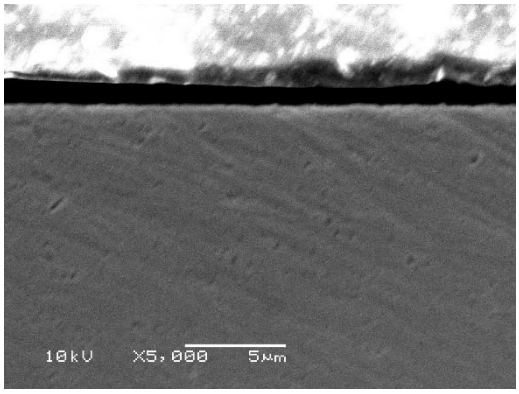

Figure 49. SEM of surface and cross section for samples ground to 1200-grit and exposed to CO-CO2-H2O at 600 C for 169 hours.

Carbon deposition in C_2H_6 atmosphere

3.7% Al

2.6% Al

HP-Nb

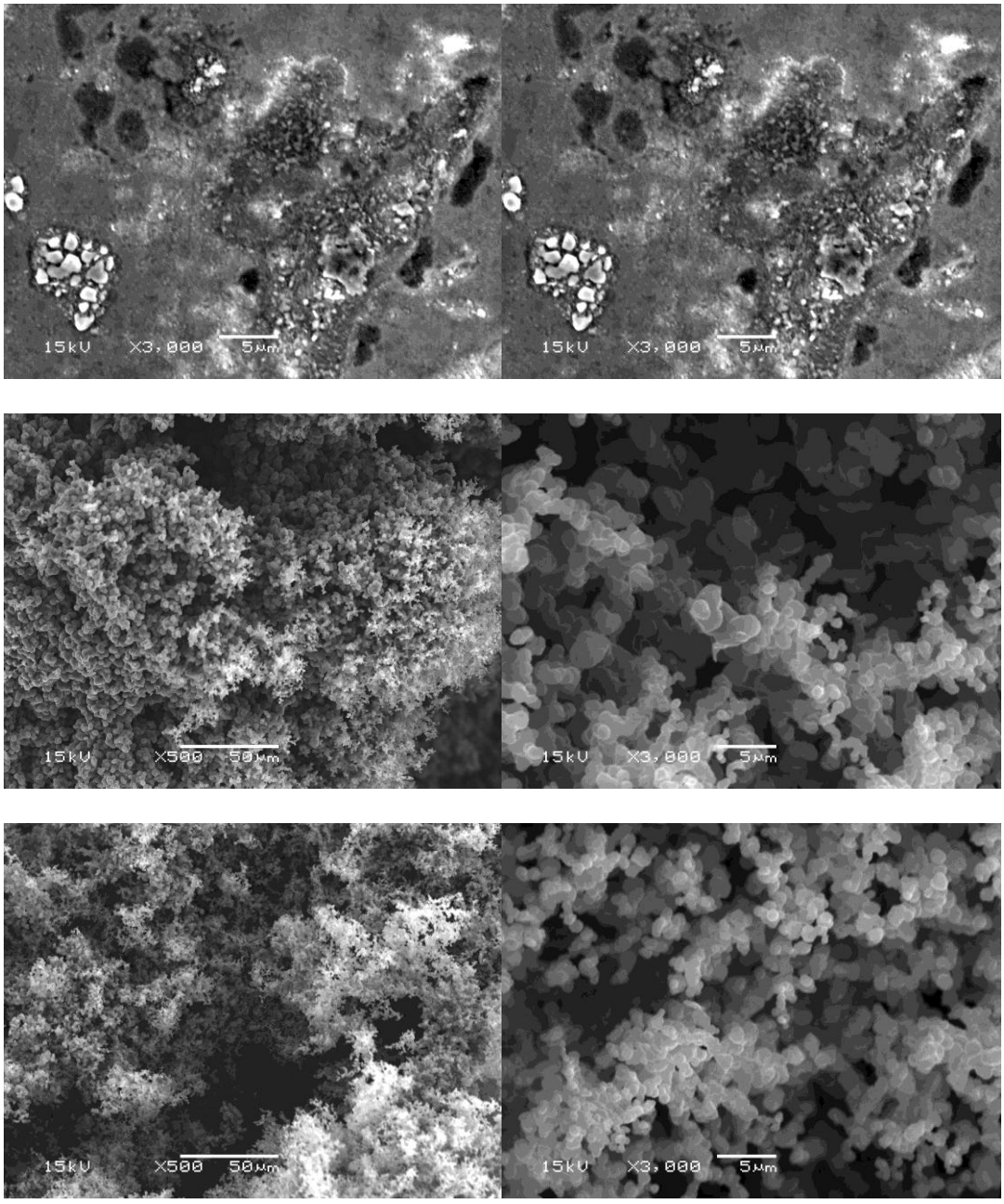

Figure 50. SEM of surface for samples ground to 1200-grit and exposed to C_2H_6-Ar at 850°C for 100 hours.

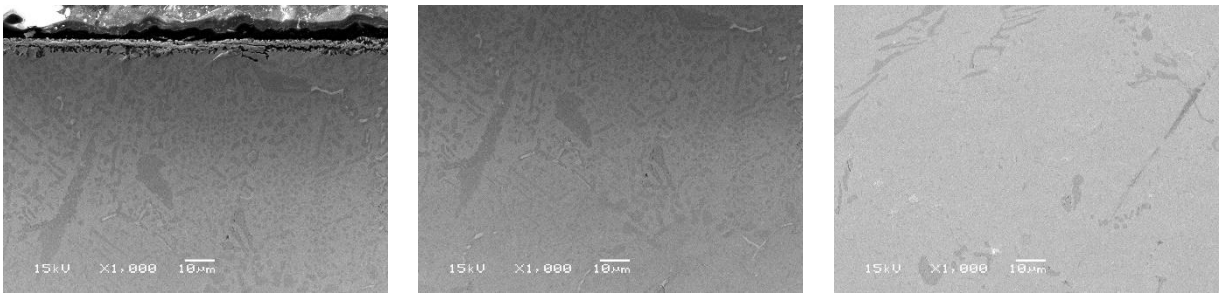

Figure 51. SEM cross section from surface (left) to base metal (right) of 2.6% Al exposed to C_2H_6 at 1050 °C for 24 hours.

APPENDIX C – SEM OF INFLUENCE OF TIME AND TEMPERATURE

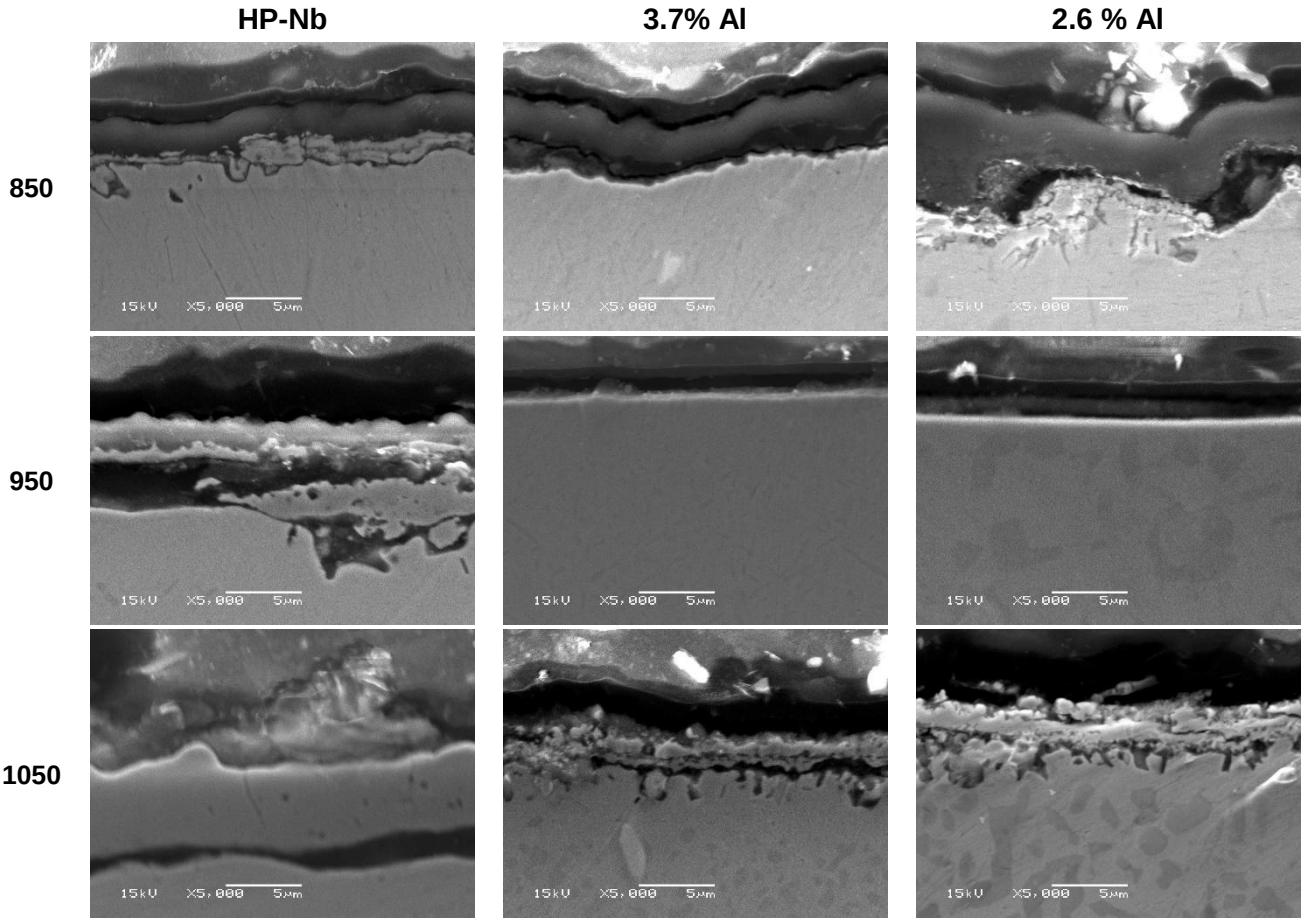

Figure 52. SEM cross section of samples after exposure to C_2H_6 for 24 hours

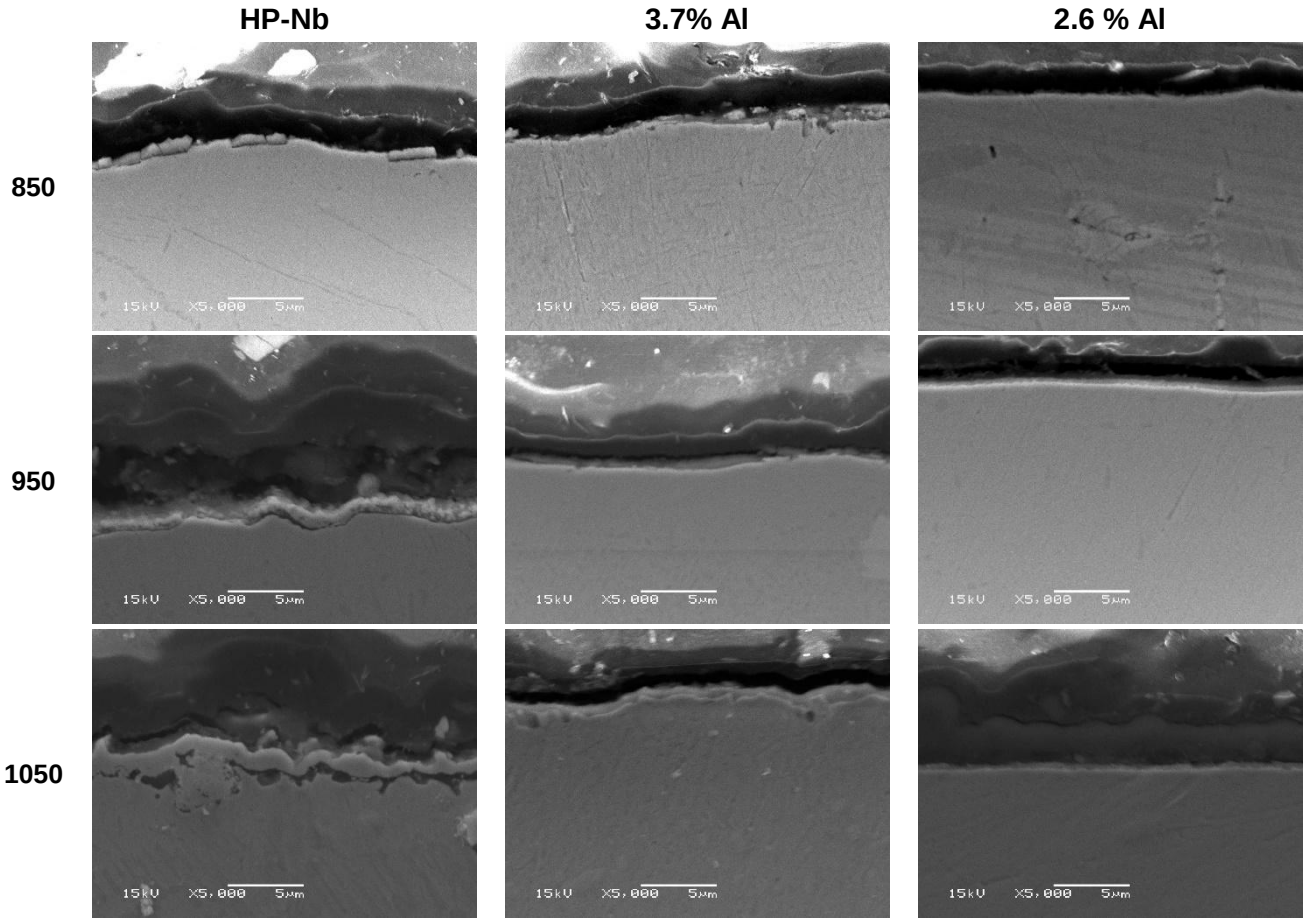

Figure 53. SEM cross section of samples after exposure to C_2H_6 for 1 hour

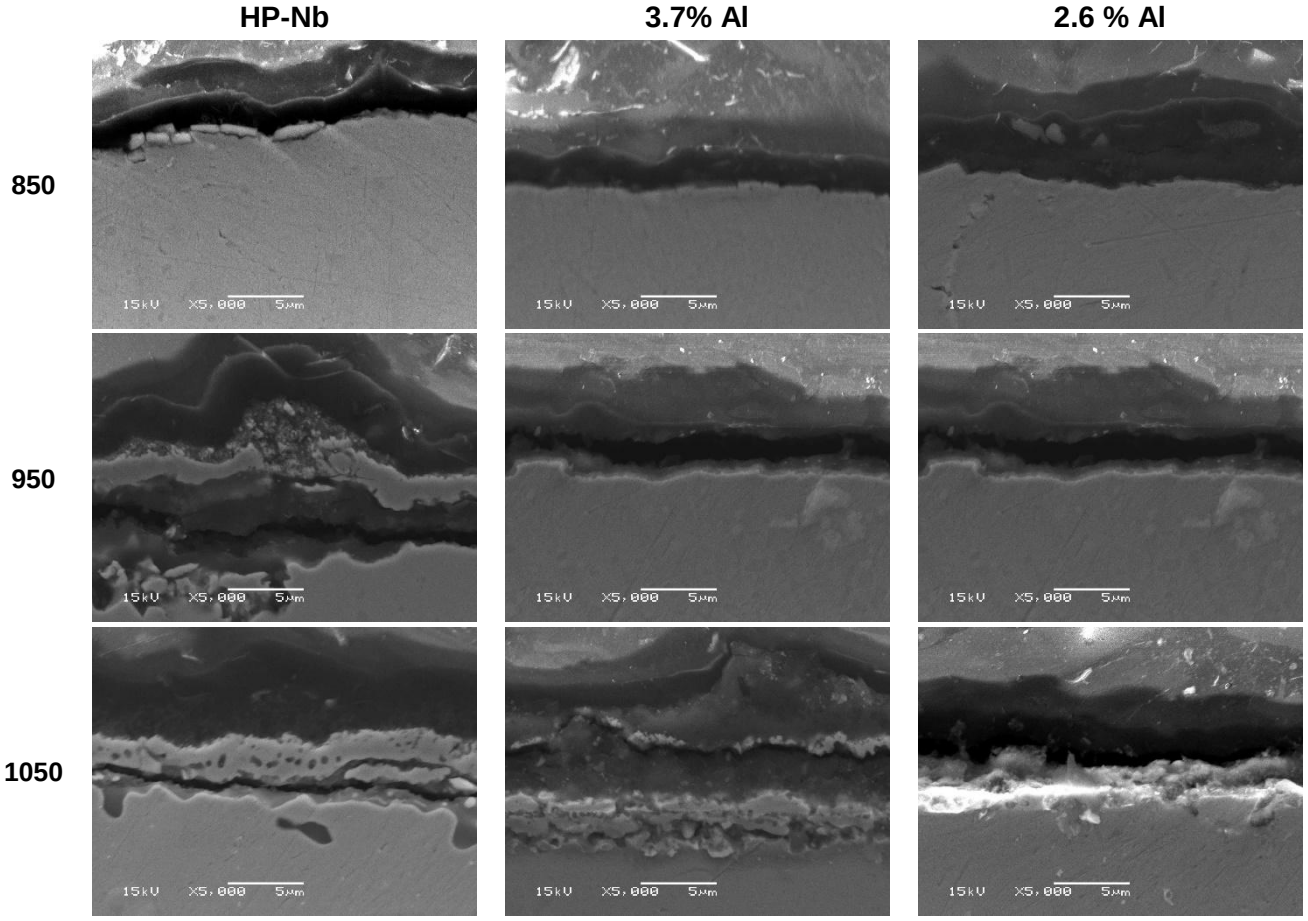

Figure 54. SEM cross section of samples after exposure to C_2H_6 for 6 hours